Fermilab Library
0 1160 0000335 4

FERMILAB
OCT 31 1988
LIBRARY

KEK-88-6

KEK Report 88- 6
September 1988
H

144

Proceedings of the Workshop on Physics of Quark-Gluon-Plasma

February 18 – 20, 1988
KEK, Tsukuba, 1988

Edited by
T. Hatsuda (KEK), J. Chiba (KEK) and O. Miyamura (Osaka)

ROUTE TO
NAME | LOCATION
RETURN TO FERMI LIBRARY

NATIONAL LABORATORY FOR
HIGH ENERGY PHYSICS

FERMI
QC793.5
.Q252W67
1988

Preface

Recent theoretical studies of nature of hadronic matter at high temperature and density have convinced us of existence of new phase. First order phase transition is suggested by lattice simulations with dynamical fermions.
Furthermore, studies of dynamical properties such as excitation mode around critical temperature have been discussed by various models and some lattice simulations. One of the purposes of this workshop is to discuss the results from the frontier in these studies.

Experimental search of phase transition and new phase by heavy ion acceralator has been started since 1986. In these years, some results in first stage have been presented. It seems quite timely to examine the experimental data in order to find the way to second stage experiments with combining the new knowledge from theoretical studies and pilot data from cosmic rays. In this respect, signals of phase transition is important and still open problem.
It seems difficult but at the same time attractive because it is problem of new type including particle physics,nuclear physics, statistical physics and hydrodynamics.

Program and Contents

February 18th, Thursday

A Comment on Formation and Development of Quark Gluon Plasma
O. Miyamura (Osaka) 1

QCD Hydrodynamics
M. Mizutani (Waseda) 12

Signals for Quark Gluon Plasma Formation
T. Hashimoto (INS) ○

Search for Quark Gluon Plasma at the CERN SPS
H. En'yo (CERN) 21

Heavy Ion Experiments at the BNL AGS
Y. Akiba (Tokyo) 41

^{16}O and $^{32}S +^{207} Pb$ Interactions in the CERN EMU-05 Experiment
J. Iyono (Okayama) 54

Cosmic Data above TeV/amu
J. Iwai (Washington) ○

February 19th, Friday

Report on QGP Workshop at India 1988
Y. Takahashi (Alabama) ○

Phenomenological Descriptions
H. Sumiyoshi (Matsusho-Gakuen) ○

Lattice QCD at Finite Temperature
C.E. DeTar (RIFP) 76

Effective Theory of QCD at Finite Temperature
S. Midorikawa (INS) ○

Hadrons at Finite Temperature
T. Kunihiro (Ryukoku) 88

Hadron-Quark Phase Transition and An Excluded Volume Effect
F. Takagi (Tohoku) 106

Temperature Effects to Anomalous Baryon Decay
T.Akiba ○

Feburary 20th, Saturday

High Energy Particle/Nuclear Astrophysics with Emulsion Chambers
Y. Takahashi (Alabama) 116

First Results from Quark Gluon Plasma Search at Fermilab
D. Koltick (Purdue) 140

A Comment on

Formation and Development of Quark Gluon Plasma

Osamu Miyamura

Department of Applied Mathematics
Faculty of Engineering Science
Osaka University
Toyonaka, Osaka 560 , Japan

1. Initial energy density formed in ultra-relativistic nucleus-nucleus collision

Formation of Quark Gluon Plasma in laboratory has been discussed mainly on phenomenological basis.[1-3] Present expectations of possible formation are 1) baryon number less plasma in central region of nucleus-nucleus collisions above TeV/amu and 2) baryon number rich plasma production in the energy region 10 ~ 100 GeV/amu. One of key quantities for these estimations is energy density at the starting time of fire ball evolution which is required to exceed critical energy density of hadron -quark phase transition.
Various estimations have been presented based on assumptions of critical energy density of 1 - 2 GeV/fm^3. On this point recent estimate of critical temperature by lattice Monte Carlo

simulations including light quarks have suggested lower value as Tc= 110 ~ 160 Mev.[4)]

The purpose of this comment is to examine the required energy of baryon numberless plasma formation in the case of such low critical temperature.

Let us examine critical energy density of quark gluon plasma (QGP) phase . Free gas model of N_f flavor quarks and gluon gives

$$\varepsilon \simeq \left(\frac{7Nf}{20} + \frac{8}{15} \right) \pi^2 T^4 \quad . \qquad (1)$$

We use (1) for order of magnitude estimation. It is noted that some lattice Monte Calro simulations have suggested emperical usefulness of it.[5)] By the use of eq.(1), critical energy density of Quark Gluon Plasma phase is estimated as

$$\varepsilon_c = \begin{matrix} 32 \\ 2 \\ 0.2 \end{matrix} \ \mathrm{GeV/fm^3} \quad \text{for} \quad T_c = \begin{matrix} 400 \\ 200 \\ 120 \end{matrix} \ \mathrm{MeV} \quad . \qquad (2)$$

Nextly, we have to estimate initial energy density of fire ball formed in central region. For this purpose, we use previous calculation of ε_{max} and ε_{th} by Sumiyoshi, suzuki, Date, Ochiai and present author.[3)]

The quantity ε_{max} is calculated by the formula according to Bjorken;[2)]

$$\varepsilon_{max} = \frac{e_o N_\pi}{V(\tau_o)} \qquad (3)$$

where $V(\tau_o)$ is volume of fire ball (disk) at the starting time of soft QCD interaction τ_o which is taken to be 1 fm/c hereafter. N_π is average number of pions and e_o is average energy per pion involved in $V(\tau_o)$. e_o is taken to be 0.4 GeV . N_π is average number of pions in rapidity interval $|y| < 0.5$ and estimated by Multi-Chain model.[6] We take into account spreading of collision points between constituent to estimate $V(\tau_o)$. In addition to the spreading due to (Lorentz contracted) incident nucleon distributions,inherent spreading of collision points due to virtual parton structure is considered [3] (Fig.2). ε_{th} is calculated in similar way as eq.(2) except for the use of $V(\tau_3)$ where τ_3 is the time that average number of collisions per pions exceeds 3.

In Fig.1 and 2, contour of ε_{max} and ε_{th} are shown. Vertical (horizontal) axis corresponds to mass number of projectile (target) or target (projectile) nucleus. Effect of spreading of collision points are (not) taken into account in Fig.2 (Fig.1). Head-on collision is assumed. We see that both ε_{Max} and ε_{th} exceed 0.2 GeV/fm^3 even for collisions of middle and heavy projectile nuclei at 0.4 TeV/amu. However energy density of 2 GeV/fm^3 can not be achieved in this energy region. It is remarked that recent estimations $\varepsilon_{Max} \simeq 3.5$ GeV/fm^3 based on CERN SPS experiments(O^{16} 200 GeV/amu

GeV/amu) have used the formula with factor 2 difference.[7,8] Furthermore spreading due to finiteness of lorentz contraction has been neglected. Thus present analysis suggest that if T_c is as low as 120 MeV, initial energy density exceeds ε_c in the collisions at energies above several hundred GeV per nucleon. In this case, CERN SPS has some chance of QGP formation. On the other hand, if T_c is 200 MeV, collisions at energies above TeV/amu are required. If, unfortunately, T_c is above 400 MeV, QGP formation seems hard even by collisions at RHIC energies.[9] Fig.1 and 2 suggests that such high value of energy density will be formed at energies above several hundred TeV/amu.

2. Durations of quark gluon plasma phase, mixed phase and hadronic gas phase

Let us discuss durations of QGP, mixed- and hadronic gas phases in fire ball expansion. In the energy region above several hundred GeV/amu, the centrally produced fire ball would expand longitudinally in the initial stage. Here we rely on one-dimensional hydrodynamical expansion model of ideal gas in which time development is given by

$$\tau \sim s^{-1} \sim \bar{T}^{3} \quad . \qquad (4)$$

Using eq.(4), duration of quark gluon plasma phase is

estimated as

$$\tau_{QGP} = (T_i/T_c)^3 \tau_o = (\varepsilon_i/\varepsilon_c)^{3/4} \tau_o \quad . \qquad (5)$$

Using the previous estimation of ε_{Max} as ε_i ,we can estimate duration of QGP era at different energy regions.
Results for several combination of nuclei in the cases of T_c = 120 MeV and 200 MeV are summerized in Table 1. If T_c = 200 MeV, QGP era is only several fm/c even at 10 TeV/amu. However if it is 120 MeV, the duration becomes around 10 fm/c at RHIC energies. At energies 0.4 GeV/amu , the duration is still a few fm/c in this case.

Nextly let us discuss duration of mixed phase.
In the case of first order phase transition, super- cooling is expected and there would be era of mixed phase.
It seems hard to discuss the duration of mixed phase from present knowledge. In case of smooth transition (no entropy production) , the mixed phase proceeds to exhaust gap of entropy between QGP phase and hadron gas phase and we have in scaling expansion

$$\tau_{mix} \sim (\tau_{QGP} + \tau_o)(s_Q^c / s_H^c - 1) \quad , \qquad (6)$$

where s_Q^c and s_H^c are entropy densities of QGP and hadronic gas at T_c. As smooth transition is an extreme case, actual duration of mixed phase would be shorter than (6).

If we utilize free gas models of QGP and pion gas, τ_{mix} is estimated as

$$\tau_{mix} \lesssim 10\ \tau_{QGP} \qquad (7)$$

Duration of hadronic gas phase proceeds from T_c to the decoupling temperature. If we use the scaling solution again, it is given by

$$\tau_H = [\ (T_c / T_f)^3 - 1\ ]\ (\ \tau_o + \tau_{QGP} + \tau_{mix}\ ) \quad . \qquad (8)$$

Although validity of the scaling solution in this stage is poor due to inhomoginuity after super-cooling, eq.(8) gives following observation. If T_c / T_f is around unity , duration of hadronic era does not overcome $\tau_{QGP}+\tau_{mix}$. This is good condition for observation and detection of formation of new phase. As temperature become lower than pion mass, pion density is significantly suppressed. Decoupling temperature cannot be much lower than pion mass even for large fire ball. Thus if T_c =120 MeV , we can expect this good situation.
expect the good situation. For example , for T_c =120 MeV and T_f = 80 - 100 MeV, τ_H is less than 3(τ_{QGP} + τ_{mix}) as shown in Table 1.

3. Summary

We have discussed formation and development of quark gluon plasma in the case of low critical temperature. If T_c is as low as 120 MeV, initial energy density of fire disk by head-on collisions at energies above several hundred GeV/amu exceeds the critical energy density. Furthermore , durations of QGP and mixed phase are comparable to that of hadronic phase in this case. These are good conditions for observation and detections of new phase.

On the contrary if T_c is higher than 400 MeV, formation of new phase seems to be hard even at RHIC energies.

References

1) R.Anishetty,P.Koehler,L.McLerran Phys.Rev. D22 2793 (1980); M.Gyulassy , Proceedings of the Quark Matter 83 at BNL , Nucl.Phys. A418 59c (1984).

2) J.D.Bjorken, Phys.Rev. D27 140 (1983)

3) H.Sumiyoshi, S.Date, N.Suzuki, O.Miyamura and T.Ochiai, Z.Phys. C23 391 (1984)

4) S.Gottlieb, W.Liu,D.Toussaint,R.L.Renken and R.L.Suger, Phys.Rev.Lett. 59 1513 (1987).

5) J.Engels,F.Karsch,H.Satz and I.Montvay, Nucl.Phys. B205 545 (1982); J.B.Kogut and D.K.Sinclair, Phys.Rev.Lett. 60 1250 (1988).

6) K.Kinoshita,A.Minaka and H.Sumiyoshi, Z.Phys. C8 205 (1981)

7) A.Bamberger et al.(NA35) , Phys. Lett. B184 271 .

8) R.Albrecht et al. (WA80) , Phys.Lett. B190 297 (1987).

9) T.Ludlam , Proceedings of the Nucleus-Nucleus CollisionII at Visby, 1985, Nucl.Phys. A447 349c (1986).

		ε_{Max} (GeV/fm^3)	ε_{th} (GeV/fm^3)	$(\varepsilon_{Max}/\varepsilon_c)^{3/4}$ ε_c=0.2 GeV/fm^3	2.0 GeV/fm^3
S-Pb	(a)	1.2	0.5	3.8	/
0.4TeV/amu	(b)	0.7	0.3	2.6	/
Pb-Pb	(a)	1.5	0.9	4.5	/
0.4TeV/amu	(b)	0.9	0.5	3.0	/
S-Pb	(a)	2.0	1.1	5.6	1.0
1TeV/amu	(b)	1.0	0.6	3.3	/
S-Pb	(a)	5.1	3.5	11	2.0
10TeV/amu	(b)	2.4	1.8	6.4	1.1
Pb-Pb	(a)	7.5	6.0	15	2.7
10TeV/amu	(b)	3.5	2.8	8.6	1.5

Table 1. Initial energy densities and duration of quark gluon plasma phase

Case (a) represents the values by Bjorken's formula.[2)]

Case (b) corresponds to the calculations including space-time spreading of collision point (S_h=1 fm) in ref.2.

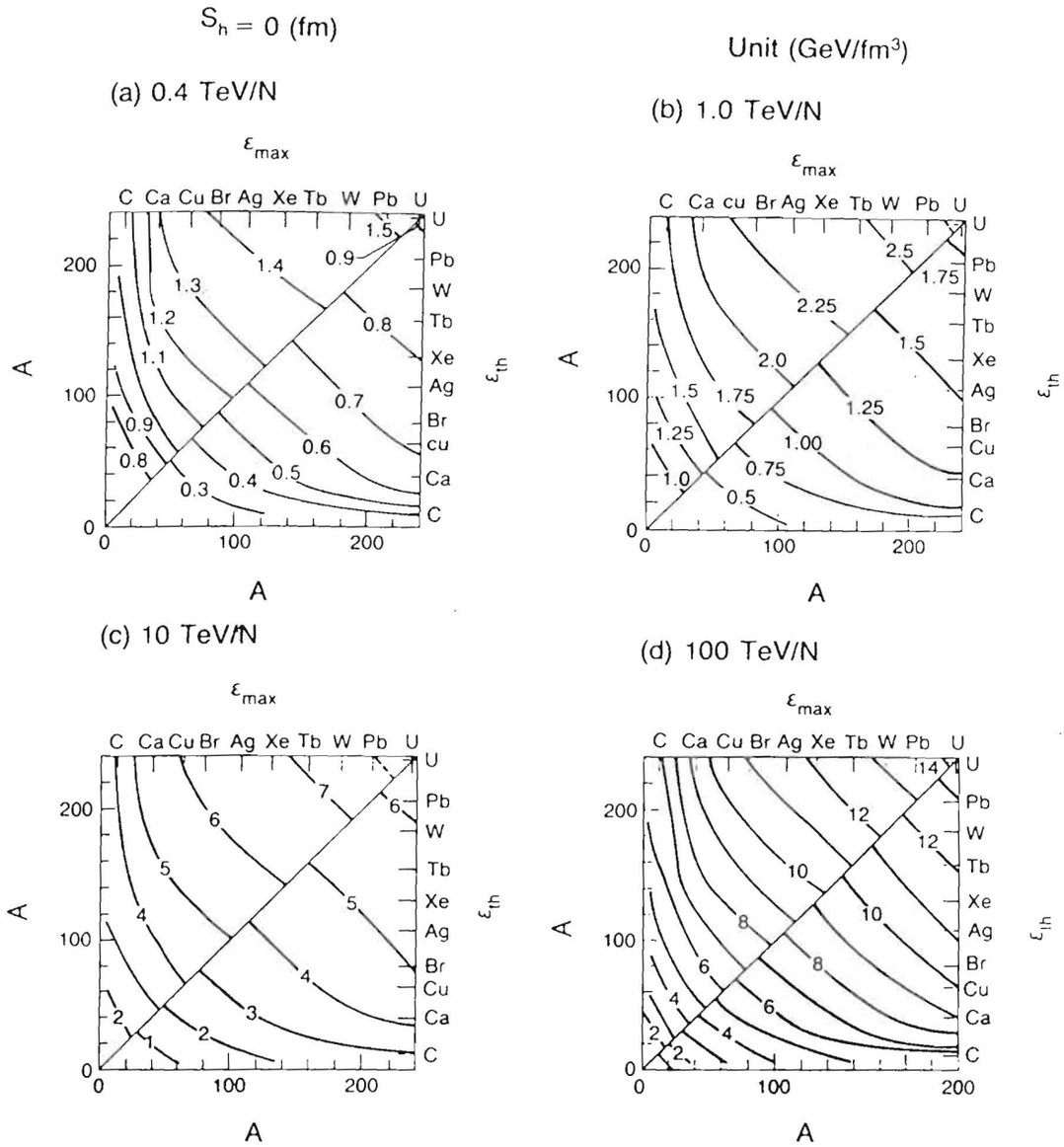
S_h = 0 (fm)
Unit (GeV/fm^3)
(a) 0.4 TeV/N
(b) 1.0 TeV/N
(c) 10 TeV/N
(d) 100 TeV/N
ε_{max}
ε_{th}
A
C Ca Cu Br Ag Xe Tb W Pb U
Pb W Tb Xe Ag Br Cu Ca C
0 100 200

Figure 1.

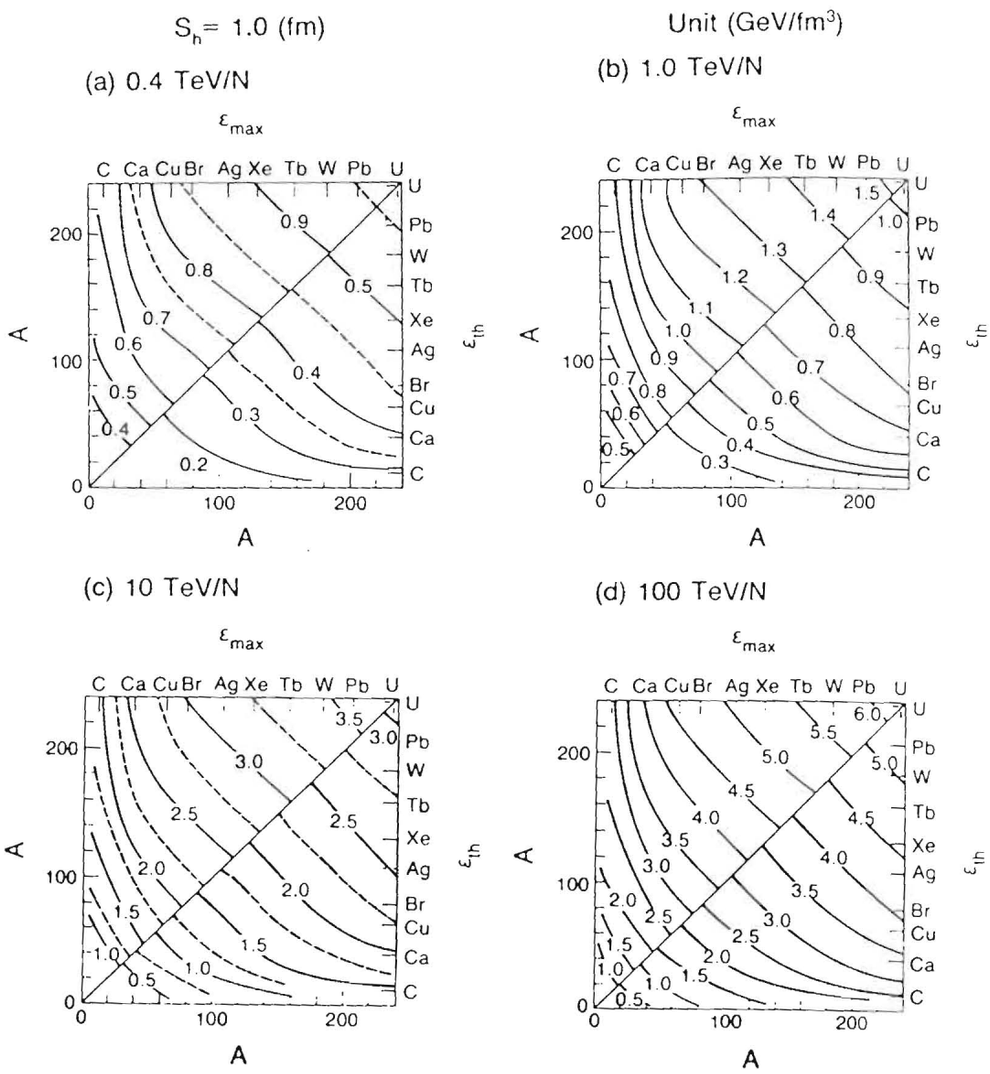
S_h= 1.0 (fm)
Unit (GeV/fm^3)
(a) 0.4 TeV/N
(b) 1.0 TeV/N
(c) 10 TeV/N
(d) 100 TeV/N
ε_{max}
ε_{th}
A
C Ca Cu Br Ag Xe Tb W Pb U

Figure 2.

QCD Hydrodynamics

Masashi Mizutani

Department of Physics, Waseda University, Tokyo 160, Japan

The relativistic hydrodynamical model is reviewed for a phenomenological approach to quark-gluon plasma. First, we formulate the relativistic hydrodynamics by which we discuss high energy nuclear reactions. Next, we introduce transport theory based on the operator field Langevin equation we proposed. This theory provides an intermediate theoretical step from first principles, QCD, towards the phenomenolgy, the hydrodynamical model. Using our operator field Langevin equation, we derive the temperature dependence around a phase transition point of thermodynamical quantities and transport coefficients. Using these results, we solve a hydrodynamical equation for the quark-gluon system and analyse how its initially hot system approaches phase phase transition point.

The details of this review will be published on another occasion.

1. Introduction

First of all, we must establish phenomenology in order to understand complicated phenomena such as high energy nuclear reactions. Next, we derive the phenomenology from first principles. However, in most cases, the phenomenological theories would be very far from first principles. Thus, it is often useful to introduce an intermediate theoretical step between them.

We consider the relativistic hydrodynamical model of quark-gluon plasma as one of the phenomenological theories. On the other hand, here, first principles is QCD. In general, it is very difficult to derive the hydrodynamical model from QCD. Thus, we have proposed a transport theory based on an operator field Langevin equation which mediates between the hydrodynamical model and QCD.

2. Relativistic hydrodynamics

In hydrodynamics, we assume a local equilibrium. Consider that a space-time region which is macroscopically small but microscopically large around the point of a fluid on the macroscopic scale. A thermal equilibrium of this region is the local equilibrium.

In general, the relativistic hydrodynamics starts with giving the energy-momentum tensor $T^{\mu\nu}(x)$ and the conserved current vecter $J^{\mu}(x)$. They obey the following equations:

$$\partial_\nu T^{\mu\nu}=0, \qquad \partial_\mu J^\mu=0. \tag{2.1}$$

It is easy to generalize the above equations to those of a mixed fluid. We define the local velosity of a fluid $U^\mu(x)$ with J^μ[2,3] or $T^{\mu\nu}$.[4,5] In this review, we use the definition by $T^{\mu\nu}$:

$$U^\mu=T^{\mu\nu}U_\nu/(U_\rho T^{\rho\sigma}T_{\sigma\tau}U^\tau)^{1/2}=T^{\mu\nu}U_\nu/U_\rho T^{\rho\sigma}U_\sigma. \tag{2.2}$$

We need equation of state which provides a relation between energy density ε and static pressure P in order to solve a system of hydrodynamical equations. We get

$$P=\frac{1}{3}\varepsilon \tag{2.4}$$

in the high energy limit for the interaction of the first kind.[15,16] In addition to equation of state, we need phenomenological relations in order to analyze a motion of a viscous fluid.[2]

3. Applications of relativistic hydrodynamics to high energy nuclear reactions.

1) perfect fluid. Assume that the produced fluid by high energy nuclear reactions is a 1+1 dimensional perfect fluid with zero baryon chemical potential. Following Bjorken,[8] we assume:

a) thermodynamical quantities must be functions of only proper time $\tau=(t^2-z^2)^{1/2}$ independent of rapidity $y=\frac{1}{2}\ln[(t+z)/(t-z)]$, and

b) a particular solution of hydrodynamical equation

$$U^\mu=x^\mu/\tau \tag{3.1}$$

describes phenomena. Then, we give the temperature change of the fluid:

$$T=T_0\left(\frac{\tau_0}{\tau}\right)^{1/3}, \tag{3.2}$$

where T_0 and τ_0 are the initial temperature and time of the fluid, respectively.

Next, let us consider the relation with observed quantities. Suppose that hadronization takes place at $\tau=\tau_f$. We assume:

$$n_f \propto s_f, \tag{3.3}$$

where n_f and s_f are the produced number density and the entrpy density of the quark-gluon fluid at $\tau=\tau_f$, respectively. Using (3.2), (3.3) and Stephan-Boltzmann law, we derive

$$\varepsilon_0 \propto \left(\frac{dN}{dy}\right)^{4/3}, \tag{3.4}$$

where ε_0 and dN/dy are the initial entropy density and the rapidity distribution, respectively.[9]

2) viscous fluid. Let us include the effect of viscosity. We assume a) and b) in 1). Thus, we assume that transport coefficients are functions of only proper time τ through temperature. From dimensional analysis, assuming that

c) $$\frac{2}{3}\eta_{(s)}+\eta_{(v)}=aT^3, \tag{3.5}$$

where $\eta_{(s)}$ and $\eta_{(v)}$ are shear and bulk viscosity, respectively, and a is an unknown constant. Temperature change of the fluid is

$$T=T_0\left(\frac{\tau_0}{\tau}\right)^{1/3}+\frac{3a}{8K_{SB}\tau_0}\left(\frac{\tau_0}{\tau}\right)^{1/3}\left[1-\left(\frac{\tau_0}{\tau}\right)^{2/3}\right], \tag{3.6}$$

where K_{SB} is the Stephan-Boltzmann constant.[20,21,22]

4. QCD transport theory

In this section, we introduce transport theory to mediate between the hydrodynamical model and QCD. Transport theory based

ate theoretical steps.[19,20,21,22] This theory may not be justified because of non-Markoffian character of the process rooted in quantum property. Speaking in principle, we should find a collective mode which describes essence of phenomena. Our motivation is to make an intermediate theoretical step in the form of a collective mode and fluctuations around it, which are responsible for the dissipation effect to give transport coefficients, on the basis of an operator valued equation.[27]

Suppose that we find a collective mode to describe essence of quark-gluon plasma, and that the mode is represented by a canonical operater $a(\mathbf{k},t)$. For simplisity, we deal with $a(\mathbf{k},t)$ as if it were a single boson or fermion operator. Then, assume that $a(\mathbf{k},t)$ obeys an operater-valued Langevin equation:

$$i\frac{\partial}{\partial t}a(\mathbf{k},t)=\int_0^t K(\mathbf{k},t-t')a(\mathbf{k},t')dt'+f(\mathbf{k},t), \qquad (4.1)$$

where $K(\mathbf{k},t)$ is a kernel function and $f(\mathbf{k},t)$ is a random source operator. It is plausible to assume that a Green's function $[\omega-E(\mathbf{k},\omega)]^{-1}$ of Eq.(4.1) has simple poles at $\omega=\varepsilon_j(\mathbf{k})-i\frac{1}{2}\gamma_j(\mathbf{k})$ $(\gamma_j(\mathbf{k})\geqq 0)$ on the lower-half of plane of complex ω, where $E(\mathbf{k},\omega)$ is a Fourier transform of $K(\mathbf{k},t)$. $\varepsilon_j(\mathbf{k})$ and $\gamma_j(\mathbf{k})$ are inputs of our theory.

We can have $a(\mathbf{k},t)$ satisfying the canonical commutation relation:

$$[a(\mathbf{k},t),a\dagger(\mathbf{k}',t)]_{\pm}=\delta^3(\mathbf{k}-\mathbf{k}') \qquad \text{for all } t\geqq 0. \qquad (4.2)$$

Further, we can obtain the quantum fluctuation-dissipation theorem, assuming a thermal average satisfied Kubo-Martin-Schwinger conditon. This theorem indicates the present stochastic process is not Markoffian.[27]

Using the above operator, $a(\mathbf{k},t)$ and $a^{\dagger}(\mathbf{k},t)$, we can derive formulas of thermodynamical quantities and transport coefficients written in terms of $\varepsilon_j(\mathbf{k})$ and $\gamma_j(\mathbf{k})$. Giving simple models to inputs $\varepsilon_j(\mathbf{k})$ and $\gamma_j(\mathbf{k})$, we can obtain phase transition-like behaviors to the temperature dependence of thermodynamical quantities. Using the above quantities, we solve numerically equation of a 1+1 dimensional viscous fluid with zero baryon chemical potential:

$$\frac{dT}{d\tau}=\left(\frac{d\varepsilon}{dT}\right)^{-1}\left[-(\varepsilon+P)/\tau+\left(\frac{2}{3}\eta_{(s)}+\eta_{(v)}\right)/\tau^{2}\right]. \tag{4.3}$$

We have found that the life time of quark-gluon phase gets long by viscosity and transition to hadron phase is late by phase trasition.[28]

5. Summary

We have discussed the relativistic hydrodynamical model of quark-gluon plasma as one of the phenomenology, and have proposed a transport theory based on an operator field Langevin equation which mediates between the hydrodynamical model and QCD. We have derived temperature dependences of thermodynamical quantities. Using these results, we have solved hydrodynamical equation numerically, and have discussed approach to phase transition point.

Acknowledgment

The auther would like to express his sincere thanks to

Professor M. Namiki and Drs. S. Daté and S. Muroya for collaborations and to Professor M. Namiki for his useful advices.

References

[1] Relativistic Hydrodynamics

1. S. R. de Groot, W. A. van Leeuwen and Ch. G. van Weert, Relativistic Kinetic Theory (North Holland, Amsterdam, 1980). (Eckart's Method)
2. C. Eckart, Phys. Rev. 58 (1944), 919.
3. G. A. Kluitenberg, S. R. de Groot and P. Mazur, Physica 19 (1953), 689, 1079.
   (Landau-Lifshitz's Method)
4. L. D. Landau and E. M. Lifshitz, Fluid Mechanics (Pergamon Press, London, 1959).
5. C. Møller, Theory of Relativity (Oxford University Press, Oxford, 1952).

[2] Landau's Hydrodynamical Model

6. L. D. Landau, Izv. Akad. Nauk. S.S.S.R. 17 (1953), 51.
7. S. Z. Belen'kij and L. D. Landau, Usp. Phys. Nauk 56 (1955), 309; Nuovo Cim. Suppl. 3 (1956), 3.

[3] Bjorken's Scaling Hydrodynamical Model

8. J. D. Bjorken, Phys. Rev. D27 (1983), 140.
9. M. Gyulassy and T. Matsui, Phys. Rev. D29 (1984), 419.
10. J. Cleymans, R. V. Gavai and E. Suhonen, Phys. Rep. 130

(1986), 218.

[4*] Cylinderical Scaling Hydrodynamical Model

11. G. Baym, B. Friman, J.-P. Blaizot, M. Soyeur and W. Czyż, Nucl. Phys. A407 (1983), 541.
12. A. Białas and W. Czyż, Acta Phys. Pol. B15 (1984), 229.
13. H. van Gersdorff, L. McLerran, M. Kataja and P. Ruuskanen, Phys. Rev. D34 (1986), 794, 2755.
14. S. Kagiyama, A. Nakamura and A. Minaka, Prog. Theor. Phys. 76 (1986), 118.

*We do not enter this topic in this talk.

[5] Field Theoretical Approach to The Hydrodynamical Model

15. M. Namiki and C. Iso, Prog. Theor. Phys. 18 (1957), 591.
16. H. Ezawa, Y. Tomozawa, and H. Umezawa, Nuovo Cim. 5 (1957), 810.
17. C. Iso, K. Mori and M. Namiki, Prog. Theor. Phys. 22 (1959), 403.

[6] Transport Theory Based on The Boltzmann Equation

18. S. R. de Groot, W. A. van Leeuwen and Ch. van Weert, in ref. 1.

(Quark-Gluon Plasma)

19. U. Heintz, Phys. Rev. Lett. 51 (1983), 351; Ann. Phys. 161 (1985), 48; 165 (1986), 148.
20. A. Hosoya and K. Kajantie, Nucl. Phys. B250 (1985), 666.
21. P. Danielewicz and M. Gyulassy, Phys. Rev. D31 (1985), 53.

22. S. Gavin, Nucl. Phys. A435 (1986), 826.

[7*] Transport Theory Based on The Wigner Operator

23. S. R. de Groot, W. A. van Leeuwen and Ch. G. van Weert, in ref. 1.

24. P. Carruthers and F. Zachariasen, Phys. Rev. D13 (1976), 950 (Quark-Gluon Plasma)

25. U. Heintz, in ref. 6.

26. H. Th. Elze, M. Gyulassy and D. Vasak, Nucl. Phys. B276 (1986), 706; Phys. Lett. 177B (1986), 402.

*We do not enter this topic in this talk.

[8] Transport Theory Based on The Quantum Langevin Equation

27. M. Mizutani, S. Muroya and M. Namiki, to be published in Phys. Rev. D.

28. S. Daté, M. Mizutani, S. Muroya and M. Namiki, in preparation.

Search for Quark Gluon Plasma at the CERN SPS

H.En'yo
CERN, Geneva, Switzerland

ABSTRACT

The experimental results from 200 GeV/N and 60 GeV/N oxygen nucleus interactions measured in the CERN SPS experiment are reviewed. I discuss these results attempting to figure out how close we are to the detection of a phase transition of nuclear matter.

1 INTRODUCTION

The aim of this manuscript is to review the experimental results from the CERN SPS ion projects. In 1986 200 GeV/N oxygen ions have been accelerated in the CERN SPS, in 1987 sulphur ions have been and lead ions are planned for 1991. Recently the experimental results obtained with oxygen beams have become available from several experimental groups. I am trying to find out what we have learned through the results and which direction our future research should take. Since reviewing all the detectors and their results is beyond my ability, I, a member of the HELIOS-NA34 collaboration, shall describe the experimental results through my eyes.

Figure 1 shows a plausible phase diagram of nuclear matter. By bombarding nuclei with high energy beams, we hope to get high enough an energy density to reach the quark deconfined state known as "Quark Gluon Plasma (QGP)", but it is natural to believe that we have a partially deconfined state ("mixed phase") along the dynamical path.

1.1 Keys to the phase transition

Nobody knows precisely at which energy density the phase actually changes, but there are theoretical predictions [1]. According to theorists, QGP may occur at about 2.5 GeV/fm^3. The energy density can be linked to experimental observable. The relation between energy density (ε) and transverse energy (E_t) has been

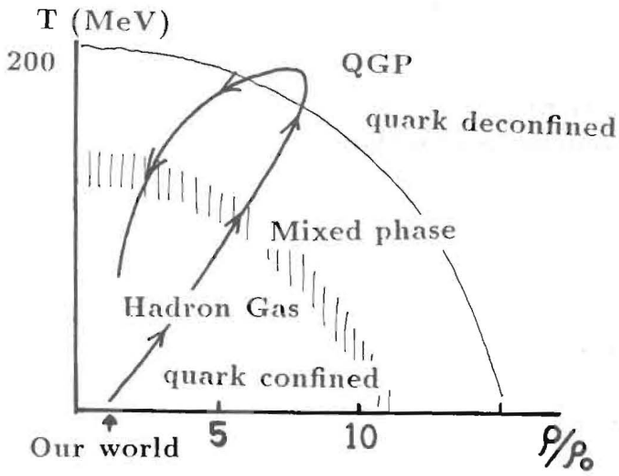

Figure 1: Phase diagram of nuclear matter. The line indicates a possible dynamical path in a collision.

derived by Bjorken [3]:

$$\varepsilon = \frac{1}{\pi(r_0 A^{1/3})^2} \frac{dE_t}{d\eta} \frac{1}{\tau_0} \tag{1}$$

where $r_0 A^{1/3}$ is the nuclear radius, $dE_t/d\eta$ the transverse energy per unit of pseudo rapidity and τ_0 the formation time of the high energy density state. This formula tells us that we can select a high energy density state experimentally by measuring E_t, even though one must be careful when applying this formula directly to estimate energy densities [1].

Once the phase changes, an increase of temperature (average p_t rises) has been expected. Already a long time ago a striking result (Fig. 2) has been reported by a cosmic-ray emulsion experiment (the JACEE collaboration) [4]. They found that the average p_t tends to increase when the estimated energy density exceeds 2-3 GeV/fm^3. If we apply formula 1 the corresponding energy density is 4-6 GeV/fm^3 (see footnote).

In the SPS the NA38 collaboration has measured J/ψ suppression which was predicted by Matsui and Satz [2] as a QGP candidate signal. The results are reviewed in this manuscript.

The study of elementary process may already have revealed the mixed phase. Recently the AFS collaboration at the ISR reported their results for single electron and electron pair production in proton-proton collisions at $\sqrt{s} = 63\ GeV$ [6]. They found an excess of electrons over their known sources in the low p_t region

[1]There seems to be confusion of a factor 2 in the energy density estimation between emulsion groups and CERN group. Here I stick to formula 1.

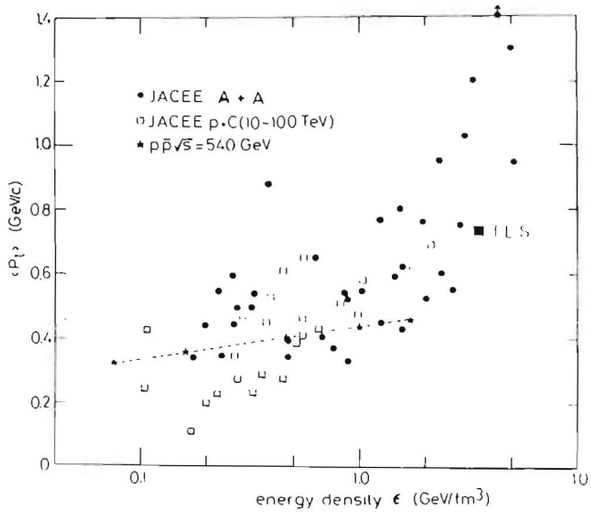

Figure 2: Scatter plot of estimated energy density and average p_t of each cosmic-ray event (from Ref. [4])

($< 500 MeV/c$). This excess is proportional to the square of the pion multiplicity, which can be understood by assuming electron production from the mixed phase [6]. It has been suggested [7] that the low p_t photon excess found in 70 GeV K^+-p interactions [8] could have the same origin as this electron excess.

As a last point I would like to mention what we can expect from the SPS ion projects. The energy density which can be achieved with the SPS, can be estimated as follows. Let me take a 200 GeV/N oxygen nucleus hitting the centre of a tungsten target nucleus and interacting with 50 nucleons at rest. This leads to $\gamma_{cm} = 5.8$, providing 7.0 GeV/fm^3, which is certainly higher than the theoretical estimate of 2.5 GeV/fm^3 for the transition energy density. If this high energy density stays long enough to ensure thermalization, we should see a new phase.

2 THE EXPERIMENTS

In the SPS ion project, six counter-experiments and several emulsion experiments have been participating. The counter experiments are listed in Table 1.

Details of the experiments can be found elsewhere [9]; here I discuss only four big experiments, NA34, NA35, NA38 and WA80, whose results are reviewed in this manuscript.

HELIOS (NA34) is characterized by full η-coverage ($0 < \eta < 6$) of calorimeters [2], U/scintillator calorimeters in the backward region ($-0.1 < \eta < 2.2$) and U/liq.Ar calorimeter in the forward region. The mid rapidity region is covered by silicon detectors to measure multiplicities. Muons in the forward region are measured in full azimuth, but hadron particle identification is limited to the small acceptance.

[2]Beam rapidity is 6 for 200GeV/N ions.

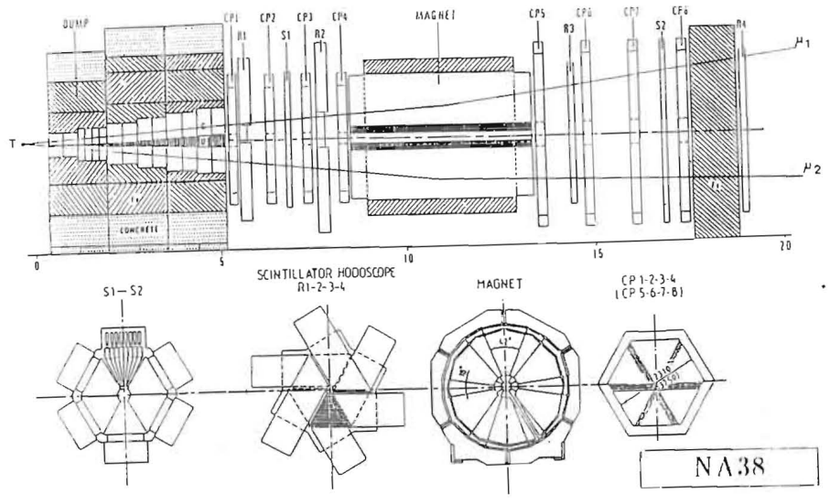

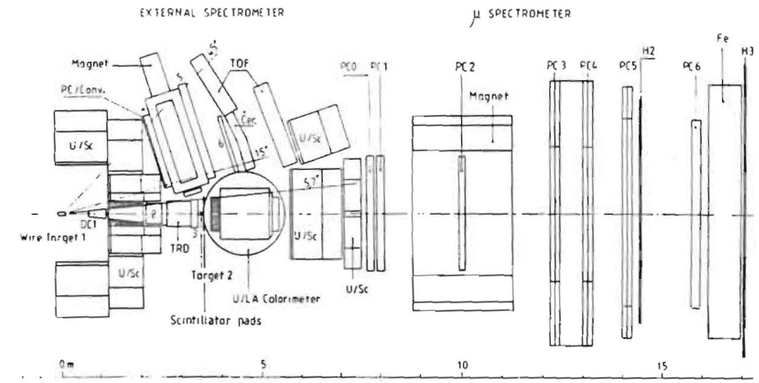

HELIOS setup

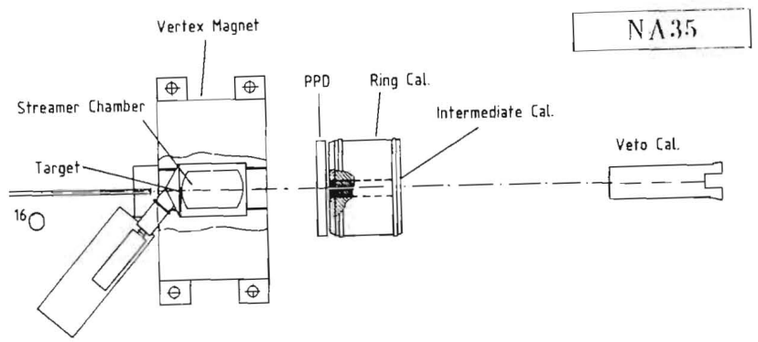

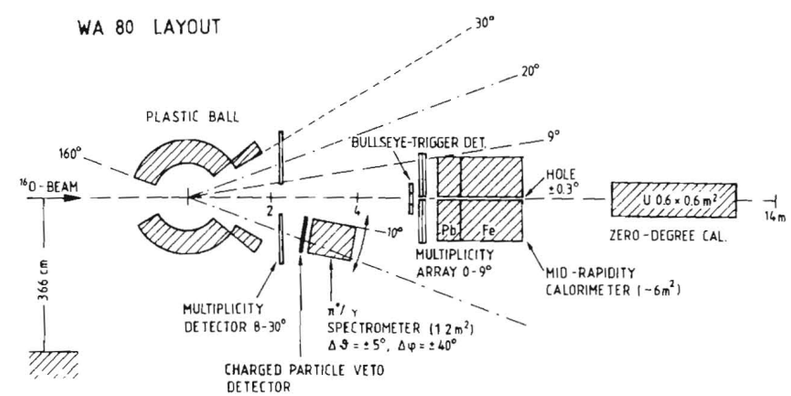

Figure 3: The detector setups

Experiment	characteristics	spokesman	Collab.
NA34	HELIOS, 4πCal. lepton hadron	H.J.Specht	130
NA35	Streamer chamber	R.Stock	66
NA36	EHS+TPC Strange-Baryons	C.R.Gruhn	54
NA38	NA10 $\mu\mu$spectrometer (J/ψ)	L.Kluberg	47
WA80	Plastic-ball, 4πmultiplicity, photon	H.H.Gutbrod	37
WA85	Ωspectrometer, Strange particles,	E.Quercigh	39

Table 1: SPS ion experiments (counter exp. only

WA80 covers full η with multiplicity measurements by the plastic-ball and streamer tubes, which give information complimentary to E_t. The calorimeter covers the mid rapidity region and the zero degree calorimeter vetos the projectile fragmentation region. The plastic ball performs π/p/d identification in the target region in full azimuth. Photons are measured by a single arm photon detector consisting of lead glass counters.

NA35 has a calorimeter setup similar to WA80, and its heart is the streamer chamber covering wide rapidity range. Momentum is measured with 1% precision.

NA38 is the dedicated experiment for J/ψ production. Beside a μ-spectrometer they have an EM calorimeter in the central region (measuring mainly π^0 energy). They can run with very high beam intensities ($> 10^7$).

2.1 Triggers

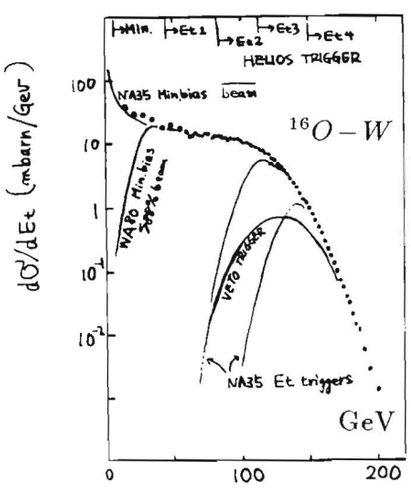

Figure 4: Rough sketch for the trigger conditions for each experiments overdrown on the HELIOS E_t spectrum

Figure 4 gives you an idea of trigger biases of each experiments. Approximate trigger setting are superimposed on the HELIOS E_t spectrum which will be ex-

plained in the next section. HELIOS has several E_t thresholds and a minimum bias trigger determined by a silicon pad detector. WA80 selects the "centrality" by the energy deposition in the "Zero degree calorimeter". NA35 uses their zero degree calorimeter either for a minimum bias trigger (reject beam) or a veto trigger, and the EM part of the mid-rapidity calorimeter is used to select "central events".

3 EXPERIMENTAL RESULTS AND INTERPRETATIONS

I describe the results and try to interpret them. More detailed information can be found in Ref. [12,13,14,15].

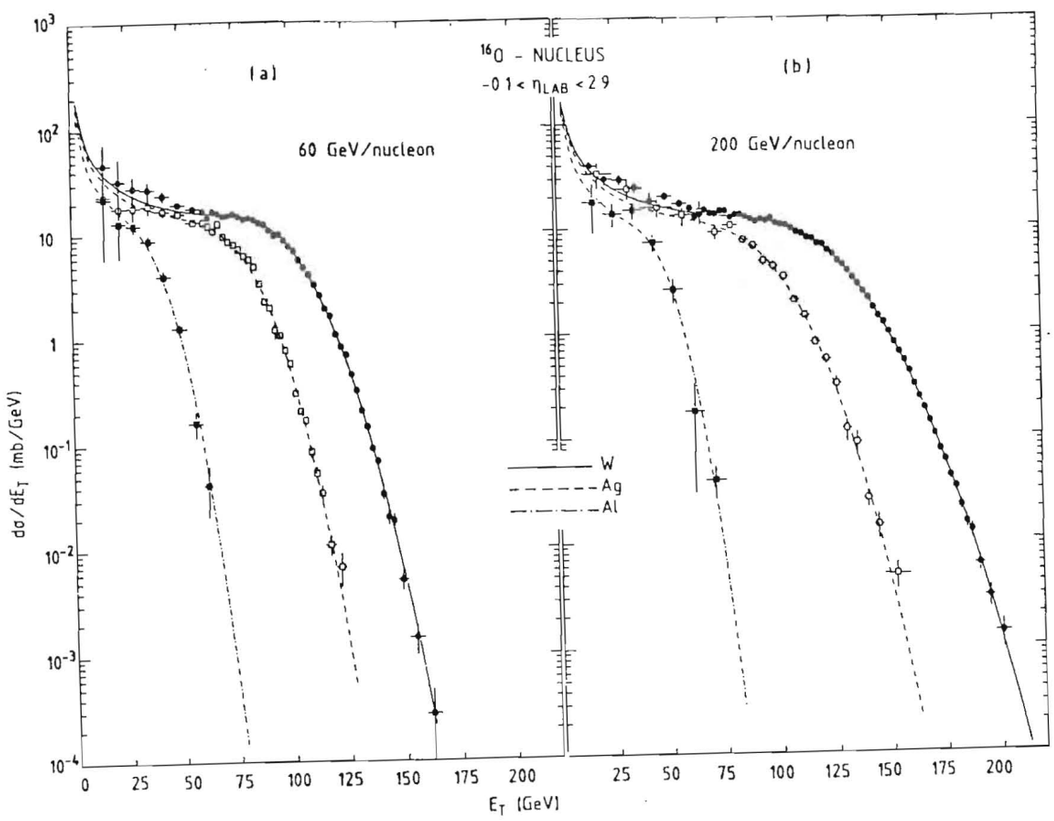

Figure 5: $d\sigma/dE_t$ distribution for $-0.1 < \eta < 2.9$ in 60 and 200 GeV/N $^{16}O \rightarrow W, Ag, Al$ reactions. The lines are the results of the geometrical parametrization (see text). HELIOS

3.1 E_t spectrum

Figure 5 shows the E_t distributions in the pseudo-rapidity range $-0.1 < \eta < 2.9$ for 60 and 200 GeV/N ^{16}O nucleus interactions on W,Ag and Al targets.

We first try to understand the spectra on the basis of a geometrical picture. We assume the number of participant nucleons in a collision at a given impact parameter b to be described by:

$$N(b) = \sigma_0 \int \rho_1 \rho_2 ds \tag{2}$$

where the ρ_i are the nuclear density distributions including nuclear deformation and where σ_0 is the p-p inelastic cross section (32mb). The integration is to be done over the overlap region of the two nuclei.

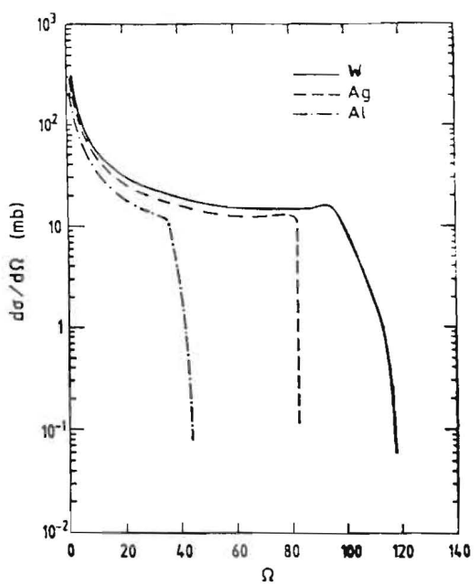

Figure 6: The geometrical cross section as a function of the number of collisions (see text).

Beam energy	60GeV/N			200GeV/N		
Target	Al	Ag	W	Al	Ag	W
$\varepsilon_0(GeV)$	1.02	0.95	0.98	1.26	1.14	1.19
w	1.99	2.20	1.75	1.05	2.64	2.53

Table 2: Results of the geometrical parametrization

Then the geometrical cross section can be described as a function of the impact parameter as well as the number of the participants as shown in Fig. 6; it's shape is quite similar to the E_t distribution, which imply the close relation of E_t and the impact parameter.

We parametrized the E_t distribution assuming that collisions at a given impact parameter, i.e. given N, give Gaussian distributed E_t with mean $E_t = N\varepsilon_0$ and variance $\sigma^2 = wN\varepsilon_0^2$, where ε_0, w are free parameters. This parametrization gives excellent fits as shown in Fig. 5. The parameters we obtained are listed in Table 2.

It should be noted that energy conservation and secondary cascading are not taken into account in this approach. However, the most important thing we have learned from this approach is that the E_t spectrum is in first order explained by pure geometry.

3.1.1 Monte Carlo Generator

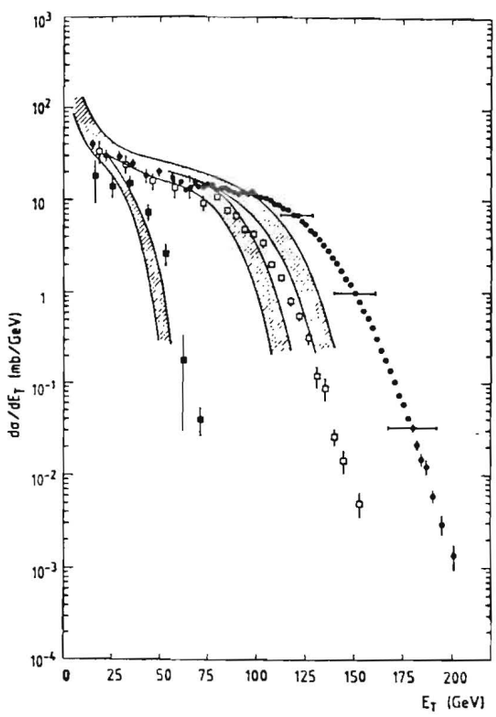

Figure 7: The comparison of the IRIS prediction (shaded bands) with the data. The horizontal error bar indicates a systematic error on the E_t scale.

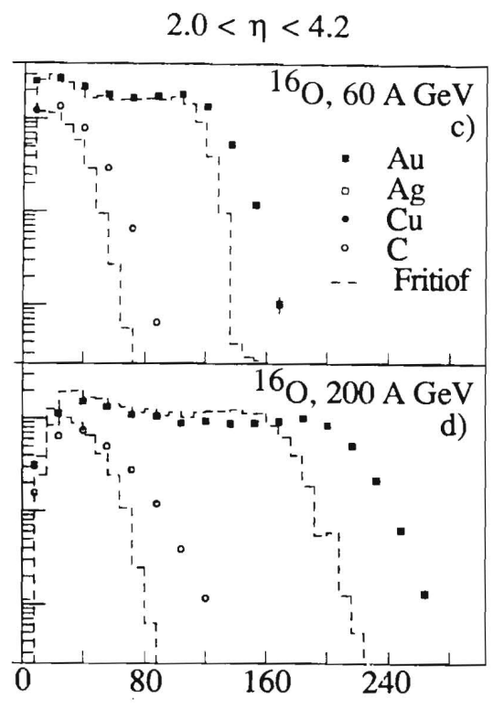

Figure 8: Charged particle multiplicity distributions for O^{16} induced reactions at 60 GeV/N and 200 GeV/N together with the FRITIOF prediction. (WA80)

Another approach is comparing the data with results from a Monte Carlo particle generator. In the CERN SPS ion experiments, majorly two different Monte Carlo programs are used. One of them is IRIS [16] based on the Dual Parton Model

and the other is FRITIOF [18] based on the LUND string model. Both of them have three basic assumptions:

- strings are formed independently,
- string decays independently and
- final state interaction of secondary is negligible.

The LUND fragmentation scheme [17] is used to represent the decays. The parameters for fragmantations are adjusted for p-p and e^+e^- data. By taking the known nuclear density profile, the generators are used for the nucleus-nucleus interactions without new additional free parameters being introduced.

The IRIS prediction is shown in Fig. 7 together with the HELIOS E_t spectrum. The global shape is reproduced fairly well, but IRIS underestimates the high E_t tail.

A similar discrepancy is found in the multiplicity distribution. WA80 measured multiplicity distributions(Fig. [14]) and compared them to the FRITIOF prediction in the pseudo-rapidity range $2.0 < \eta < 4.2$ where the contribution from target fragments should be negligible.

These discrepancies from the models tell us that the nucleus-nucleus interaction is not a superposition of nucleon-nucleon interactions. One could say that the secondary cascading (or final state interactions) must be important, which is neglected in the models. There are some reports saying that by putting secondary cascading into the model, the agreements to the data becomes better.

3.2 Stopping of projectile and baryon density

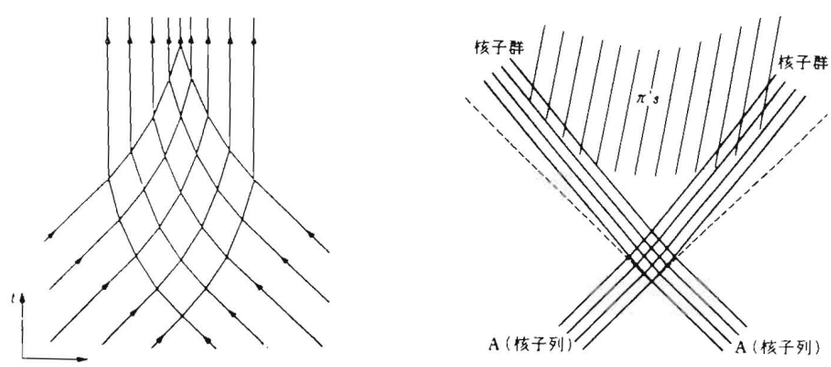

Figure 9: Sketch of the space-time evolution for the stopping of incident baryons in the centre-of-mass frame. (a) shows ideal complete stopping, (b) is a plausible picture in the SPS region.
(from Ref. [20])

The width of the E_t distributions increases with the mass of the target nuclei. This tendency is not observed at lower energies as reported by BNL-AGS experiments [19].

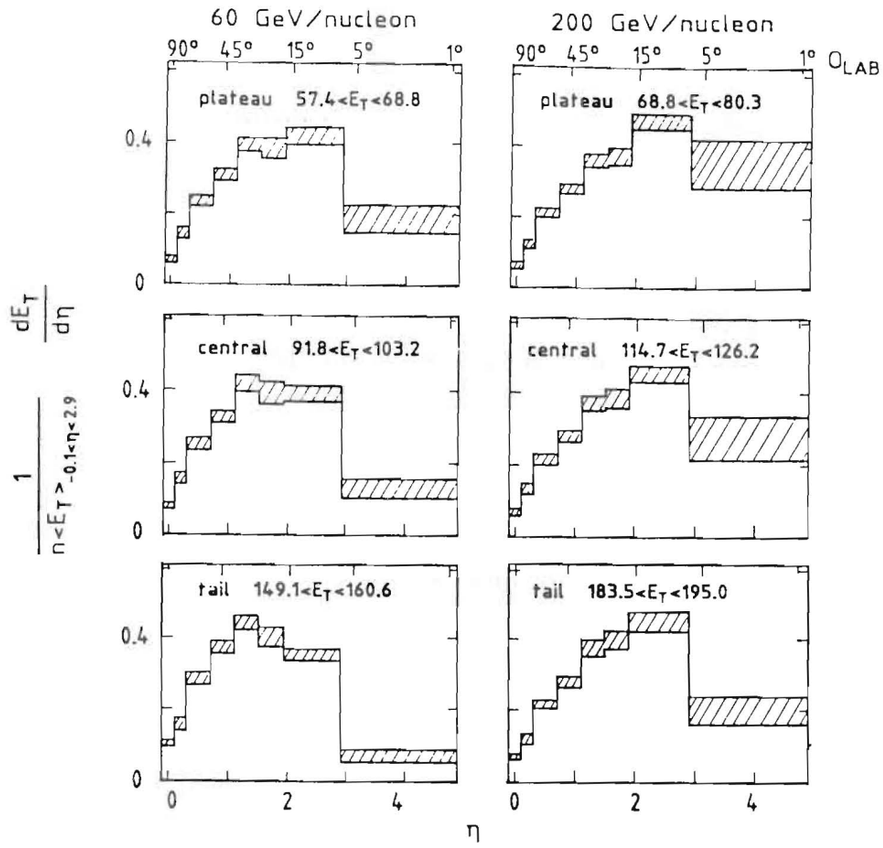

Figure 10: The distribution of $dE_t/d\eta$ as a function of η, for $^{16}O-W$ interaction in three selected E_t windows for 60 and 200 GeV/N beam energy (from Ref.[12]

This fact can be related to the stopping power of nuclei. The situation of ideal stopping is illustrated in Fig. 9a). In a stopping process most participant nucleons loose more than half their rapidity in the centre-of-mass frame. Fuki and Sumiyoshi have estimated the stopping power of a nucleus in the framework of the multi-chain model [20]. They conclude that a full stopping process only occurs when the beam energy is less than 15-30 GeV/N for nuclei as big as Uranium.

This energy corresponds to the AGS region. On the other hand, in the SPS energy region which is clearly above the stopping limit, the situation must be as shown in Fig. 9b) where all participant nucleons more or less punch through and dissipate energy by producing many pions.

This interpretation is confirmed by Fig. 10, where $dE_t/d\eta$ distributions are

shown for three different E_t bins for 60 and 200 GeV/N incident beam energy. In the 200 GeV/N reaction, the peak of the distribution stays at a constant value of about $\eta = 2.4$, but in the 60 GeV/N case the peak moves backwards when high E_t (central) events are selected. Hence, an energy of 60 GeV/N or less is more suitable to obtain a high baryon density. At 200 GeV, however, we could expect a higher energy density. Note that the highest $dE_t/d\eta$ observed, corresponds to 90 GeV per unit of rapidity and 3.5 Gev/fm^3 of energy density by Eq. 1.

3.3 Particle spectra

Figure 11 shows negative particle spectra measured by the HELIOS External Spectrometer [12]. The shapes are identical for p-W and O-W interactions within statistical errors, indicating that an oxygen interaction is just a superposition of proton-nucleus interactions. The broken line in Fig. 11 is the prediction of a pion generator which parametrizes the ISR π^- data and the high p_t nuclear enhancement measured by Cronin *etal.* [21]. The shape of the spectrum is very well reproduced except in the low p_t region.

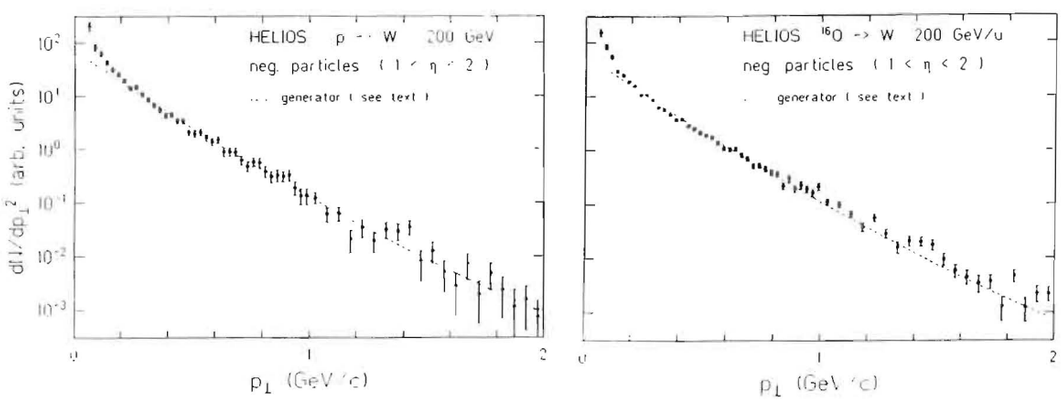

Figure 11: Negative particle p_t spectra (mainly π^-) in the range $1 < \eta < 2$ for p-W and O-W interactions.

The E_t dependence of the average p_t/particle is shown in Fig. 12. Complimentary information is the average $E_t/(charged\ particle)$ (Fig. 13) obtained by the calorimeter E_t measurement together with the multiplicity measurement in the silicon detectors. NA35 and WA80 did a similar analysis. None of the experiments found a rise. Thus we can conclude that no rise of the average p_t has been observed in 200 GeV/N oxygen interactions.

The photon spectra are shown in Fig. 14. Here again the spectra are identical for p-W and O-W reactions. The shape of the spectra is well reproduced by a Monte Carlo simulation assuming the γ's are coming from neutral meson decays [12].

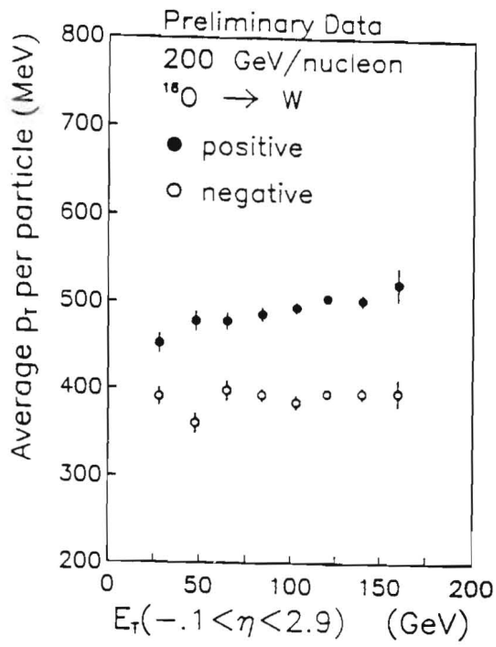

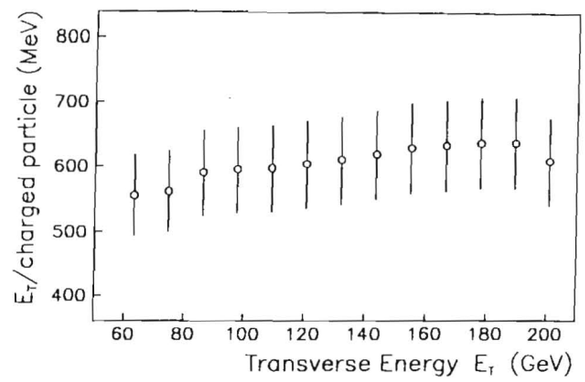

Figure 12: Left: Average p_t per particle $(1 < \eta < 2)$ as a function of E_t.

Figure 13: Up: The E_t/charged particle as a function of E_t.(HELIOS)

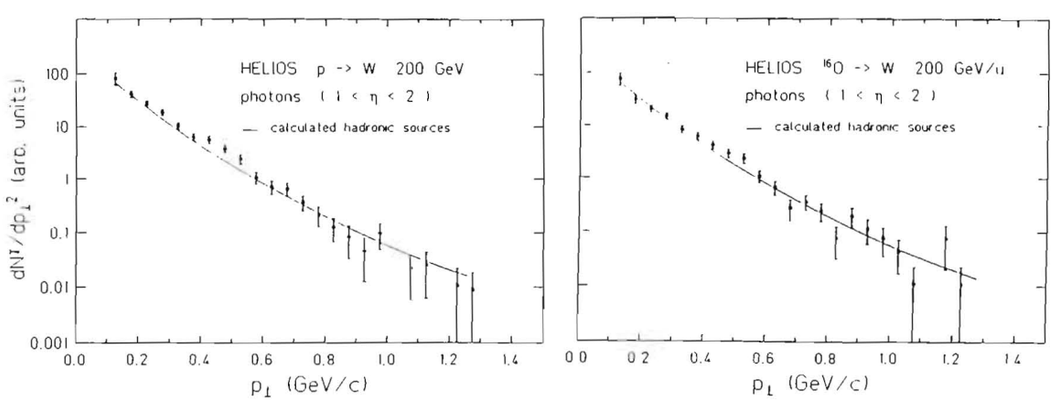

Figure 14: Photon p_t spectra in $1 < \eta < 2$.

3.3.1 Low p_t excess of the negative particle spectrum

A key to the low p_t excess was given by the NA35 streamer chamber results [13]. NA35 compare negative particle p_t spectra of p-p interactions to p-Au and O-Au interactions in the central rapidity region. According to their analysis, the p_t spectrum can be reproduced assuming one thermodynamical source in the p-p interaction, but in the case of O-Au and p-Au two thermal sources have to be introduced to reproduce the spectrum as shown in Fig. 15.

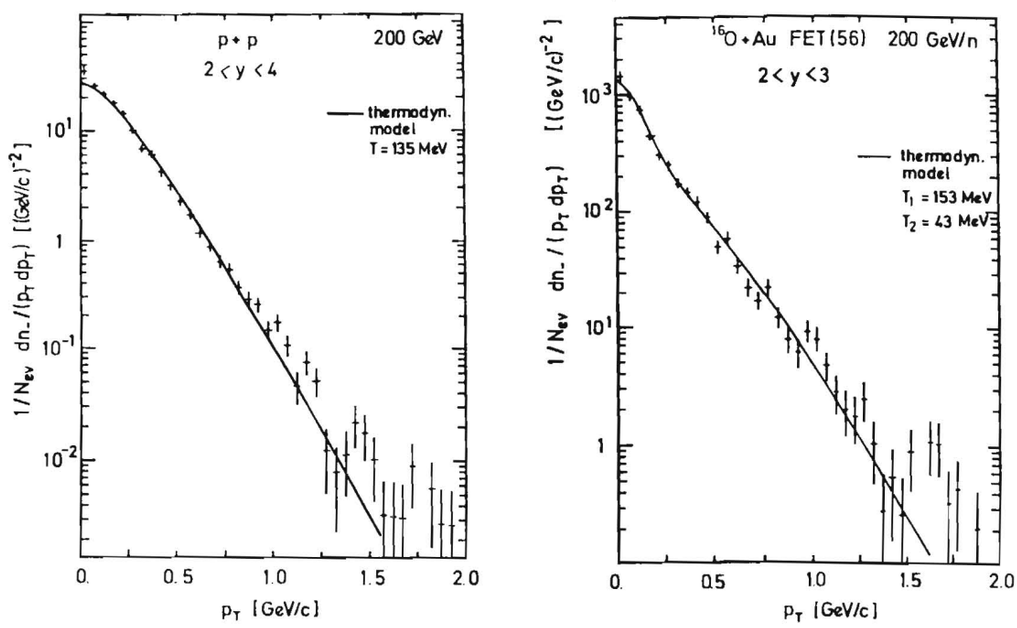

Figure 15: Transverse momentum distributions for minimum bias p+p interactions and central ^{16}O+Au interactions at 200 GeV/N. Also shown are thermal model fits.

This type of two-component spectra has also been observed the lower energy p-A studies such as KEK-E90 who measured 4 GeV p-A interactions. The spectra of protons and pions are well reproduced by the "two moving source model" which amounts to assuming two thermal sources [10]. The temperatures of the two sources are similar to those that are observed in 200GeV/N oxygen interactions. The lower energy component is only visible in the high multiplicity events. This is analogous to the difference between 200 GeV p+p and p+A interactions. In the few GeV region, pions are predominantly produced via isobars (Δ N*), which, I presume, could be one explanation for this lower component of the p_t spectra.

There have been observations of low p_t in the central region of ISR p-p and $\alpha - \alpha$ [11]. They observed a low p_t excess in the high multiplicity events, a shape

similar to that observed in the ion case. However, the central region at the ISR energy range isobars cannot play an important role.

There seems to be no clear explanation for the low p_t excess yet. The angular distribution for this low p_t excess, which will be available in the near future, is hoped to give a clue.

3.4 Interaction volume

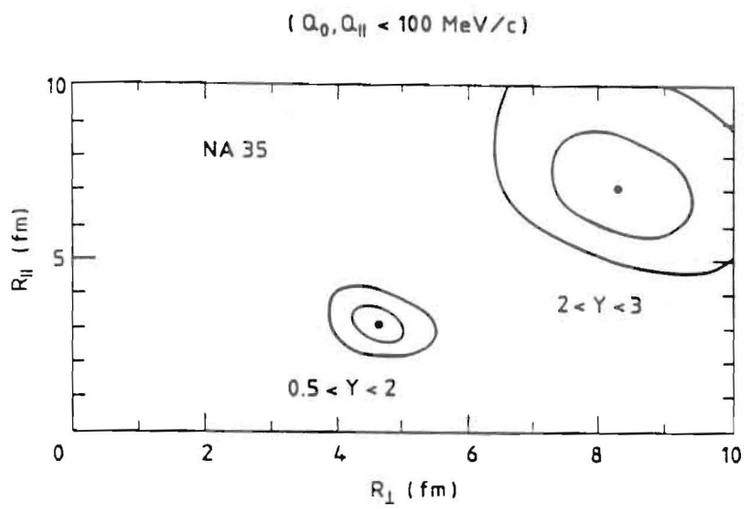

Figure 16: The transverse and longitudinal radii from negative particle HBT correlation for two different rapidity intervals. (NA35)

Interesting measurements to find the interaction volume, have been done with the NA35 streamer chamber using two pion interferometry. In their central collision data sample, they study negative-particle HBT correlations. For the negative particles, which are produced in the backward region ($0.5 < Y < 2$), they found a radius of about 3 fm, but for the central rapidity region ($2 < Y < 3$) 6-8 fm is observed, which is much bigger than the size of the projectile (Fig. 16). Their interpretation is that this big radius corresponds to the stage when rescattering of pions stops (freeze out). This implies that secondary scattering is important and that thermalization has been achieved somewhere.

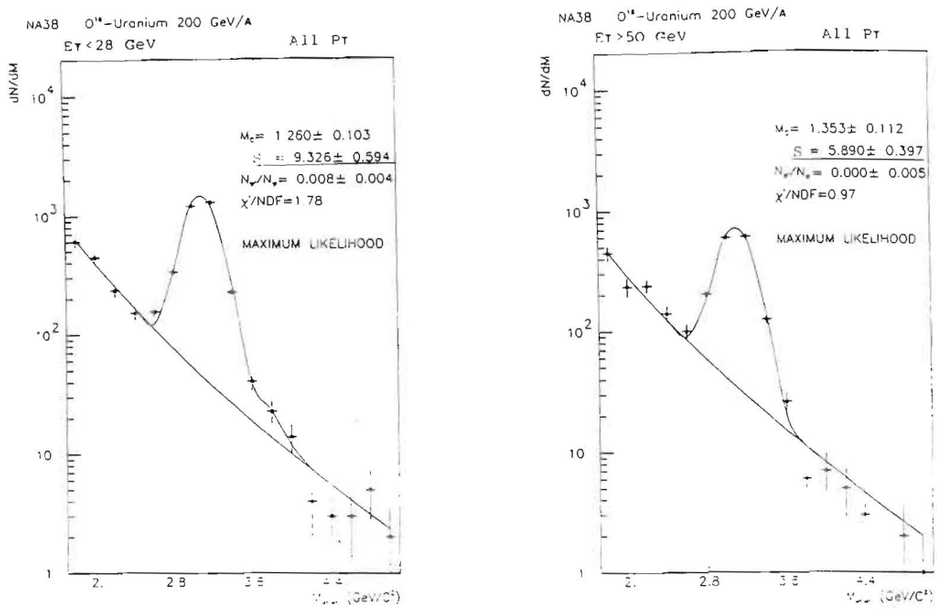

Figure 17: NA38, $J\psi$ spectrum for low E_t (left) and high E_t (right) events.

3.5 J/ψ suppression

The most exciting measurements have been done by the NA38 collaboration. Although many things remain to be confirmed, this signal could indicate the formation of Quark-Gluon Plasma.

The theoretical details can be found in Ref. [2]. The basic idea is that the J/ψ can only be produced when the density of the plasma is low enough since Debye screening forbids resonance formation. An estimate of the critical temperature for J/ψ production $T_{J/\psi}$ is 1.2-1.5 times T_c, the QGP critical temperature.

The finite size of the plasma plays a significant role In the real experimental situation. The lifetime of J/ψ competes with the lifetime of the plasma and the size of the plasma, e.g. it is easier for a high p_t J/ψ to leave the plasma than a low p_t one. Thus the time evolution of the density (or temperature) profile of the high density state determines the J/ψ suppression.

NA38 selects an event when the E_t measured with the EM calorimeter ($2<Y<4$) is more than 50 GeV (QGP is expected) and also when E_t is below 28 GeV (QGP is not expected). The ratio of the number of J/ψ to the continuum is smaller in the high E_t sample than in the low E_t sample [15](Fig. 17).

Fig. 18 shows the ratio of $N_{J/\psi}$(high E_t) to $N_{J/\psi}$(low E_t) as a function of the p_t of the di-muon system. This shows a clear suppression pattern. The same quantities

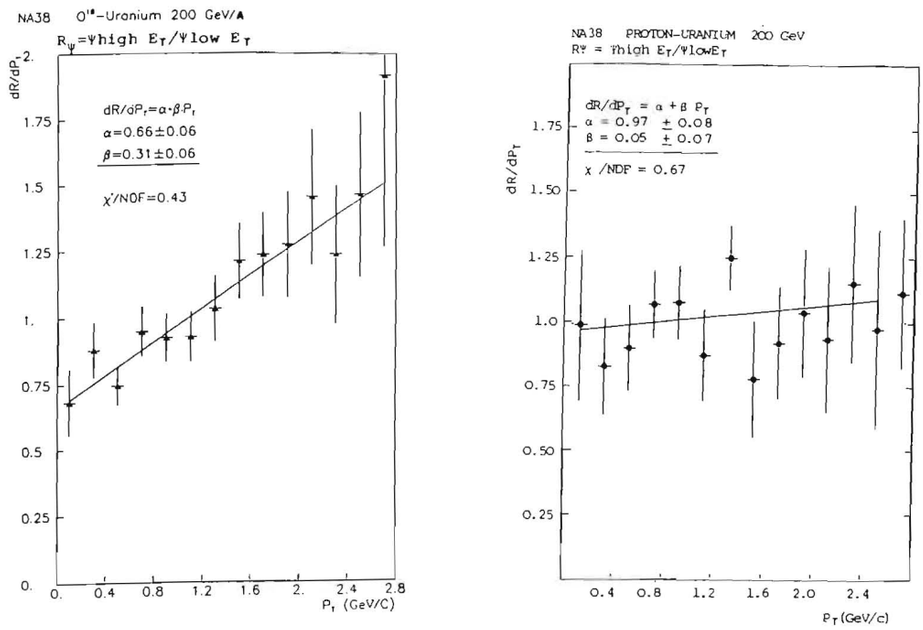

Figure 18: NA38, p_t dependence of J/psi suppression. (left:O+U, right:p+U)

for p-U interactions and for the continuum do not show any clear suppression. Thus this suppression is correlated to the bulk size of ion interactions.

Karsch *et al.* [22], assuming the formation of QGP, have parametrized the density profile and used it as an input for their theory. They have well reproduced this suppression pattern.

There are other approaches without assuming QGP [23]. Ftacnic *et al.* and Capella *et al.* have tried to explain the data by J/ψ disintegration in nuclear matter (or pion gas). For the moment the suppression cannot be fully understood by the disintegration mechanisms.

4 DISCUSSION

4.1 Summary of the experimental results

First of all, I summarize what we have learned from the results. The E_t distribution is mainly geometrical and reproducible by a Monte Carlo calculation based on p-p interactions. The particle distributions (hadronic probes) indicate that nucleus-nucleus interactions are superimposed proton-nucleus interactions. No increase of the average p_t/particle is observed. Thus, the results except the J/ψ suppression can be understood without assuming any phase transition.

To understand the situation better, we should recall an energy density estimate based on the data. With the Bjorken type estimate (Eq. 1) our observed maximum energy density is 3.5 GeV/fm^3, well above the predicted critical density of $2.5 GeV/fm^3$. Now we need to estimate the time evolution of the reaction to know how long this high energy density is maintained.

4.2 Time evolution of energy density

To understand the time evolution, the information of the initial energy density and the dynamics of the expansion are important. One objection against applying the Bjorken type estimate (Eq. 1) is the fact that the observed density of particles or E_t is, due to the expansion of the interaction volume, only indirect information of the initial stage. Gyulassy and Matsui made a calculation to connect the observed density to the initial density [24], assuming a QGP hydrodynamical model with one-dimensional expansion. Their results are shown in Fig. 19. The initial energy density corresponding to our $(dE_t/d\eta)_{max}$ is about 7 GeV/fm^3, which coincides nicely with the maximum energy density estimated for our beam energy in the first chapter ! This can be just a chance coincidence, but could indicate the possibility of QGP formation.

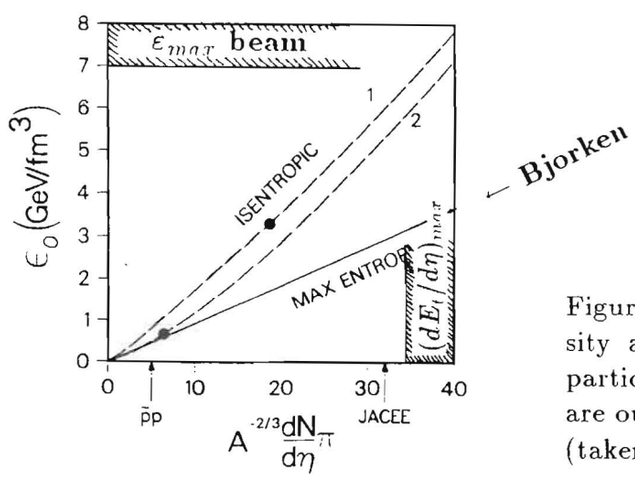

Figure 19: Initial energy density as a function of observed particle density. Hatched areas are our "maxima" (see text). (taken from Ref. [24])

If this assumption holds, one can plot the time evolution of the energy density. During the expansion, the product of the time and the entropy density is constant. By taking the Boltzmann equation, the energy density as a function of time is:

$$\varepsilon = \varepsilon_0(\tau_0/\tau)^{4/3} \tag{3}$$

where ε_0 is the initial energy density and τ_0 the formation time of the QGP. The situation will look like in Fig. 20. The vertical scale is determined from Fig. 19. The high energy density at which QGP can exist is kept only for about 1 fm/c. Then presumably the mixed phase starts until hadronization is finished.

During hadronization in the mixed phase, latent heat which is used to form a bag for a hadron can reduce the effective temperature observed via $< p_t >$ for example. The produced hadrons will be rescattered in the hadron gas phase. The NA35 two pion interferometry results indicate a "freezing out" (end of rescattering) size of 8 fm [13], which can be long enough to forget the initial information again. Thus it is not surprising that our hadron probes have not shown any spectacular behavior, even if QGP has been formed.

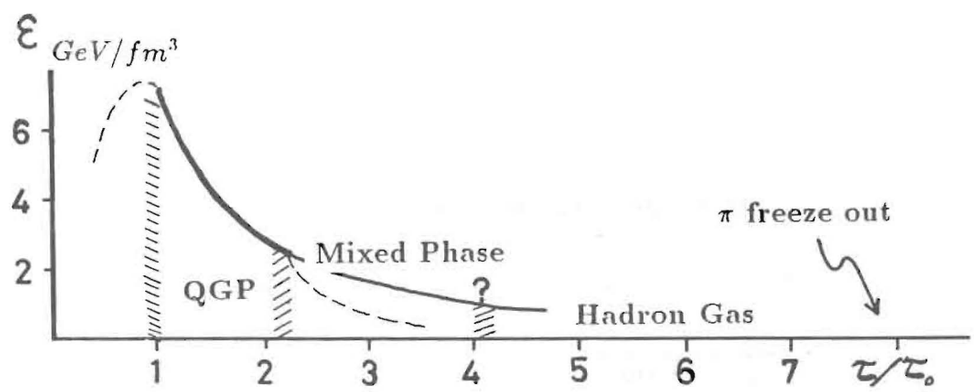

Figure 20: Time evolution of energy density (solid line) in the central rapidity region of central collisions. After the QGP phase the line should be incorrect. τ_0 can be about 1 fm/c.

I cannot claim that keeping a high energy density for about 1 fm/c is long enough to produce observable signals. At least, however, we can say that we need to study less interacting particles to detect any phase beyond the hadron gas phase. Unfortunately our photon probe is not yet overcoming the big π^0 background. The J/ψ is the only other less interacting particle we have at hand.

5 CONCLUSION

One can classify the results into two categories. The first is the set of results using hadronic probes (E_t, multiplicity, π spectra) which do not yet show a "QGP candidate" signal. However, the big interaction volume measured by NA35 is one surprise. The other is the data using less interacting probes of which we have only J/ψ at our disposal. The J/ψ suppression is a really interesting signal although we need a better understanding. By assuming a QGP formation succeeded by a long ($> 6fm/c$) "mixed phase" and/or a "hadron gas phase" for rescatterings, we get a natural explanation for all our observations.

6 Acknowledgement

The author is grateful to all the HELIOS collaborators. Especially the author owes to Prof. W.J.Willis, Dr. K.H.Dederichs and drs. R.J.Veenhof to polish up this manuscript. The author has been supported by the Japan Society for the Promotion of Science.

References

[1] See contribution by others to this workshop.

[2] T.Matsui and H.Satz, Phys. Lett. B178 (1987) 416.

[3] J.D.Bjorken, Phys. Rev. D27 (1983) 1409

[4] T.H.Burnett et al., Nucl. Phys. A447 (1985) 189.

[5] T.H.Burnett et al., Phys. Rev. Lett. 50 (1983) 2062.

[6] AFS collaboration. T.Åkesson et al., Phys. Lett. B 192 (1987) 463.
V. Hedberg, Thesis Univ. of LUND (1987).

[7] W.J.Willis, to appear in Proc. Uppsala conference (1987).

[8] P.V.Chliapnikov et al., Phys. Lett. 141B (1984) 276.

[9] Proposals to the SPSC, NA34: SPSC/84-43/P203, NA35: SPSC/85-36/M407, NA36: SPSC/85-70/M419, NA38: SPSC/85-20/P211, WA80: SPSC/85-35/M406, WA85: SPSC/85-35/M406.

[10] H.Enyo et al., Phys. Lett. 158B 1 (1985). H.Enyo, Thesis, Univ. of Tokyo (1985), UTPN-200.

[11] W.Bell et al., Z. Phys. C 27, 191-203 (1985).

[12] E_t: T.Åkesson et al., CERN-EP/87-16 submitted to Z. Phys. C.
p_t spectrum: H.W.Bartels, HELIOS collaboration, Contribution to the Nordkirchen conference '87, to appear in Z. Phys. C.

Multiplicity: J.Schukraft, HELIOS collaboration, Contribution to the Nordkirchen conference '87, to appear in Z. Phys. C.

[13] p_t *spectrum*: NA35 collaboration, GSI-88-07. Contribution to the Nordkirchen conference '87, to appear in Z. Phys. C.
Interferometry: T.J.Humanic, NA35 collaboration Contribution to the Nordkirchen conference '87, to appear in Z. Phys. C.

[14] R.Albrecht et al., WA80 collaboration, GSI-87-81, to appear in Phys. Lett. B. GSI-87-82, to appear Z. Phys. C.

[15] M.C.Abreu et al. NA38, CERN-EP/88-25, to appear in Z. Phys. C.

[16] J.P.Pansart, Nucl.Phys.A461,521 (1987). A.Capella and J.Tran Thanh Van, Phys. Lett. 93B, 146 (1980).

[17] B.Andersson, G.Gustafson and T.Sjöstrand, Z.Phys.C6,235(1980).

[18] B.Andersson et al., Nucl. Phys. B281 (1987) 289. B.Nilsson-Almquist et al., Lund Preprint LU-TP 86-14(1986).

[19] Y.Akiba, contribution to this workshop.

[20] M.Fuki and H.Sumiyoshi, Prog. Theor. Phys. 76, 879 (1986). H.Sumiyoshi, Butsurigagu-saizensen 18 (1987) Kyoritsu publishing Co. (in Japanese).

[21] J.W.CRONIN et al., Phys. Rev. D11 (1975)3105.

[22] F.Karsch and R.Petronzio, CERN-TH-4699/87.

[23] Capella et al. CERN-TH.4974/88. J.Ftacnic et al. internal repport from Dept. Theoretical Physics, Comenius Univ., Czechoslovakia.

[24] M.Gyulassy and T.Matsui, Phys. Rev. D29 (1984) 419.

Heavy Ion Experiments at BNL AGS
by Y.Akiba (University of Tokyo)

Introduction

In this talk, I will briefly report the experimental results from BNL AGS heavy ion experiments. The AGS provides heavy ion beam with 14.5 GeV/c per nucleon. So far, oxygen and silicon beams are accelerated.

There are three major counter experiments approved at the AGS, namely E802, E810, and E814. The primary purposes of E802 are (i) to measure the particle spectra from the heavy ion reaction with a good particle identification, and to study the correlation of these spectra with measures of centrality such as multiplicity or energy flow. E810 uses a visual tracking detector to study the production of V-particles in H.I.Collisions. E814 studies the projectile fragmentation in ultra-forward region as well as transverse energy flow around the target. I myself belong to E802 experiment, so my talk is mainly about the results from E802.

So far, we had three periods of beam time of heavy ions. In November of 1986, a subset of E802 measured neutral energy flow and multiplicity from O + A reactions(1). In April 1987, we had Si beam with 10 GeV/c per nucleon and 14.5 GeV/c per nucleon. In this beam time, a part of E814 measured transverse energy from Si + A collisions at 10 GeV/c(2), and E802 measured Si + A reactions at 14.5 GeV/c(3,4). In November and December 1987, we had 14.5 GeV/c Si beam, and E802 accumulated data more than ten times as much as that in the April run. However, the data from this run is now being analysed, so I will not discuss about the new data. Though most of the data in my talk were already reported in the last Quark Matter Conference(5), they should be considered as preliminary.

Neutral Energy Flow in mid rapidity

I start with measurements of neutral energy from O + A collisions(1) by E802. The experimental setup consisted of 96 lead glass counters (PBGL) arranged in 10 × 10 square array with 2 × 2 block hole in the center for the beam pass through. The acceptance of the detector in the nucleon-nucleon c.m.s were about $-0.5 < \eta^* < 0.7$.

The PBGL measures the amount of Cerenkov light from the electromagnetic shower caused by high energy photons. A fast charged hadron ($\beta > 0.8$) also produces a signal in PBGL, approximately equivalent to 0.5 GeV photons. Therefore, the observed energy, E^0_{TOT} is approximately expressed as

$$E^0_{TOT} = \Sigma E_{\pi^0,\eta} + 0.5GeV \times n_{rel},$$

where n_{rel} is the number of relativistic particles. The value of E^0_{TOT} is about 50 % of total hadronic energy in the detector.

The spectra of energy observed in the PBGL is shown in Fig.1 for O+Au, O+Cu, and O+Mylar reactions. Neutral energy spectrum from h^+(protons)+Au at 14.5 GeV/c is also plotted with a scale down of factor 20. The spectrum for O+Au shows a broad plateau, a bump centered at 40 GeV, and then a sharp drop-off. O+Cu data shows similar feature. These spectra shapes are easily understood from the geometry of the reaction. In fact, the observed O+A spectrum is quantitatively reproduced by adding 16 geometry weighted convolutions of p+Au spectra as

$$d\sigma/dE^0 \sim \Sigma w_n f^{(n)}(E^0),$$

where

$d\sigma/dE^0$ is the differential energy spectra for O+Au,

w_n id the probability for n nucleons in the oxygen being struck in the collision, and

$f^{(n)}$ is the n-fold convolutions of the p+Au energy spectrum.

In Fig.2, this calculation is compared with experimental O+Au spectrum. The calculation reproduces the data reasonably well.

An interesting feature of this data is that the edge of the E^0_{TOT} distribution for O+Au and O+Cu is almost equivalent. The ratio of the cross sections at the high E^0_{TOT} tail for O+Au and O+Cu is about 6. This ratio is explained as the ratio of the cross sections for complete overlap of the projectile and the target ($(R(Au)-R(O))/(R(Cu)-R(O)))^2$), indicating that the energy produced in the mid-rapidity is almost the same for central O+Au and for central O+Cu collisions.

Transverse Energy distribution

Similar results are obtained by E814 for Si+A collision at 10 GeV/c per nucleon[2]. The experimental setup of E814 consisted of a a square shaped hadron calorimeter and an array of NaI(Tl) detectors in front of it. The segmentation of the hadron calorimeter and the NaI(Tl) detector was 12 × 12 and 20 × 30, respectively. The acceptance of the detector covered $1.5 < \eta < 2.5$, corresponding to the forward hemisphere in N-N c.m.s.

The transverse energy spectra for Si+Pb, Si+Cu, and Si+Al are shown in Fig.3. The tail of the transverse energy for Si+Pb and Si+Cu reactions almost coincide. This result is consistent with the data of E802 PBGL detector for O+A collisions. However, this

situation is quite different from what is observed in the CERN SPS energy. The data of E_T at CERN energy show that more and more transverse energy is produced as the target mass is increased.

Multiplicity Distribution

The charged particle multiplicity from O+A and Si+A collisions measured by the TMA detector of E802 are shown in Fig. 4(a) and (b), respectively. The TMA is an array of proportional counters with cathode pads readout, and is sensitive to all charged particles with a range greater than that of 30 MeV protons. The acceptance of the detector is $1.1 < \eta < 3.0$ for O+A data, and is $-1. < \eta < 3.0$ for Si+A data.

The overall shapes of the spectra is very similar to that of E^0_{TOT} or E_T. Note however that the multiplicity distributions show larger target mass dependences. For example, the tail of multiplicity distribution for O+Au well extends to that of O+Cu. Also, the difference between Si+Al and Si+Au is much larger than that for E_T reported by E814. I think this difference between multiplicity and E^0_{TOT} or E_T is due to slow protons produced in the reaction. Though these protons are counted by the the TMA detector, they does not contribute much to E^0_{TOT} or E_T because of its small velocity and/or energy.

Pseudo-rapidity distributions of charged particles for central O+Au and Si+Au collisions are shown in Fig.5. The peaks of the distributions are approximately at the rapidities of O+A c.m.s. or Si+A c.m.s., and are significantly shifted backwards from the rapidity of p-p c.m.s. (y = 1.73 at this energy)for heavy targets.

Zero Degree Energy flow

E802 have a hadron calorimeter (ZCAL) at 0 degree of the beam line, and this detector is used to measured how much energy is left in the beam fragments. If we observe zero energy in ZCAL, it might be taken as an operational definition of "full stopping" of projectile. The ZCAL detector subtended an angular aperture of ± 2 deg. In front of it there was a beam pipe whose angular aperture is ± 0.7 deg. The energy resolution of the detector is 6 % r.m.s. for 406 (=28 $\times$ 14.5) GeV/c Si.

Preliminary results of energy distributions measured by ZCAL detector are shown in Fig.6 for Si+Au and for Si+Al collisions with minimum bias and with high multiplicity triggers[7]. For minimum bias trigger, the spectra (Fig.6(a) and 6(b)) shows broad distribution from just below the beam energy of 406 GeV, while for high multiplicity trigger the events concentrate to lower ZCAL energy. The Si+Au spectra shows a large peak at zero energy, indicating that all energy of the projectile is absorbed by the target. On the

other hand, the energy distribution for Si+Au collision shows few events at zero energy. Even for high multiplicity trigger, the spectrum shows a peak around 80 GeV, indicating that approximately 5 nucleons go forwards as spectators.

Let's summarize the data presented so far. The E^0_{TOT} and E_T distributions as well as zero degree energy distributions indicates that most of the energy of projectile is absorbed in the target, and is used for particle production. The data with heavy target seems to be consistent with "full stopping" of the projectile. However, these data can be explained by a simple superposition of N-N collisions. This is because the behavior of these data are largely determined by the geometry of the reaction.

Spectrometer Results

Inclusive momentum spectra of charged particles from Si+A collisions were measured by E802 magnetic spectrometer. The spectrometer consists of a magnet with bending power up to 1.5 Tm and 4 sets of drift chambers (two in front of and two behind the magnet). Particle ID is provided by an array of 160 time-of-flight counters (TOF), and 96 cells of segmented Aerogel Cerenkov counters. The TOF counters have an average r.m.s resolution of 100 ps that allows 5 σ separation between pions and kaons to above 2.0 GeV/c. The Aerogel counter is a threshold Cerenkov counter with index of refraction of 1.02. The spectrometer covers production angle from 5 deg to above 50 deg in laboratory system with several angle settings of the magnet. However, the data presented here corresponds to only one angle setting that covers $\theta_{lab} = 14 - 28$ deg.

Fig.7 shows a scatter plot between the TOF and the inverse of momentum for both positive and negative particles from Si+Au collisions at 14.5 GeV/c per nucleon. The K/π separation up to 2.2 GeV is achieved by the TOF counter. Parts of corresponding mass spectra are shown in Fig.8. The obtained K/π ratios, after a correction of decay in flight, are summarized in Table 1. The errors cited include estimated systematic errors. As a comparison, a summary of experimental values of K/π ratios from p-p and p-A collision experiments at comparable energy are listed in Table 2. Our value of K^+/π^+ ratio seems to be larger compared with p-p or p-A data. However, as listed in Table 2, the K/π ratios are strongly dependent on the parameters such as production angle, transverse momentum, etc. We need more data (more nucleus targets, angle, etc) and detailed comparison with p-A collisions to conclude something about the K/π ratio in H.I. reactions.

References

1. E802 Collaboration, T. Abbott et al., Phys. Lett. 197B, 285 (1987).

2. E814 Collaboration, B. Bassaleck al., to be published in Z. Phys. C.
3. E802 Collaboration, T. Abbott et al., to be published in Z. Phys. C.
4. E802 Collaboration, T. Abbott et al., to be published in Z. Phys. C.
5. Sixth Int. Conf. on Ultrarelativistic Nucleus-Nucleus Collisions (Quark Matter '87), Schloss Nordkirchen, West Germany, August 1987. The proceedings of the conference is to be published in Z. Phys. C.
6. L. Remsberg, private communication.
7. E. Duek, private communiation.
8. A. N. Diddens et al., Nuovo Cimento 31, 961 (1964).
9. G. J. Marmer et al., Phys. Rev. 179, 1294 (1969).
10. W. F. Baker et al., Phys. Rev. Lett. 7, 101 (1961).

Table captions

Table 1. K/π ratios measured at 14.5 GeV/c per nucleon for Si + Au collisions at $14-28$ deg, $p_{lab} \leq 2.0$ GeV/c (preliminary).

Table 2. K/π ratios in p-p and p-nucleus collisions.

Figure captions

Fig.1 Neutral energy (E^0_{TOT}) spectra measured by PBGL detector of E802 for O+A and p+Au collisions at 14.5 GeV/c per nucleon.

Fig.2 O+Au E^0_{TOT} spectrum compared with sum of convolutions of p+Au E^0_{TOT} spectrum.

Fig.3 Transverse energy spectra for Si+A collisions at 10 GeV/c per nucleon. This figure is from ref.2.

Fig.4 Multiplicity distributions for (a) O+A and for (b) Si+A collisions at 14.5 GeV/c per nucleon.

Fig.5 Pseudo-rapidity distributions of charged particles for (a) central O+A and for (b) central Si+A collisions at 14.5 GeV/c per nucleon. The data was taken with a trigger that required large energy being recorded in PBGL detector.

Fig.6 ZCAL energy distributions for Si+Au collisions with (a) INT trigger (minimum bias trigger) and with (c) TMA trigger (high multiplicity trigger), and for Si+Al collision with (b) INT and with (d) TMA trigger.

Fig.7 A scatterplot between the TOF and inverse momentum for positive and negative

particles obtained in Si+Au collisions at 14.5 GeV/c per nucleon. The spectrometer covers production angle of $\theta_{lab} = 14 - 28\,\mathrm{deg}$.

Fig.8 The mass spectra in the π-K region for (a) positive and for (b) negative particles as derived from the data in Fig.7. The tracks with momentum less than 2.0 GeV/c are selected.

Table 1. K/π ratios measured in 14.5 GeV/c per nucleon Si + Au collisions at $14° - 28°$, $p_{lab} < 2.0$ GeV/c. (preliminary)

	Min.bias trigger	Central trigger
$(K^+/\pi^+)_{present}$	19 ± 5 %	24 ± 5 %
$(K^-/\pi^-)_{present}$	6 ± 5 %	$4\ ^{+4}_{-2}$ %

Table 2. K/π ratios in p-p and p-nucleus collisions.

	p_{inc} (GeV/c)	Reaction	Angle	Momentum (GeV/c)	Ratio (%)	Reference
K^+/π^+	19.0	p+p	6.6°	1.7	4.5 ± 2.0	8
K^-/π^-					3.4 ± 2.0	8
K^+/π^+				2.4	7.1 ± 2.0	8
K^-/π^-					3.6 ± 2.0	8
K^+/π^+	12.3	p+Be	10°	1.0	3.7 ± 0.3	9
K^-/π^-					1.3 ± 0.2	9
K^+/π^+		p+Cu	10°	1.0	5.7 ± 0.5	9
K^-/π^-					1.7 ± 0.2	9
K^+/π^+	30.0	p+Be	20°	1.25	2.7 ± 1.2	10
K^-/π^-					1.2 ± 0.5	10
K^+/π^+				2.5	23.0 ± 1.2	10
K^-/π^-					8.8 ± 0.9	10

Fig.1

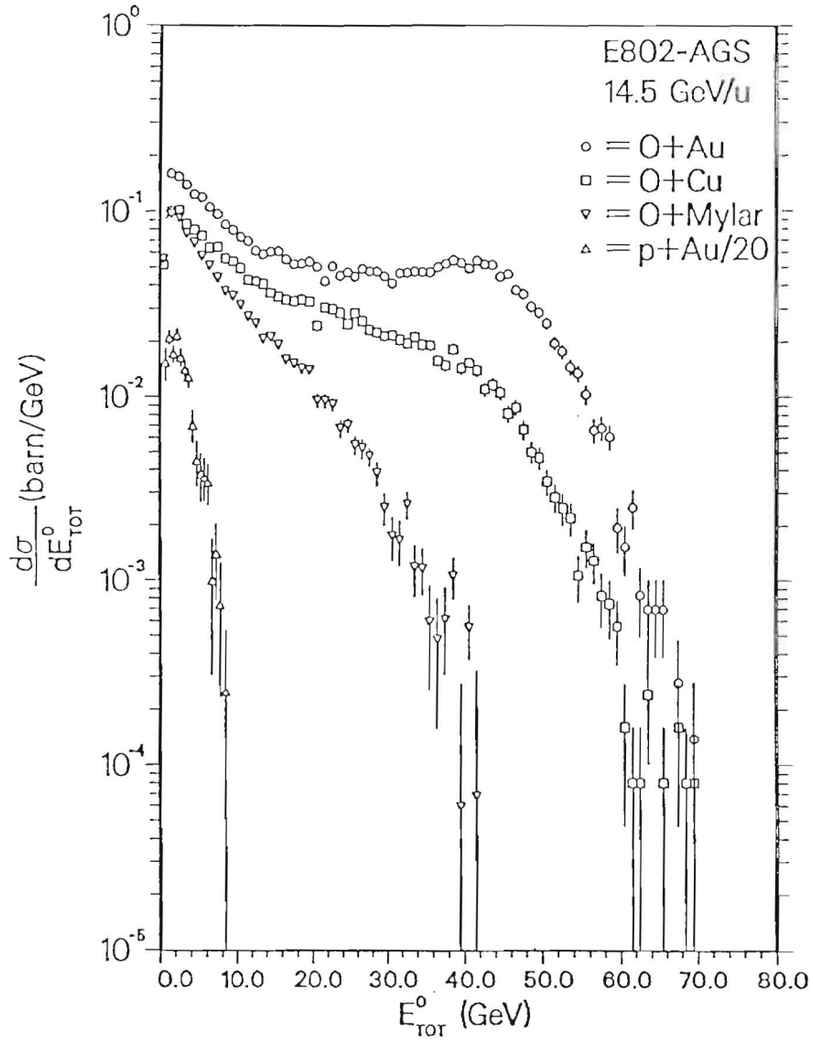
E802-AGS
14.5 GeV/u
○ = O+Au
□ = O+Cu
▽ = O+Mylar
△ = p+Au/20
$\frac{d\sigma}{dE^0_{TOT}}$ (barn/GeV)
E^0_{TOT} (GeV)

Fig.2

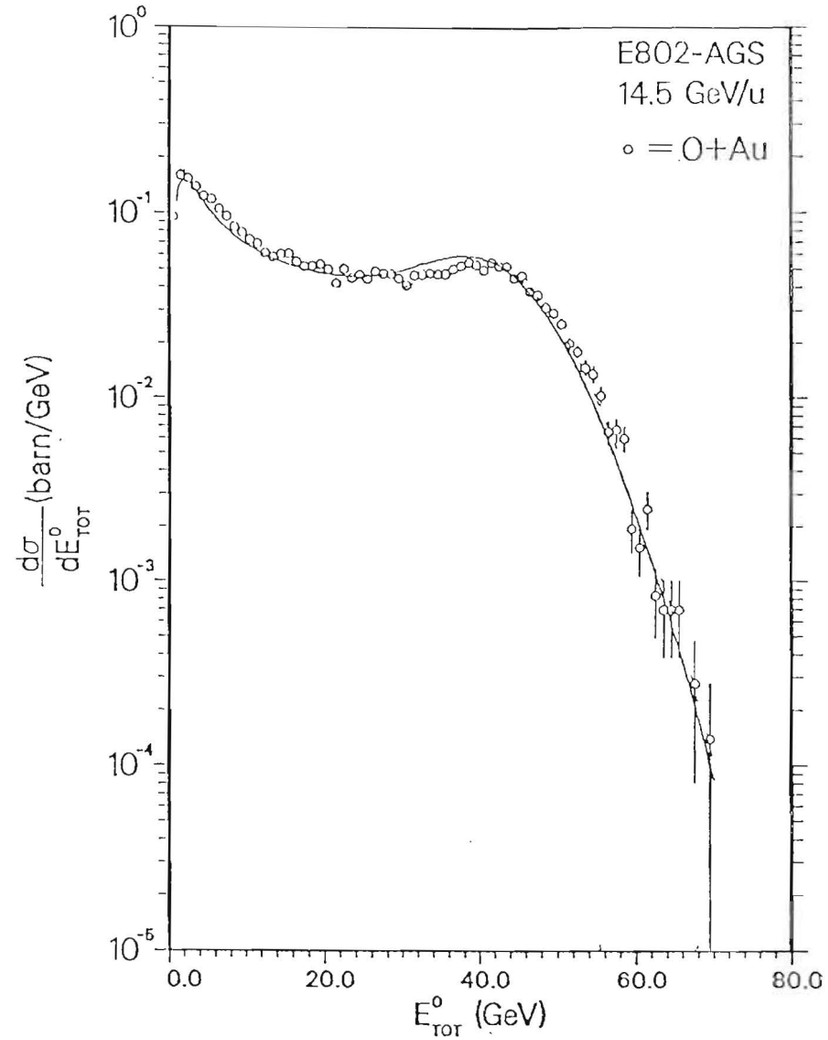
E802-AGS
14.5 GeV/u
○ = O+Au
$\frac{d\sigma}{dE^0_{TOT}}$ (barn/GeV)
E^0_{TOT} (GeV)

Fig.3

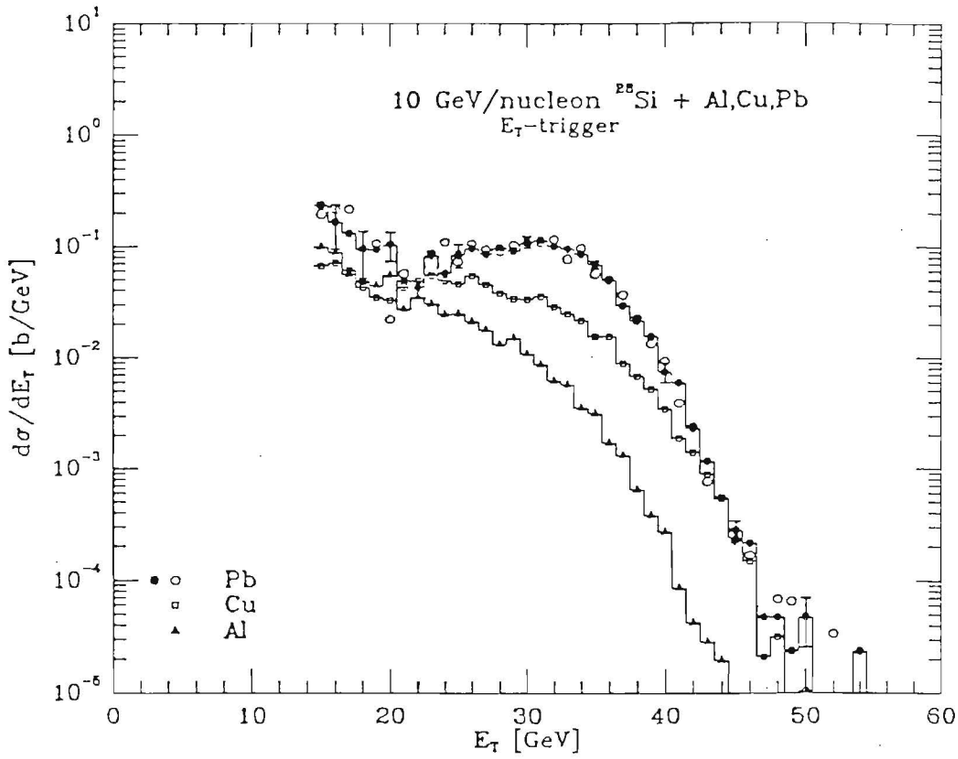
10 GeV/nucleon ^{28}Si + Al,Cu,Pb
E_T-trigger
$d\sigma/dE_T$ [b/GeV]
E_T [GeV]
Pb
Cu
Al
10^{1}
10^{0}
10^{-1}
10^{-2}
10^{-3}
10^{-4}
10^{-5}
0
10
20
30
40
50
60

Fig.4

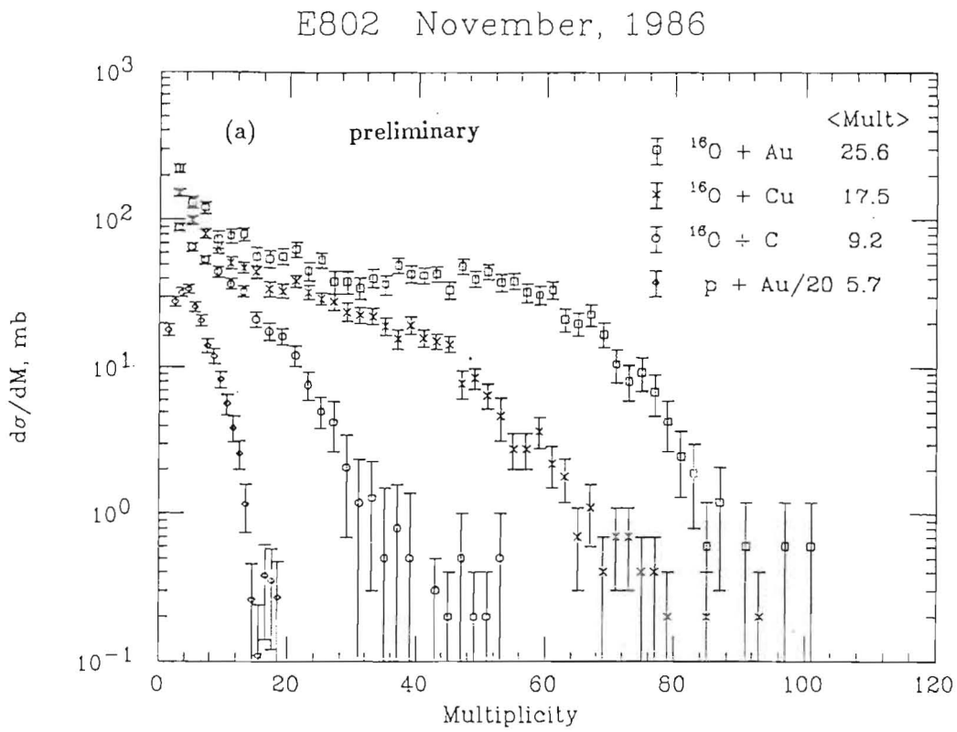
E802 November, 1986
(a)
preliminary
<Mult>
^{16}O + Au 25.6
^{16}O + Cu 17.5
^{16}O + C 9.2
p + Au/20 5.7
dσ/dM, mb
Multiplicity

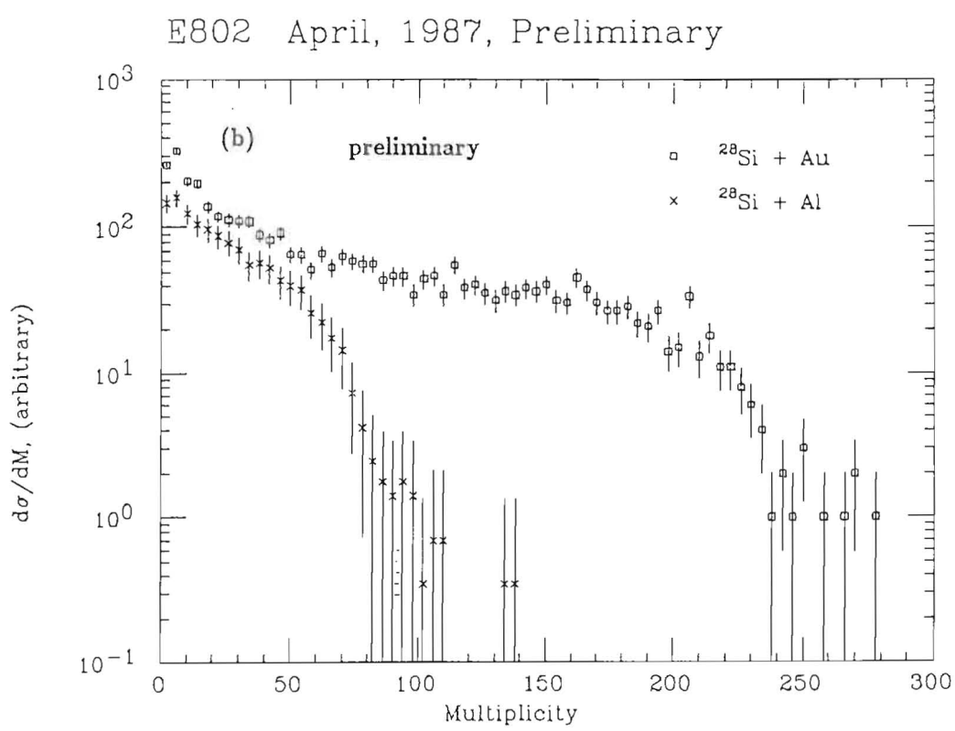
E802 April, 1987, Preliminary
(b)
preliminary
^{28}Si + Au
^{28}Si + Al
dσ/dM, (arbitrary)
Multiplicity

Fig.5

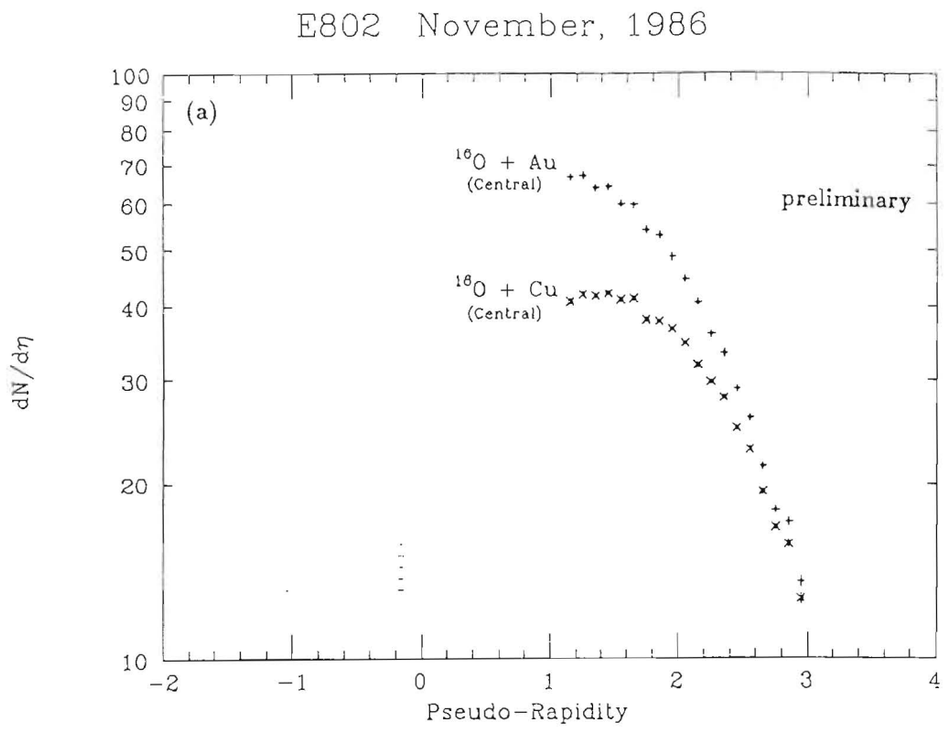
E802 November, 1986
(a)
^{16}O + Au
(Central)
^{16}O + Cu
(Central)
preliminary
dN/dη
Pseudo-Rapidity

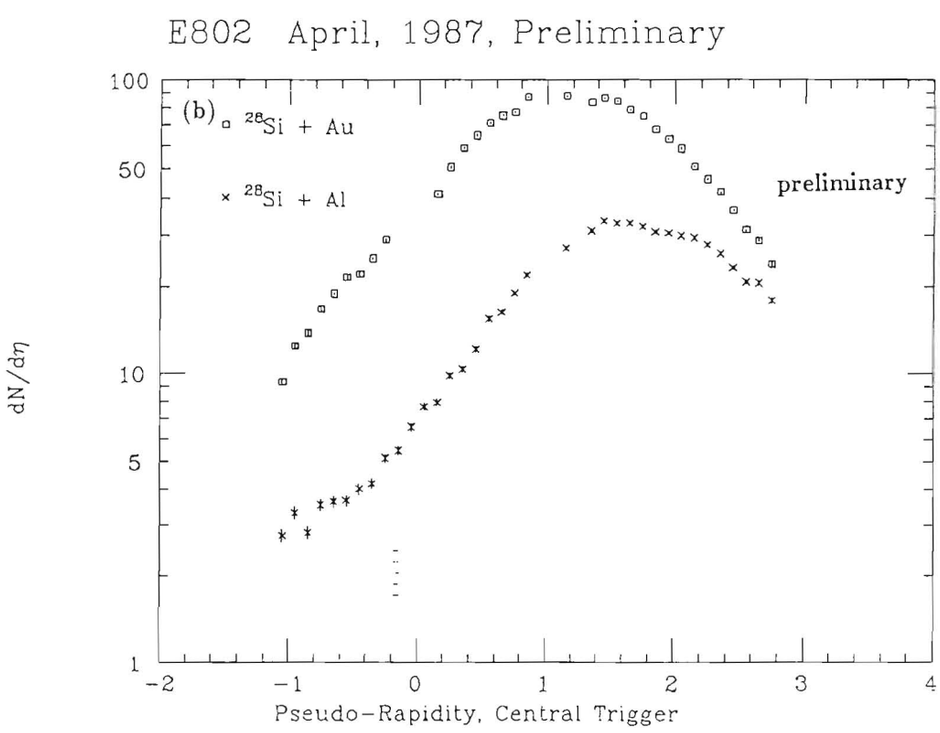
E802 April, 1987, Preliminary
(b) □ ^{28}Si + Au
× ^{28}Si + Al
preliminary
dN/dη
Pseudo-Rapidity, Central Trigger

Fig.6

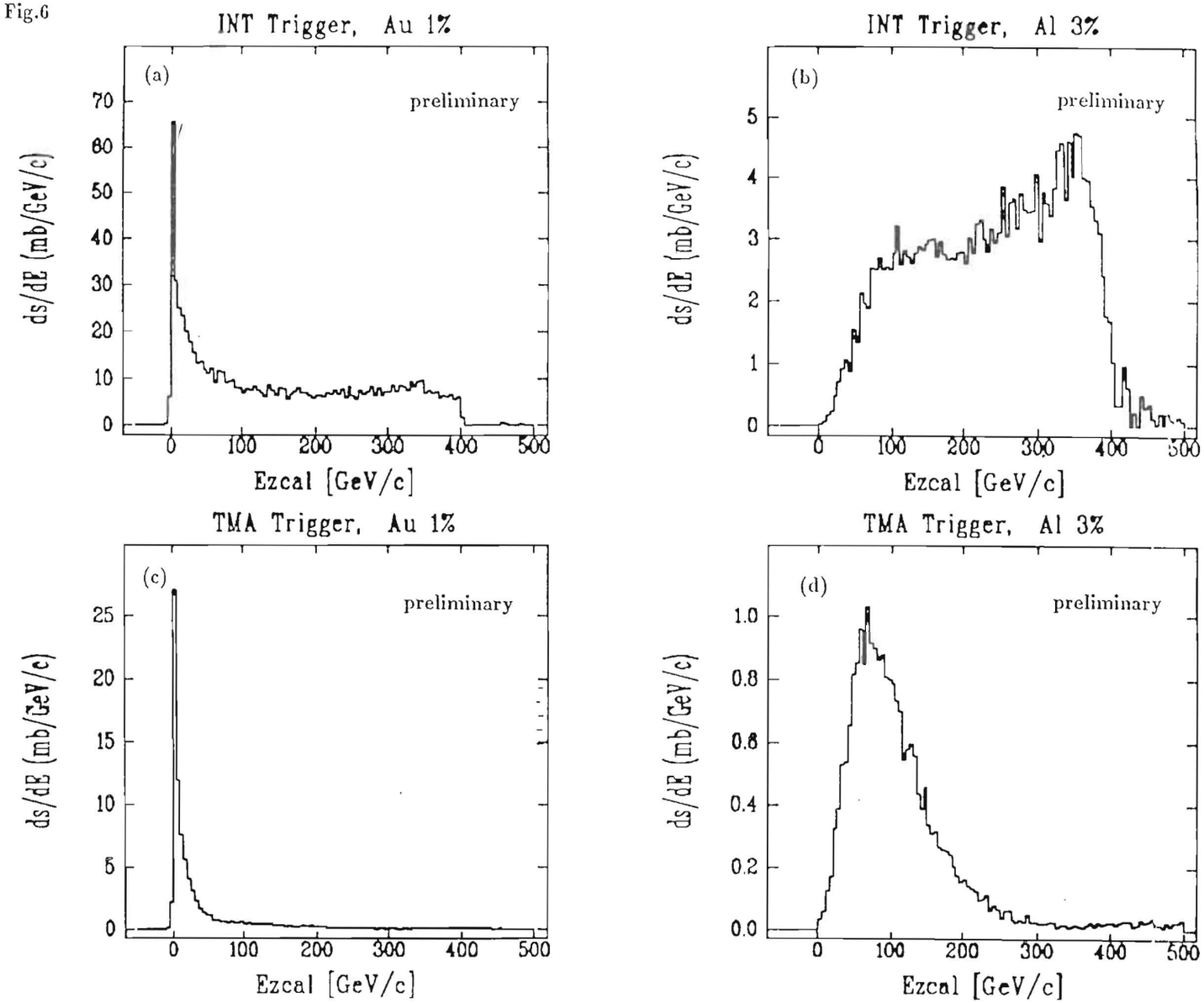
INT Trigger, Au 1%
(a)
preliminary
ds/dE (mb/GeV/c)
Ezcal [GeV/c]
INT Trigger, Al 3%
(b)
preliminary
ds/dE (mb/GeV/c)
Ezcal [GeV/c]
TMA Trigger, Au 1%
(c)
preliminary
ds/dE (mb/GeV/c)
Ezcal [GeV/c]
TMA Trigger, Al 3%
(d)
preliminary
ds/dE (mb/GeV/c)
Ezcal [GeV/c]

Fig.7

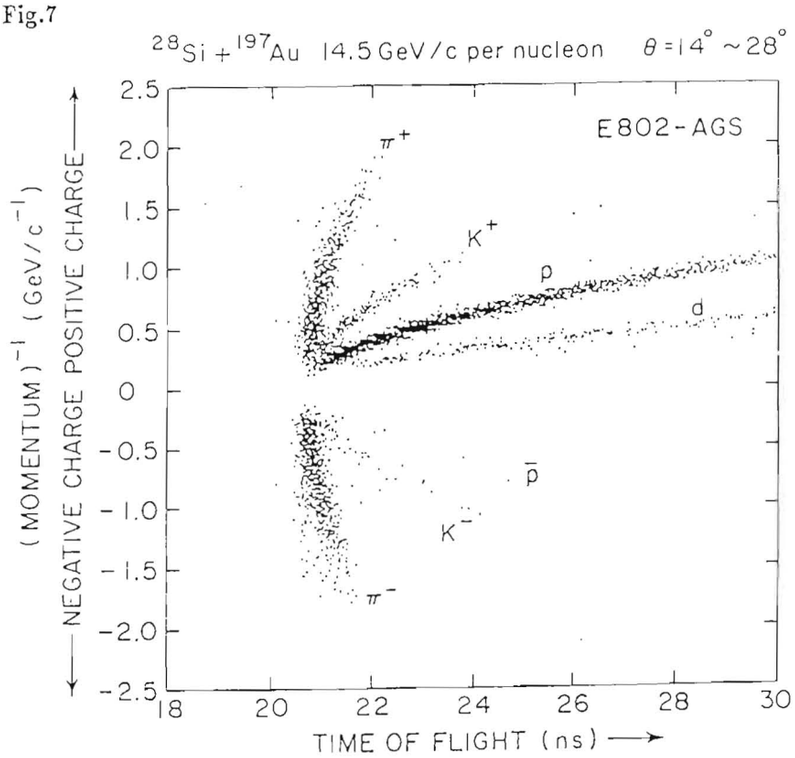
$^{28}Si + ^{197}Au$ 14.5 GeV/c per nucleon $\theta = 14^\circ \sim 28^\circ$
E802-AGS
π^+
K^+
p
d
$\bar{p}$
K^-
π^-
(MOMENTUM)$^{-1}$ (GeV/c^{-1})
NEGATIVE CHARGE POSITIVE CHARGE
TIME OF FLIGHT (ns)

Fig.8

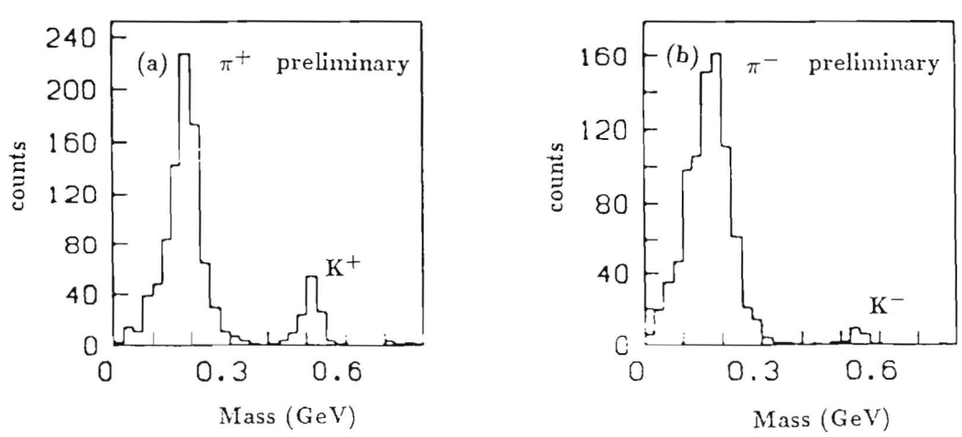
(a)
π^+ preliminary
K^+
counts
Mass (GeV)
(b)
π^- preliminary
K^-
counts
Mass (GeV)

^{16}O and ^{32}S + ^{207}Pb Interactions in the CERN EMU-05 Experiment

A.Iyono(0), S.Dake(1), T.Tominaga(1), T.Ogata(2), O.Miyamura(3), M.Fuki(4), Y.Takahashi(5), J.C.Gregory(5), T.Hayashi(5), J.H.Derrickson(6), P.B.Edy(6), W.F.Fountain(6), T.A.Parnell(6), R.E.Roberts(6), J.W.Watts(6), T.Tabuki(6), S.Nagamiya(7).

(0). Okayama University of Science,Japan
(1). Kobe University,Japan
(2). University of Tokyo,ICR,Japan
(3). Osaka University,Japan
(4). Matsusho-Gakuen Junior College,Japan
(5). University of Alabama in Huntsville,USA
(6). Space Science Laboratory,NASA/MSFC,USA
(7). Columbia University,USA

ABSTRACT

Emission angles, momenta and charge-signs of all charged particles in forard hemisphere have been measured in ^{16}O+Pb and ^{32}S+Pb interactions at incident energy of 200 GeV per nucleon. The multiplicity distributions of ^{16}O and ^{32}S nucleus interactions are almost scaling expressed as a function of scaling variable $Z(\equiv Ns/\langle Ns\rangle)$. The ratio of average pseudorapidity density of ^{16}O+Pb to that of proton(200 GeV/c)+Pb is flat almost all over the range of $\eta(\equiv -\ln \tan \theta/2)$. Measuring momentum of central-forward charged particles for high multiplicity events, we have obtained their transverse momentum(P_T) distributions as preliminary results.

§1. Introduction

The enhancement of close hadronic pairs has been observed in cosmic ray nucleus-nucleus collisions by JACEE experiments[1]. The data suggest that the HBT(Hambury-Brown/Twiss) source radius is very small(3~4 fm) with $Ns \gtrsim 1000$[2]. To investigate like and unlike charge pair correlation in detail, it is very important to measure momenta and charge-signs of pairs inhigh multiplicity events.. In EMU-05 experiments, the emulsion chamber was put within 1.8 Tesla magnetic field.

The observables in EMU-05 experiment are summarized;

(1)emission angles ; θ , ϕ
(2)momentum and charge-sign of all charged tracks ; P , P_T
(3)A part of photons(e^+e^- pairs) and short-lived decaying particles
(4)Particle identification($P \lesssim 3$ GeV/c).

We have measured minimum-biased multiplicities of 248 events for ^{16}O and of 315 events for ^{32}S+Pb interactions by initial scanning. For ^{16}O+Pb interactions, we obtained angular distributions of 35 events.

§2. Detector and Analysis

The detector in EMU-05 experiment is called the Magnetic - Interferometric - Emulsion - Chamber(MAGIC). Fig. 1 shows the layout of MAGIC apparatus in the H3 beam line at CERN-SPS. If a beam hits in the target og MAGIC, we can see the schematic picture as shown in Fig. 2. This chamber consists of thickemulsion plates, 300μm lead plates for target, and very thin emulsion films(50μm thick on both sides of 70μm polystyrene film) for tracking in a spectrometer part of the chamber. Low density styloform plates are used for gaps in a spectrometer part. Since the whole radiation length and hadronic interaction mean free path are ,respectively, 0.051 and 0.005, we can avoid confusing many tracks in following them down in the spectrometer part.

The analysis of MAGIC has been started from the scanning on the emulsion plates just under the lead plates. At first, to count multiplicities of observed event and measure the emission angles of charged tracks in each events, only a few layers are needed because of the fine geometrical resolution of emulsion plates. Figs. 3a and 3b show two photographs of one of higher multiplicity event in ^{32}S+Pb interactions, at 50μm and 180μm downstream the interaction vertex, respectively. Most of the charged tracks are easily separated at the lower plate 130μm downward from the upper plate. In order to measure momentum of charged tracks, we perform tracking on more than ten layers. Coordinates of charged tracks are measured from reference beam tracks which did not interact in the individual layers. All coordinates include the noise of the multiple Coulomb scattering. The magnetic deflection of charged tracks, however, is about seven times larger than the noise in the spectrometer. Figs. 4a and 4b show the deviations of all measured position data and the mean deviations of each track from assumed curves, respectively. This well describes the scattering deflection[3]. The accuracy of momentum is presented as

$$\Delta P/P = 13/\sqrt{N}\ \%\ \text{(upto 20 GeV/c)}$$
$$= (13/\sqrt{N})*P/20\ \%\ \text{(above 20 GeV/c)}.$$

where N is the number of observed layers, typically 10, and P is the momentum of each track in GeV/c.

§3. Results and Discussions

3-1. Multiplicity distributions of ^{16}O and ^{32}S+Pb collisions.

Initial scanning on the emulsion plates quickly served us the multiplicity distributions of 248 events for ^{16}O+Pb and 315 events for ^{32}S+Pb.

In Fig. 5, we present the multiplicity distribution for ^{16}O+Pb at incident energy of 200 GeV per nucleon. Average multiplicity $\langle N_s \rangle$ of shower particles of which ionization is less than 1.4 times of the minimum ionization, is 88. Tracks observed as gray and black tracks were eliminated from multiplicity data. The EMU-05 data of ^{16}O+Pb interactions expressed as a function of scaling variable $Z(\equiv N_s / \langle N_s \rangle)$ agree with a Glauber-scheme Monte-Carlo caluclation by Capella et al[4]. And they distribute wider than KNO scaling function of proton+proton (p+p) and proton+nucleus (p+A) interactions. Furthermore, the multiplicity distribution of ^{32}S+Pb interactions is scaling with the data of ^{16}O+Pb interaction when each data is expressed as a function of Z, as shown in Fig. 6. The preliminary $\langle N_s \rangle$ of ^{32}S+Pb is 145. In Fig. 7, however, EMU-04 experiments[5] have observed the contribution of direct Coulomb $e^{\pm}$ pairs production to very small multiplicity range. In case of ^{32}S+Pb, the $\langle N_s \rangle$ value is corrected by EMU-04 data. This contribution can be finally eliminated by the further analysis.

The ratios of $\langle N_s \rangle$ to dispersion D are about 1 for ^{16}O and ^{32}S+Pb cases. In case of p+p and p+A interactions, each ratio is twice as large as EMU-05 data. And Jain et al[6]. have reported that the ratio is 2.4 and 2.3 for central ^{16}O+AgBr and CNO interactions, respectively. The plausible explanation of EMU-05 results is the dominance of impact parameter variation over the fluctuation of elementary process. These results also agree with the observed data of 20-65 GeV/n cosmic ray "Fe"-nucleus interactions in JACEE-3 experiment[7].

Very low multiplicity data in ^{16}O+Pb collisions did not get rid of detection biases originated only from inefficiency because of rapid scanning .

We summarize the observed $\langle N_s \rangle$ and various Monte Calro calculation results in the following table.

	$\langle N_s$ (EMU-05)$\rangle$	MCM*	WNM*	DPM*
^{16}O+Pb	88^{+8}_{-6}	101	78	88
^{32}S+Pb	145^{+25}_{-8}	158	117	

* DATE et al. Phys.Rev.D36,2744(1987)
* CAPELLA et al. Phys.Rev.D35,2921(1987)
* TAKAHASHI et al. Nucl.Phys.A(1987)

3-2. Angular distributions of ^{16}O+Pb collisions at 200 GeV/n.

We obtained the angular distributions of 35 events in ^{16}O+Pb interactions. Pseudorapidity density distribution of charged particles are shown in Fig. 8. For inclusive data, central rapidity density in nucleon-nucleon center of mass system is 33 ± 2 and the position of maximum pseudorapidity density is shifted around $\eta \simeq 2$. If the distribution are separated for two cases of Ns = 200, the observed peak positions are shifted for backward as multiplicities increase.

In Fig. 9, the pseudorapidity density ratios of ^{16}O+Pb and p+Pb to p+p at 200 GeV/n[8] expressed as a function of η. These ratios are flat and almost equal to the average collision number ratio of ^{16}O+Pb to p+Pb interactions almost all over η. Clearly, this implies that the average pseudorapidity distribution of ^{16}O+Pb data is reproduced by the multiplication the collision number ratio.

In azimuth angle distributions, one bimodal type event is observed in high multiplicity events. Fig. 10 shows the angular distributions and η-ϕ scatter plot of that event. We observed large fluctuations in η and ϕ distribution.

3-3. Transverse momentum distribution of high multiplicity events.

The transverse momentum (P_T) distribution of charged particles is one of the significant observables in high multiplicity and high pseudorapidity density events. We have already measured the momentum distribution for two events in ^{16}O+Pb interactions and one event in ^{32}S+Pb interactions. Here we present one of the higher multiplicity (Ns = 535) events in ^{32}S+Pb interactions. Figs. 11a and 11b show the pseudorapidity distribution and η-ϕ scatter plot, respectively. The central pseudorapidity density is 114 around the c.m.s. of nucleons at 200 GeV/n. Fig. 12a shows the P_T distribution for the same event. The excess of low $\langle P_T \rangle$ components is also observed in the P_T range below 500 MeV/c. This character of our data is consistent with WA80[9] data for π^0's P_T spectrum in ^{16}O+Au at 200 GeV/n. We observed some the tracks whose vertex positions are more than 10μm away from the vertex position obtained by mean of reconstruction, called "off vertex tracks". Except for off vertex tracks, the low $\langle P_T \rangle$ components are suppressed as shown in fig. 12b. The average transverse momentum $\langle P_T \rangle$ value is 340 ± 20 MeV/c for both forward-central and central charged tracks. It is consistent with p+p data[10]. The existence of low $\langle P_T \rangle$ components must be given careful consideration to and being analyzed further.

§5. Conclusions

The results of ^{16}O and ^{32}S+Pb collisions in EMU-05 experiment show the followings:

1). Minimum-biased multiplicity distributions in both ^{16}O and ^{32}S+Pb collisions are consistent with a standard superposition model.

2). Inclusive pseudorapidity distribution is reproduced by that of proton+Pb collision multiplied by each collision number ratio at the same incident energy.

3). Average transverse momentum values of charged particles are measured as 340 ± 20 MeV/c.

The momentum and charge sign of charged particles are able to be measured by the MAGIC. We have been analyzing high multiplicity events in details.

REFERENCES

1) Y.Takahashi, S.Dake and JACEE Collaboration, Nucl.Phys.,A461,263c(1987).
2) Y.Takanashi, Nucl.Phys.A(1987)(PANIC 1987).
3) Y.Takahashi, private communication.
4) A.Capella et al. Phys.Rev.D35,2921,(1987).
5) Y.Takahashi et al. ,Proceeding of the Workshop on Cosmic ray and High energy Gamma ray experiments For THE SPACESTATION ERA, 390(1984).
6) P.L.Jain et al., Phys.Rev.Lett.,59,2531(1987).
7) T.H.Burnett et al., Phys.Rev.D35,824(1987).
8) J. Elias et al., Phys.Rev.D22,13(1980).
9) R.Albrecht et al., GSI-87-82.
10) G.Arnison et al., Phys.Lett.118B,167,(1982).

Figure Captions:

Fig. 1 The layout of a magnet and remote-controled chariot in H3 beam line

Fig. 2 The EMU-05 MAGIC apparatus

Fig. 3a, b Photographs of ^{32}S+Pb interaction at 50μm and 130μm downstream from the vertex point

Fig. 4a, b Distance and average distance between observed track position and assumed curve

Fig. 5 Multiplicity distributions of JACEE v.s. ^{16}O+Pb collosions

Fig. 6 Multiplicity distributions of ^{6}O+Pb v.s. ^{32}S+Pb collisions

Fig. 7 Low multiplicity events(cf EMU-04)

Fig. 8 Inclusive pseudorapidity distribution

Fig. 9 Pseudorapidity density ratio of ^{16}O+Pb to p+Pb interactions

Fig. 10 η-ϕ scatter plot of bimodal type ϕ-distribution event in ^{16}O+Pb interaction, circle denoting particle with + charge and rectangle - charge.

Fig. 11a Pseudorapidity distribution for ^{32}S+Pb event

Fig. 11b η-ϕ scatter plot for the same event

Fig. 12a P_T distribution at central and central-forward regions for all tracks

Fig. 12b P_T distribution except for "off vertex tracks"

H3 (WEST HALL)

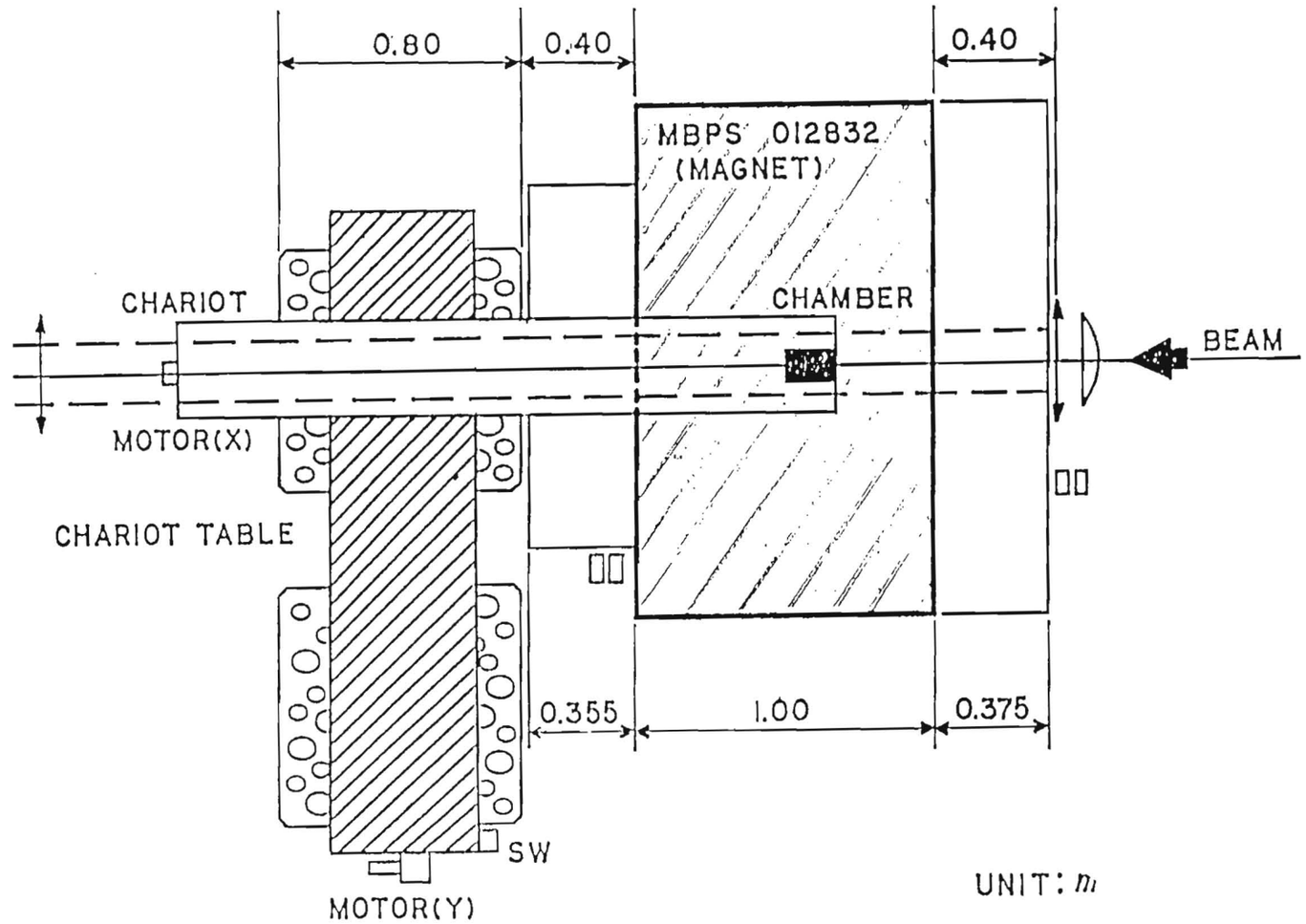

Fig. 1

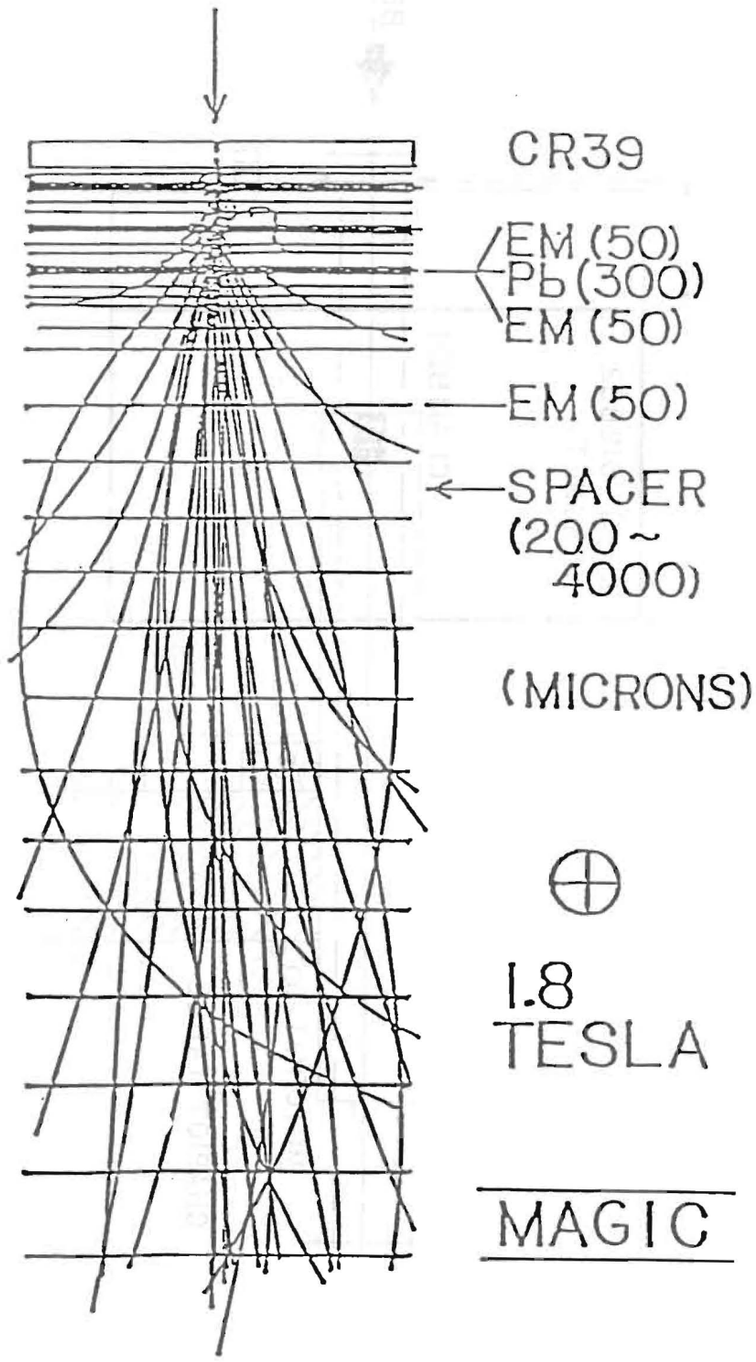
CR39
EM (50)
Pb (300)
EM (50)
EM (50)
SPACER
(200 ~
4000)
(MICRONS)
1.8
TESLA
MAGIC

Fig. 2

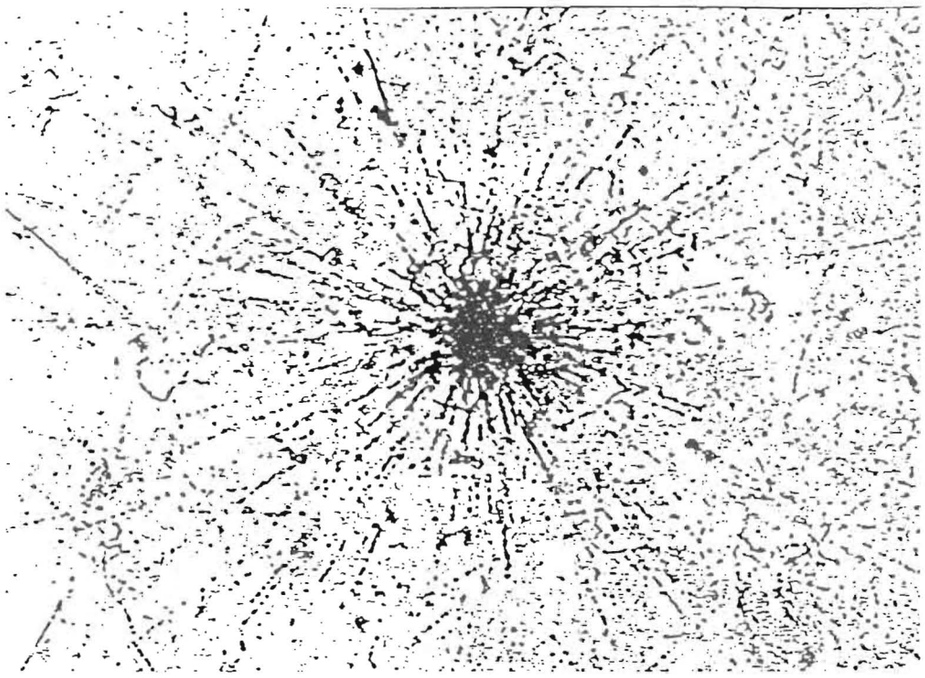

Fig. 3a

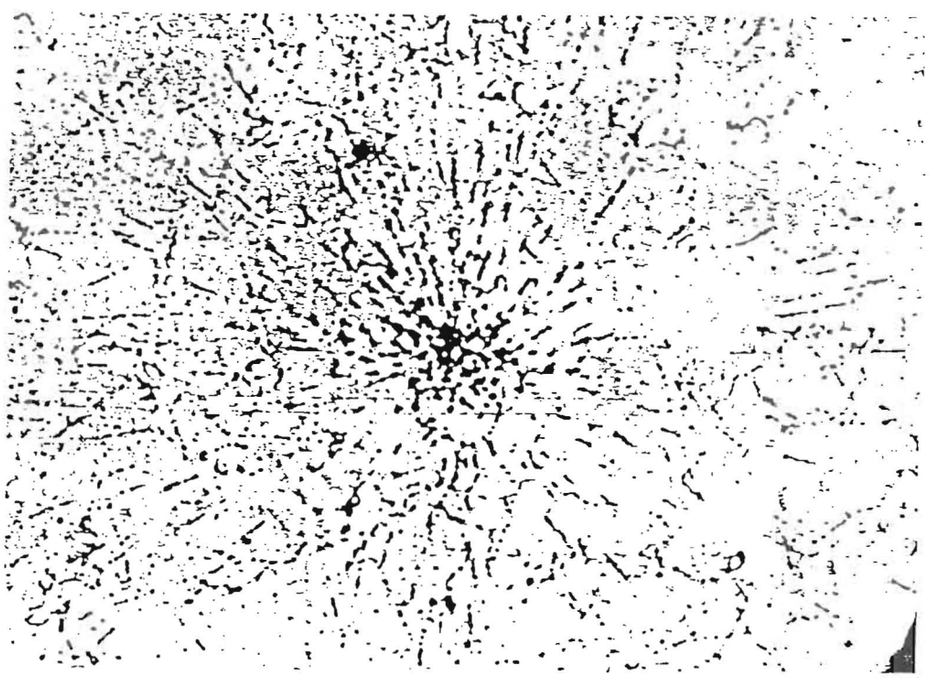

Fig. 3b

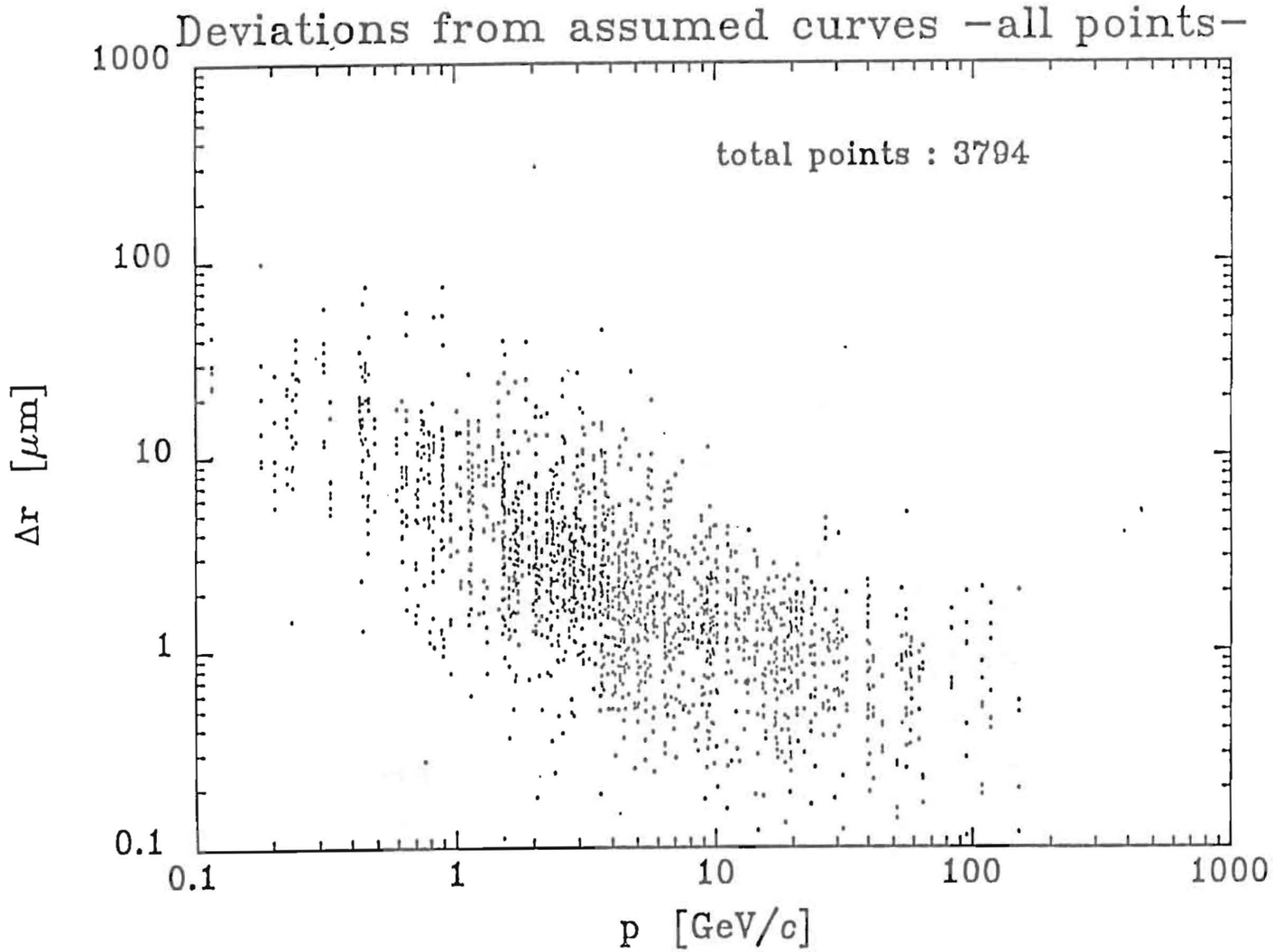
Deviations from assumed curves -all points-
total points : 3794
1000
100
10
1
0.1
Δr [μm]
0.1
1
10
100
1000
p [GeV/c]

Fig. 4a

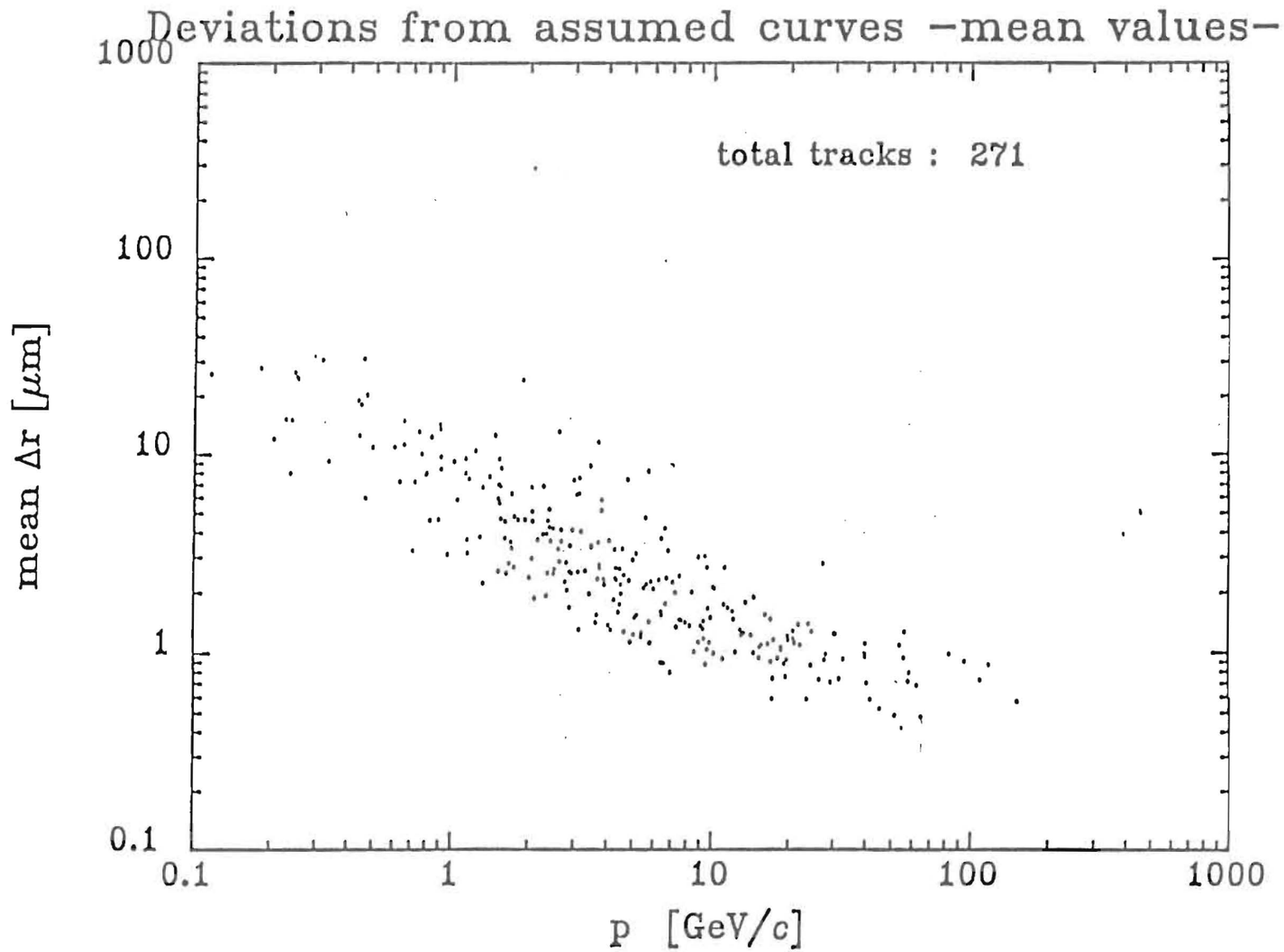
Deviations from assumed curves -mean values-
total tracks : 271
mean Δr [μm]
1000
100
10
1
0.1
0.1
1
10
100
1000
p [GeV/c]

Fig. 4b

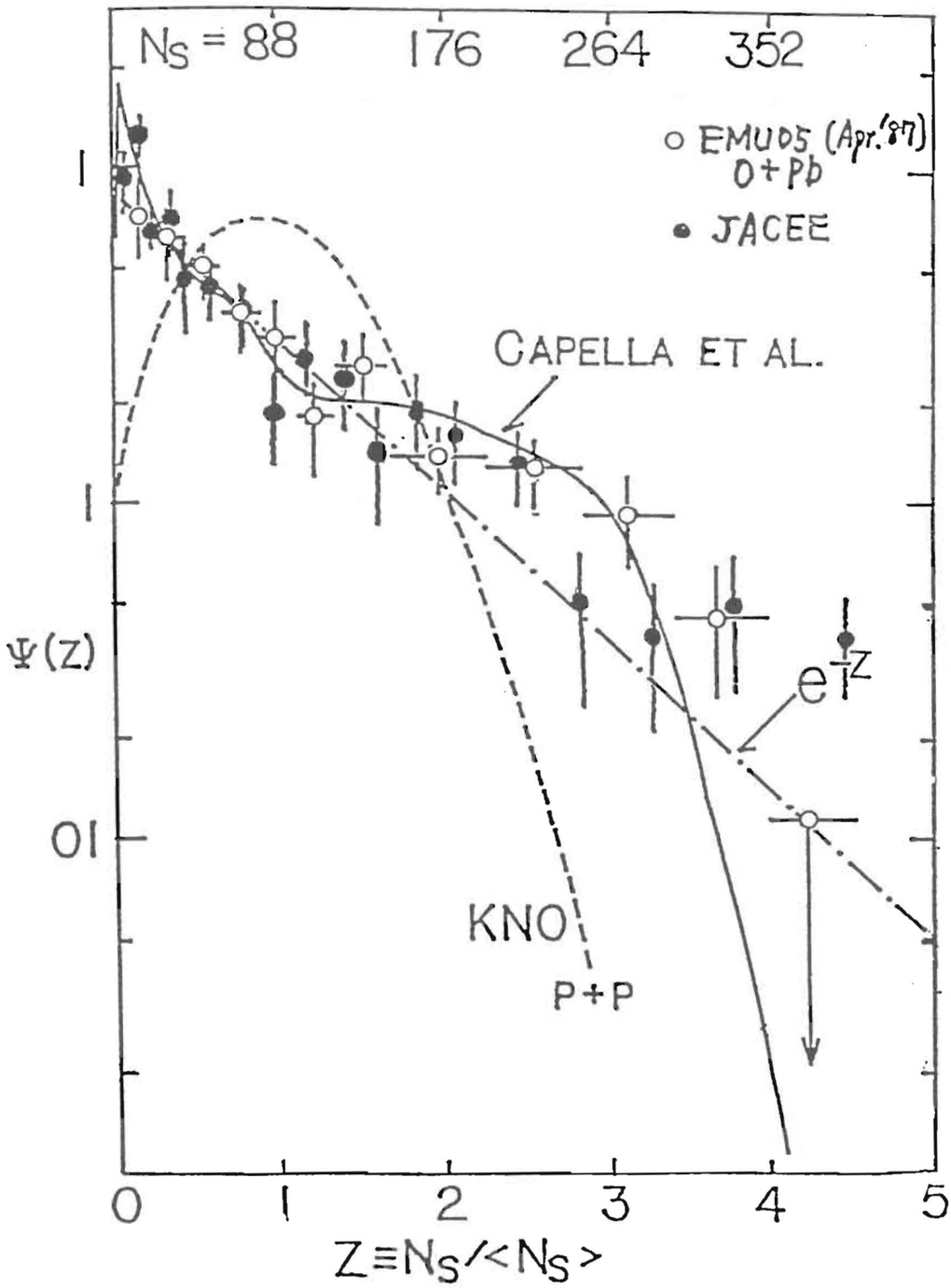
Ns = 88
176
264
352
○ EMU05 (Apr.'87)
O+Pb
● JACEE
CAPELLA ET AL.
KNO
P+P
Ψ(Z)
1
1
01
0
1
2
3
4
5
Z≡Ns/<Ns>

Fig. 5

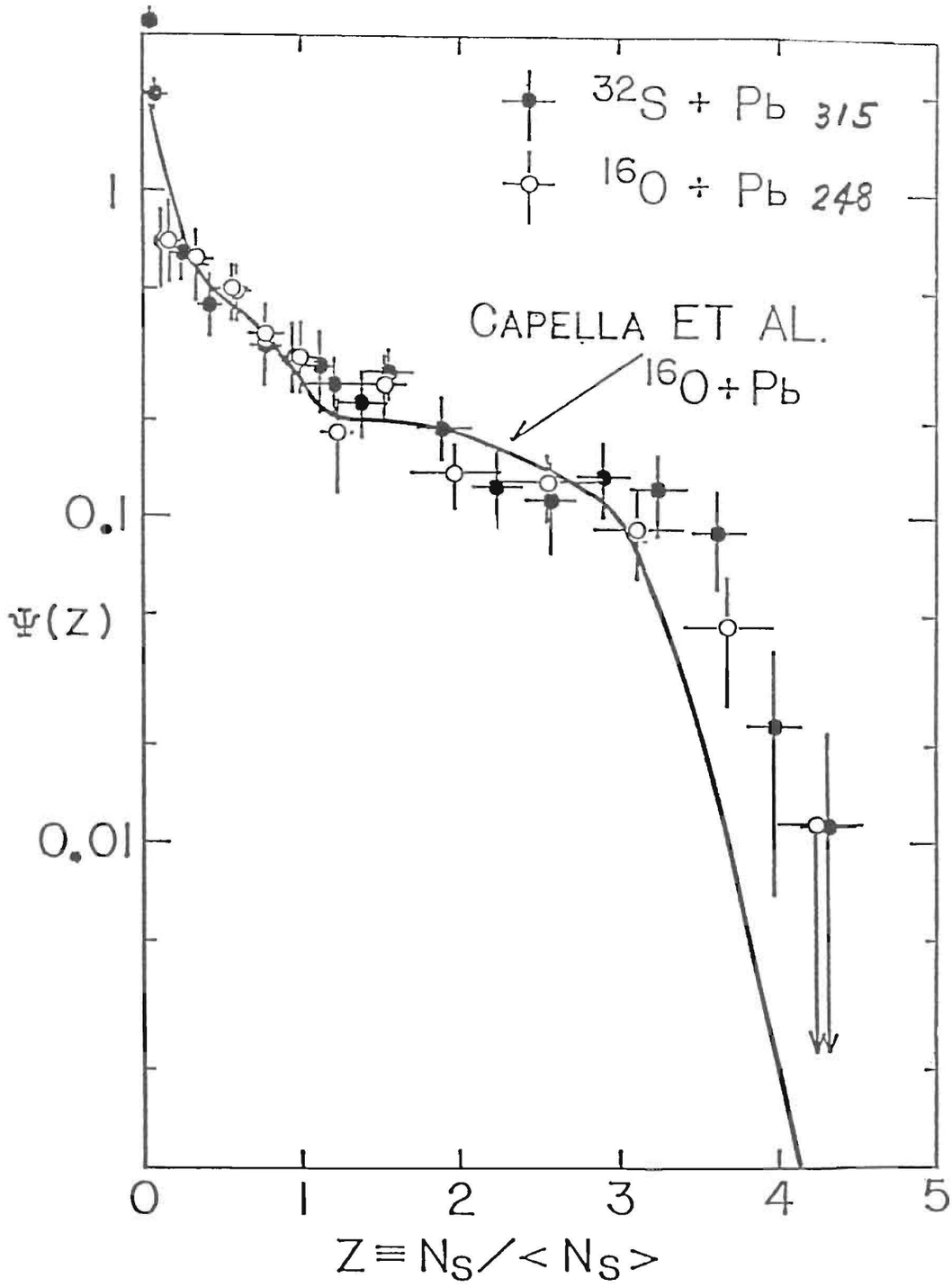
$^{32}S + Pb$ 315
$^{16}O + Pb$ 248
CAPELLA ET AL.
$^{16}O + Pb$
1
0.1
0.01
$\Psi(Z)$
0
1
2
3
4
5
$Z \equiv N_S / \langle N_S \rangle$

Fig. 6

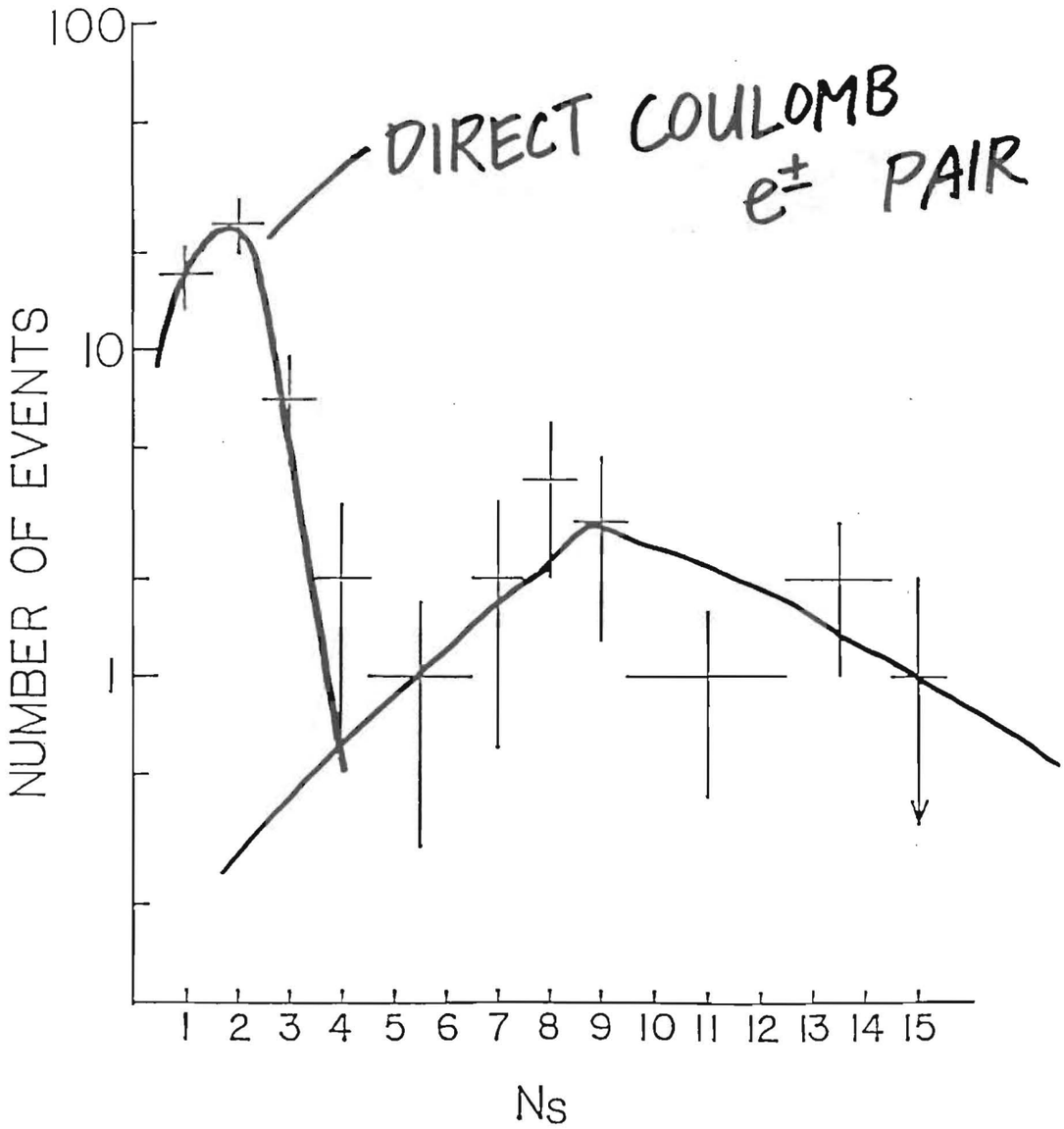
100
10
1
NUMBER OF EVENTS
DIRECT COULOMB
e± PAIR
1 2 3 4 5 6 7 8 9 10 11 12 13 14 15
Ns

Fig. 7

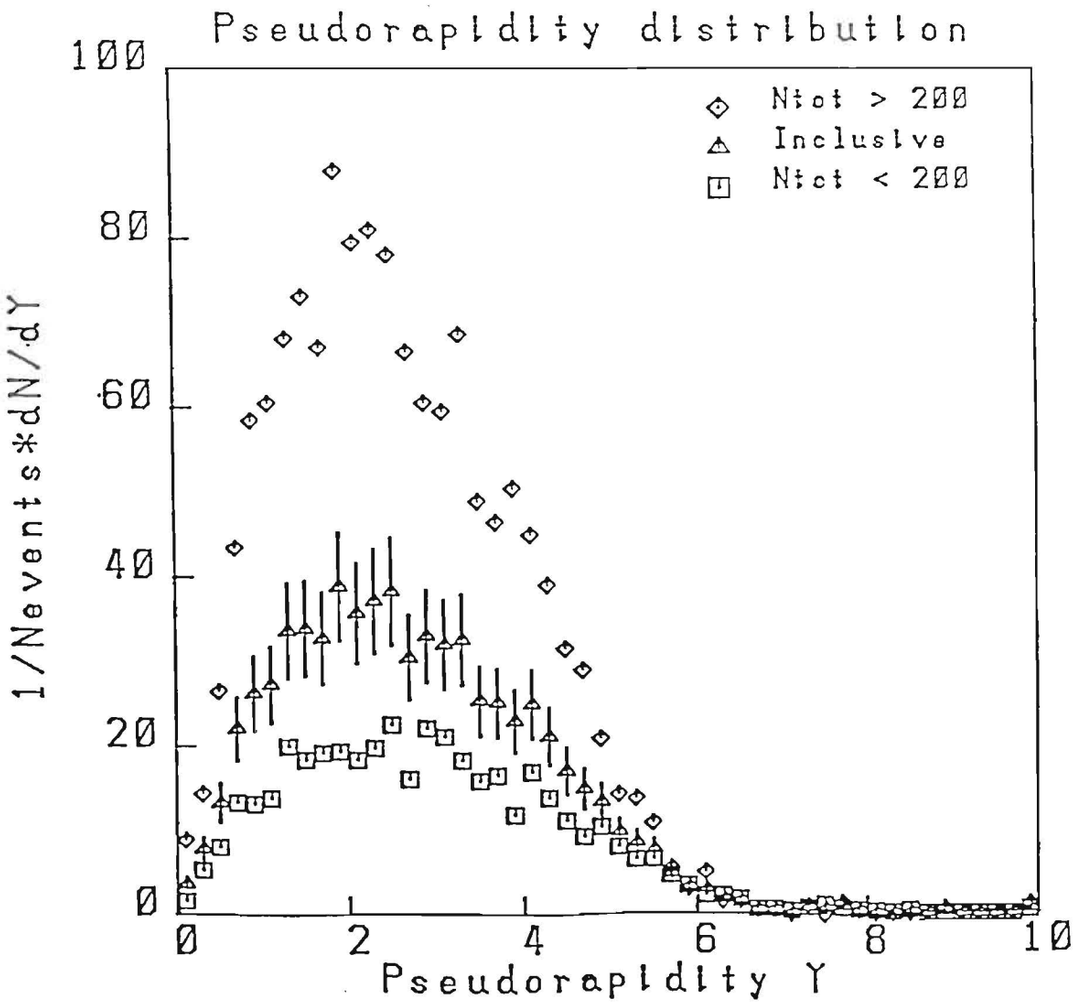
Pseudorapidity distribution
Ntot > 200
Inclusive
Ntot < 200
1/Nevents*dN/dY
100
80
60
40
20
0
0
2
4
6
8
10
Pseudorapidity Y

Fig. 8

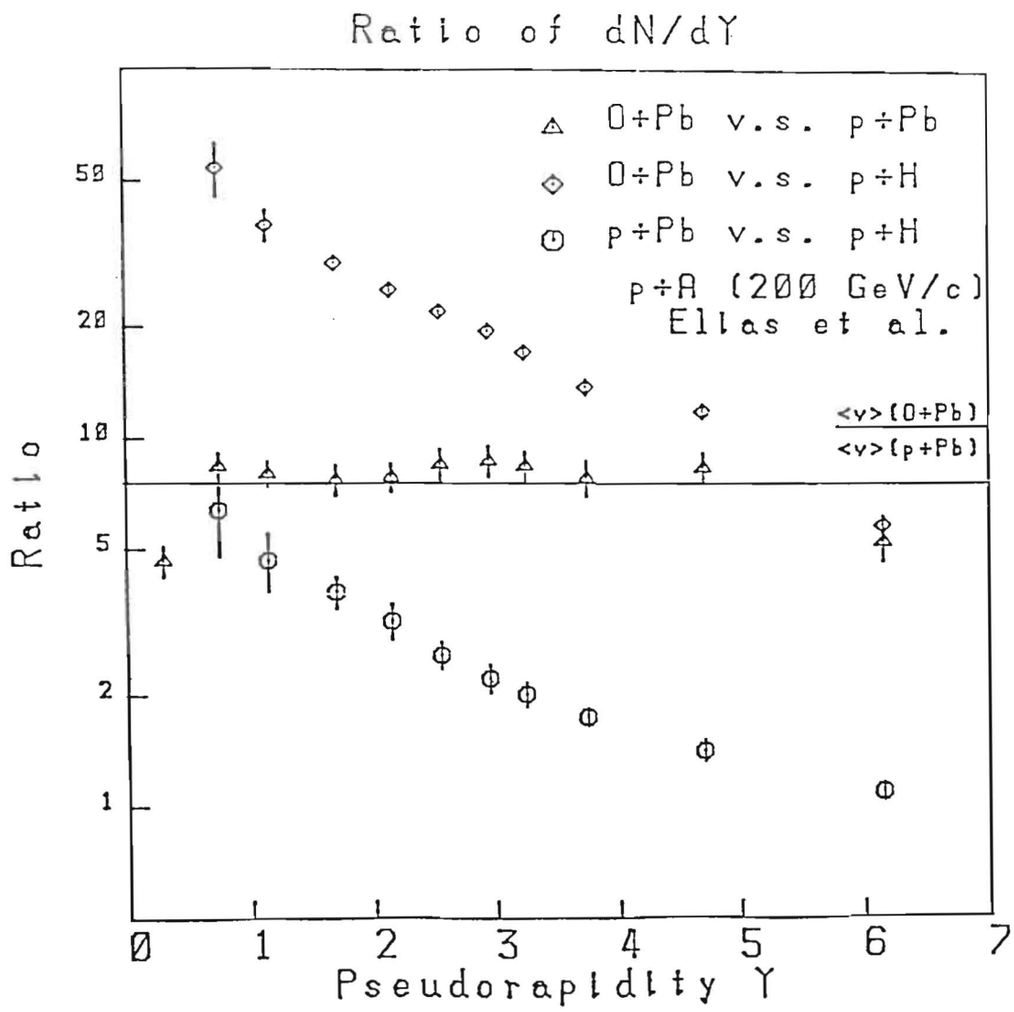
Ratio of dN/dY
O+Pb v.s. p+Pb
O+Pb v.s. p+H
p+Pb v.s. p+H
p+A (200 GeV/c)
Ellas et al.
<v>(O+Pb)
<v>(p+Pb)
Ratio
50
20
10
5
2
1
0
1
2
3
4
5
6
7
Pseudorapidity Y

Fig. 9

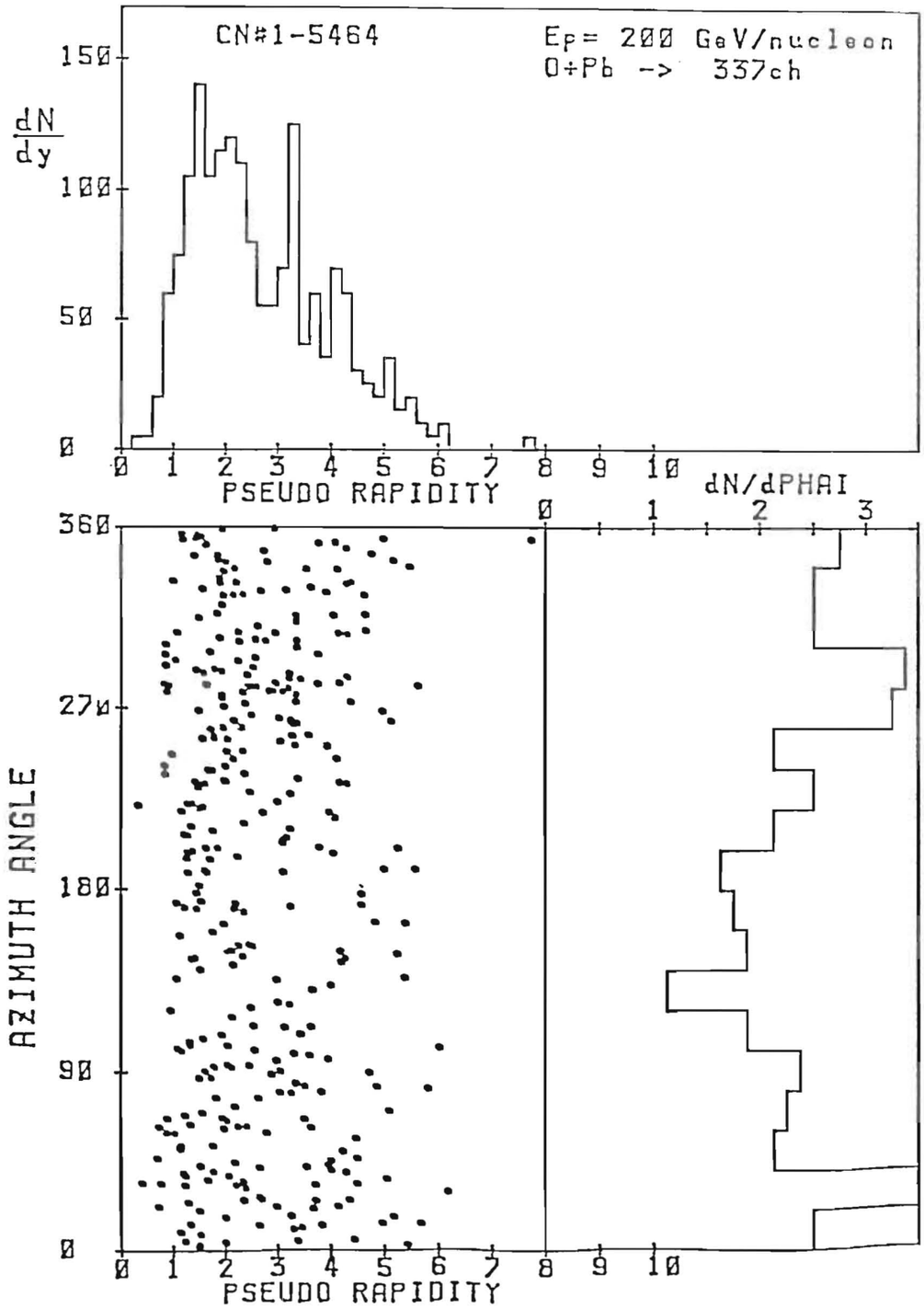
CN#1-5464
Ep= 200 GeV/nucleon
O+Pb -> 337ch
dN/dy
150
100
50
0
0 1 2 3 4 5 6 7 8 9 10
PSEUDO RAPIDITY
dN/dPHAI
0 1 2 3
360
270
180
90
0
AZIMUTH ANGLE
0 1 2 3 4 5 6 7 8 9 10
PSEUDO RAPIDITY

Fig. 10

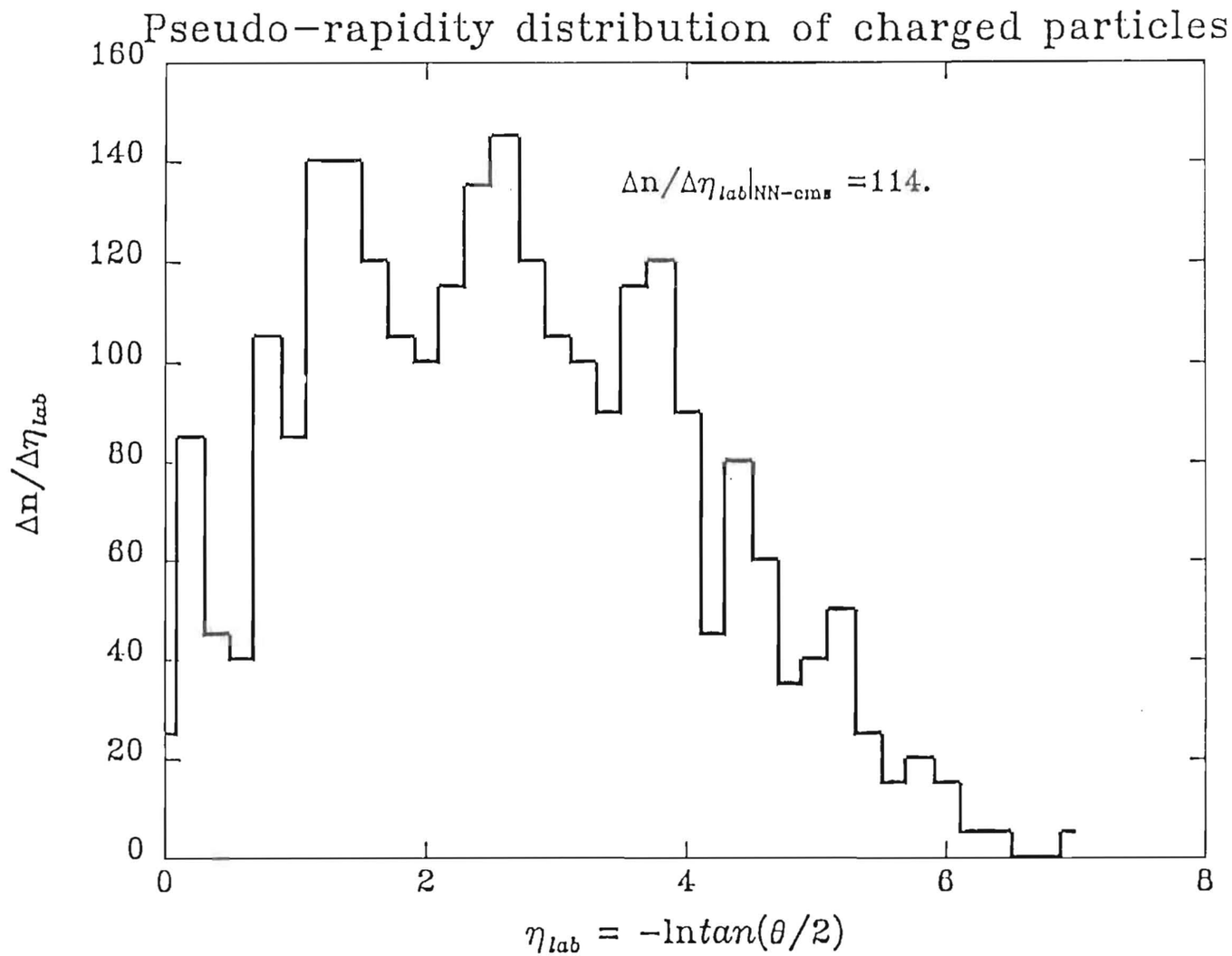
Pseudo−rapidity distribution of charged particles
$\Delta n/\Delta\eta_{lab}|_{NN-cms}$ =114.
$\Delta n/\Delta\eta_{lab}$
η_{lab} = −ln$tan(\theta/2)$
0
20
40
60
80
100
120
140
160
0
2
4
6
8

Fig. 11a

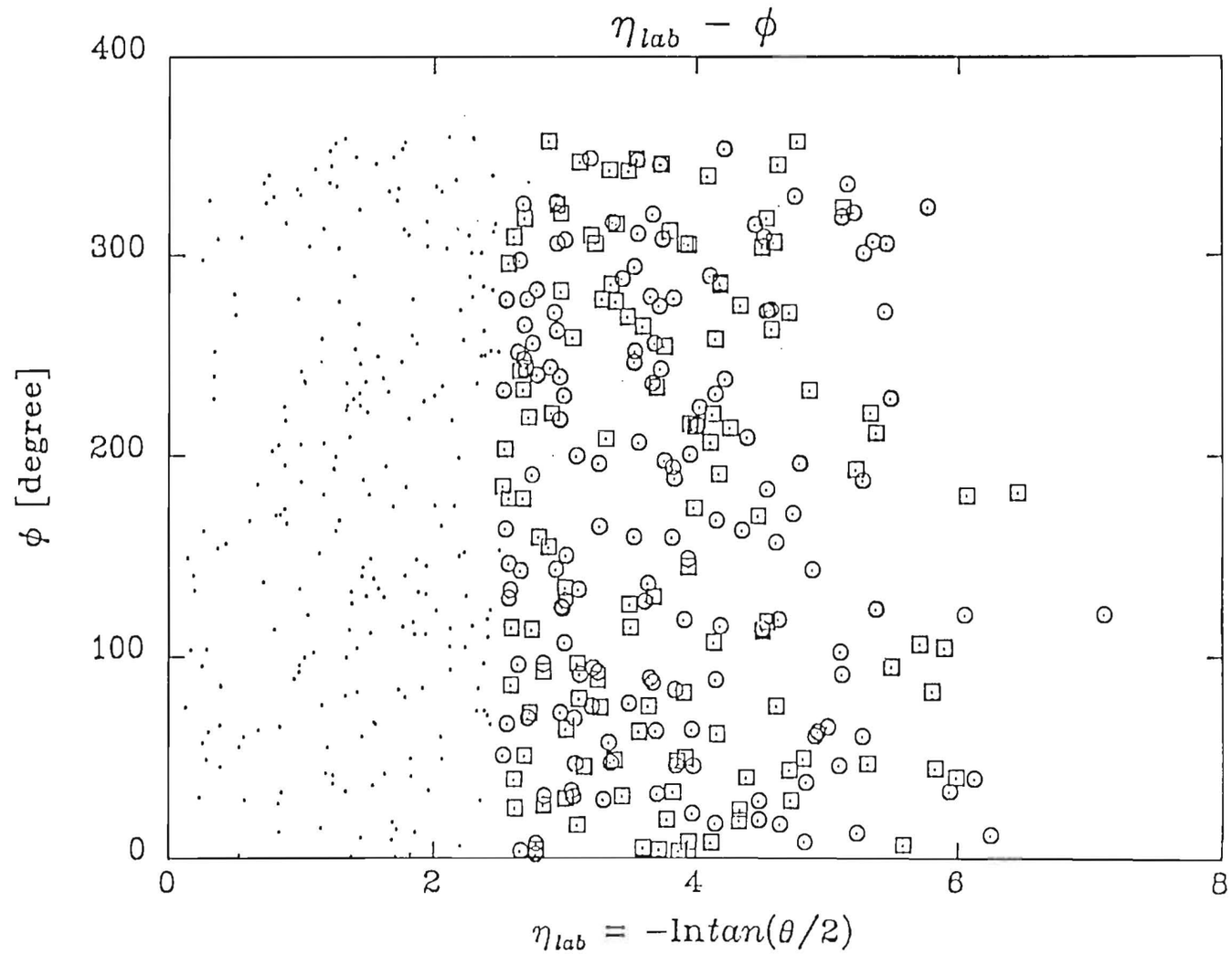
$\eta_{lab} - \phi$
400
300
200
100
0
ϕ [degree]
0
2
4
6
8
$\eta_{lab} = -\ln tan(\theta/2)$

Fig. 11b

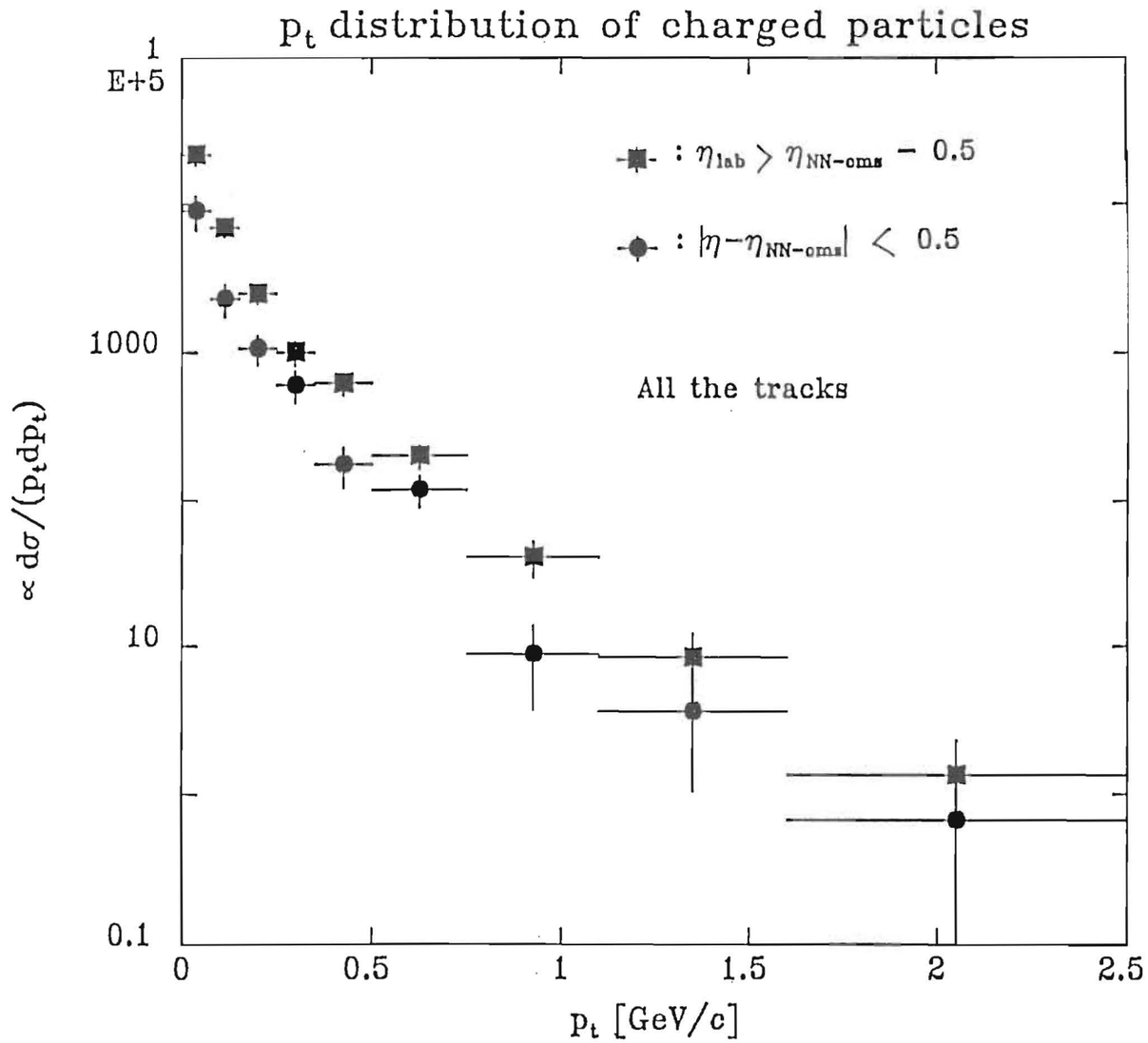
p_t distribution of charged particles
1 E+5
1000
10
0.1
$\propto d\sigma/(p_t dp_t)$
: $\eta_{lab} > \eta_{NN\text{-}oms} - 0.5$
: $|\eta - \eta_{NN\text{-}oms}| < 0.5$
All the tracks
0
0.5
1
1.5
2
2.5
p_t [GeV/c]

Fig. 12a

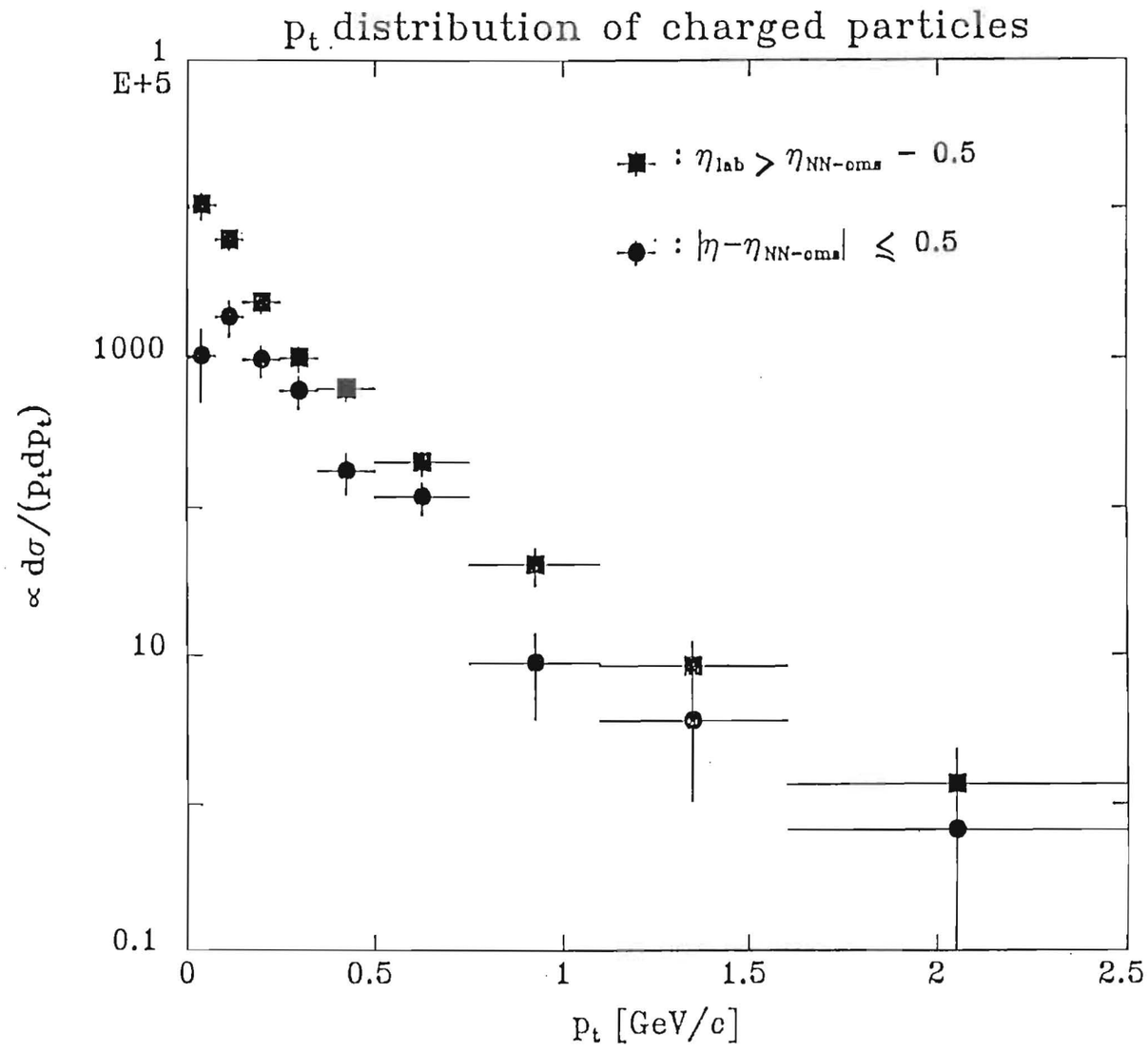
p_t distribution of charged particles
1 E+5
1000
10
0.1
$\propto d\sigma/(p_t dp_t)$
: $\eta_{lab} > \eta_{NN\text{-}cms} - 0.5$
: $|\eta - \eta_{NN\text{-}cms}| \lesssim 0.5$
0
0.5
1
1.5
2
2.5
p_t [GeV/c]

Fig. 12b

Lattice QCD at Finite Temperature

CARLETON DETAR†
Research Institute for Fundamental Physics,
Kyoto University, Kyoto 606, Japan

Recent progress in the numerical simulation of QCD at finite temperature is reviewed. Eight topics are treated briefly: (1) T_c scaling, (2) Equation of state, (3) Baryon susceptibility, (4) The QCD Phase Diagram, (5) J/Ψ Binding in the Plasma, (6) The Screening Spectrum of the Plasma, (7) Gauge Symmetry Breaking at High T, (8) Progress in Computing Power.

There are a number of excellent recent reviews of this subject. I will give only some highlights of material already contained there [1,2].

1. T_c scaling

As is well known, simulations on large lattices in quarkless QCD give hope that the deconfinement temperature T_d is approaching the asymptotic scaling prediction of the two loop beta function [3]. Simulations with quarks are less well developed. The chiral symmetry restoration temperature T_c is probably most relevant to nature. Is it scaling? Results of recent simulations [4] compiled in Fig. 1 shows that it clearly is not. Of course, there is no reason to expect a similar scaling history for these two very different physical parameters, but if it does go the same way, then we will need to double the lattice sizes before we can hope for similar improvement.

Recent simulations [5] with quarks have also studied scaling of the ratios T_c/m_N and T_c/m_ρ, shown in Fig. 2. The results are more encouraging, but since the simulations do not reproduce the correct ratio m_N/m_ρ the values for T_c are rather different, namely 135-145 MeV, using m_ρ for the scale and 108-123 MeV, using m_N for the scale. Experimentalists can take heart from these rough predictions, but until T_c/Λ is scaling properly, we can't expect other ratios to scale.

2. Equation of State

Perturbation theory predicts that the energy density ϵ and pressure p of the high temperature pure gluon plasma should be given by [6]

$$\epsilon/T^4 = \frac{8\pi^2}{15} - 8\pi\alpha_s + 128\sqrt{\pi}\alpha_s^{3/2} + \cdots$$

$$(\epsilon - 3p)/T^4 = \frac{176}{3}\alpha_s^2 - \frac{1408}{\sqrt{\pi}}\alpha_s^{5/2} + \cdots$$

In perturbation theory the plasma is a weakly interacting gas of quarks and gluons. The third term in the expansion gives the plasmon contribution to the free energy. It is known that perturbation theory breaks down at order α_s^3 in the expansion of ϵ because of infrared divergences.

These quantities can be measured in lattice gauge theory simulations. The extent of agreement with perturbation theory helps us judge the thermodynamic importance of non-perturbative or higher order perturbative effects. Of course, if agreement is found, those effects could still be important. In order to interpret results of the lattice simulations, it is important to correct for lattice discretization and finite size effects [7]. Until recently, formulas for these lattice corrections were known only for the first two terms in the perturbation expansion of ϵ. What was found can be summarized as follows: with a judicious choice of α_s the energy density ϵ for the pure gluon plasma is found to agree with the lattice corrected perturbative expression up to order α_s [1]. But the next term in order $\alpha_s^{3/2}$ has a big coefficient in the continuum expansion, and for Karsch's choice of α_s it is about the same size as the $O(\alpha_s)$ term, potentially spoiling the agreement. Recently Elze, Kajantie, and Kapusta calculated the lattice corrections for this term and found that for lattices of the size used in this comparison, it is smaller by almost an order of magnitude than the continuum prediction [8], so things now look good up to this order.

Can we now be content? No. First there is the order α_s^2 term. There is no guarantee it is small because α_s is apparently not small at the temperatures of these simulations. Second, the apparent agreement in ϵ in the pure gluon plasma might be fortuitous, since comparisons with ϵ and $\epsilon - p$ in simulations with quarks [9] show strong disagreement, especially near the phase transition, as shown in Fig. 3, taken from the review by Karsch [1].

3. Baryon Susceptibility

Recent simulations with light quarks have measured a new and useful quantity, namely the baryon susceptibility of the quark plasma; i.e. the rate of change of the baryon density with respect to baryon chemical potential [10].

$$\chi_B(T) = \frac{\partial}{\partial \mu_B} < \rho_B(\mu_B) >$$

This quantity gives a measure of the ease with which non-zero baryon number can be excited in the plasma. With present techniques such simulations are possible only at zero baryon chemical potential. This quantity also reveals some thermodynamic properties of the plasma. In the naive model of high temperature QCD, one expects baryon excitation at low temperature to be suppressed by the Boltzmann factor $g \exp(-m_N/T)$. (The degeneracy factor g is 4 for the nucleon.) In a high temperature ideal gas the susceptibility would be $N_f T^2$ for N_f flavors of massless quarks. Indeed simulations (Fig. 4) show an impressively sharp rise in the susceptibility at the phase transition in agreement with the naive expectation. Thus either the relevant baryonic plasma degrees of freedom are very light, or their multiplicity g is considerably greater in the high temperature plasma.

4. Phase Diagram for QCD

Knowing the phase diagram for QCD helps in understanding the composition of the plasma. It has been argued that if there is a "window" in the phase diagram permitting smooth passage from the low temperature phase to the high temperature phase, then it necessarily follows that the modes of excitation of the plasma are color singlets [11]. The phase diagram is multidimensional, of course, depending on the quark masses m_i, chemical potentials μ_i, and the temperature T. Thus far, simulations have been made only in a two-dimensional $m - T$ plane with all quark masses equal, but at a variety of flavors N_f. Simulations are under way with two quark masses varied. At present there is some evidence that a window exists, but there is still considerable controversy [2,4,12]. Some results for $N_f = 4$ are shown in Fig. 4. Exact simulations on a small lattice (4^4) show no window. Simulations using the Langevin method find a smaller window than simulations using the hybrid method. Clearly much more work needs to be done to resolve algorithm biases and finite size effects before this issue is settled [2].

Recent work by Fukugita and Ukawa suggests that if there is such a window, it may be a feature of only $N_f = 2, 3, 4$ quark flavors [13]. For $N_f = 1$ they find that the window, if it exists at all, must occur at quark masses smaller than $0.05/a$ in lattice units.

5. J/Ψ Binding in the Plasma

Lattice simulations can give the free energy $F_{q\bar{q}}$ of a static test quark pair in the thermal ensemble. This quantity is used in Born- Oppenheimer approximation to give the binding energy of the heavy quark system in the thermal ensemble. Elementary quantum mechanics tells us that if the free energy is of the form

$$F_{q\bar{q}}(r,T) = b(T)\frac{e^{-m_D(T)r}}{r} + 2F_0(T) \ , \tag{5.1}$$

then there is no binding if

$$m_D(T) > 1.68 m_c b(T),$$

where m_c is the mass of the charmed quark and $m_D(T)$ is the inverse color singlet Debye screening length [14]. Previous simulations have determined $m_D(T)$ to be approximately $3T$. It remains to determine the rest of the potential over the range important to the wave function. The actual form of the potential for all r is certainly not as simple as the above asymptotic term. Although high statistics simulations of the charmonium potential have been done for the pure gluon plasma at zero temperature, no comparable simulations exist for the pure gluon plasma at high temperature or for the plasma with quarks.

Recent results by Faber et al [15] for the quark plasma at high temperature are shown in Fig. 5. Reading numbers from these graphs is not easy, but assuming the asymptotic form (5.1) applies for all r and putting $m_D = 3T$, I estimate $b \approx 0.1$. Putting $m_c = 1.5$GeV, $m_D = 3T$, and $T = 150$ MeV gives 500 MeV for the left side of the inequality and 260 MeV for the right side, favoring dissociation of the heavy quarks. Many caveats go with this conclusion: one should at least use the unpublished numbers in fitting for $b(T)$ and $m_D(T)$; we don't know whether the free energy is scaling; we don't know whether the Born-Oppenheimer method is valid here.

The discussion period that followed this talk dealt with the significance of recent experimental results showing a drop in the J/ψ signal over background [16]. A summary of my view is given here:

The experimental issue to be clarified is whether the effect seen is due to a rise in background or a decrease in signal or both. If, indeed, there is a decrease in signal, what does it mean? There are a variety of processes in an ordinary hadron gas that lead to transitions between the J/ψ and other charmed states, including the open charm $D\overline{D}$ channels. Similar excitations reduce the binding strength of the free energy of a static quark pair [17]. Thus the weakening of the signal does not confirm deconfinement. However it is a useful indicator of possible thermal processes in the high temperature plasma.

6. Screening Spectrum

The screening spectrum of the plasma gives indirect information about the plasma normal modes, which are important in models. The screening spectrum is found by measuring Euclidian space-time correlations between currents of various quantum numbers at large space-like separation:

$$S_{AB}(z) = \int dxdy \int_0^\beta d\tau < A(\overrightarrow{0},0)B(x,y,z,\tau) >$$

for local operators A and B. At large separation

$$\overline{S}_{AB}(z) \underset{z\to\infty}{\sim} b(T)\exp[-\mu(T)z] \ .$$

The screening mass $\mu(T)$ is the important quantity. One question of interest is to determine in what manner the chiral symmetry is restored at high temperature. This is done by determining the screening masses in the limit of zero quark mass. (For technical reasons, it is not possible with present methods to carry out a simulation at precisely zero quark mass.) If the SU(N)×SU(N) chiral symmetry is restored then, for example, the screening masses $\mu_\pi(T)$ and $\mu_\sigma(T)$ for the π and σ should be degenerate at high temperature in the chiral limit. In Fig. 6 results for a recent simulation are shown [18]. Results are consistent with a restoration of SU(N)×SU(N). Moreover, it is found that in the baryon sector the symmetry is realized in the parity doubling mode, rather than zero mass mode.

These results have also been found by the San Diego, Santa Barbara, Indian group, using essentially the same fermion algorithm, but different, more powerful methods to analyze the propagators [19].

The measurement of the effects of color singlet modes in the quark plasma may come as a surprise to some. Their existence should be associated with color singlet real-time excitations, just as Debye screening in QED is associated with the plasmon excitation. All such modes should have a finite lifetime due to collisional processes. Unfortunately, there are no prospects for doing real-time lattice simulations to tell us what the lifetime should be. Therefore, we don't know whether these excitations are only of academic interest, or they are sufficiently long-lived to have experimental consequences. At least their appearance in screening simulations suggests that one should look for them in experiments. It won't be easy to find them, however.

7. Gauge Symmetry Breaking

In pure SU(3) gauge theory the Polyakov loop

$$L = Tr\Omega$$

where

$$\Omega = P\exp\left(i\int A^o(\tau,\vec{x})d\tau\right) \in SU(3)$$

is the order parameter for the high temperature phase transition. The matrix Ω is also related to a Higgs field in the adjoint representation of SU(3) in the high temperature three-dimensional reduction of the theory. Over the past few years there has been some interest in whether this Higgs field develops a non-vanishing expectation value, signaling a breakdown of the gauge symmetry, and, depending on the symmetry breaking pattern, the appearance of monopoles [20]. There are three parts to this unfinished story.

7.1 Old Story: Global Z(3) Breaking

The gauge symmetry of the functional integral

$$L \to e^{2\pi i n/3}L \qquad n = 0, 1, 2$$

is an exact symmetry for the confined phase, but a spontanteously broken symmetry of the deconfined phase. This is the widely accepted reason for the phase transition in the pure gauge theory.

7.2 Newer Story: SU(3) → U(1)×U(1)

Although Ω is not gauge invariant, its eigenvalues are. Defining

$$\mathrm{diag}\Omega = \exp(i\phi\lambda_3 + i\nu\lambda_8) \ ,$$

Polonyi and Wyld found in a pure gauge theory simulation that $< \phi > \neq 0$ in the deconfined phase, but that $< \nu >$ was apparently zero [20,21]. To extract the probability distribution for ϕ is tricky and requires a careful statistical analysis. Thus the result certainly needs to be confirmed and understood.

7.3 Newest Story: SU(3) → SU(2)×U(1)

Recently Mandula and Ogilvie carried out a simulation in the pure gluon plasma, fixing Landau gauge [22]. With their gauge fixing procedure, the quantity

$$\mu_n = Tr\left(< \int dx d\tau A_0(x,\tau) >^n \right)$$

is invariant and can be measured. However, they found the opposite symmetry breaking pattern, associated with a vanishing $< \phi >$ and non-vanishing $< \nu >$. This result is surprising, since it would presumably lead to a breakdown of color hypercharge reversal, i.e. it would distinguish between quarks and antiquarks [21].

This bizarre story needs to be resolved, and the effect of quarks on the symmetry, both at low and high temperatures needs to be understood.

8. Computing Power

In Table 1 I have tried to summarize the computing power of a variety of supercomputers and processors in order to get a rough assessment of current progress in computing power. The comparison of link update times on pure SU(3) gauge theory is somewhat misleading, since the comparison depends on the skills of the programmer and on the algorithm chosen. Ideally, one should be comparing time required to obtain a particular result with a given variance, using the best algorithm suited for the machine. However, this is not intended to be a "buyer's guide".

A few comments are in order. The world record speed for link updates on a single processor appears to be that of Berg et al [23] at 9μsec per link update on the ETA-10. One can get a faster time by running simultaneously on more than one processor. De Forcrand et al report a time of 6μsec on the Cray X-MP/48 with all four processors in operation [24]. However, this speedup over a single processor entails an algorithm synchronization loss of about 10%. Since most simulations involve making several runs with different starting configurations and different parameters, there is no particular advantage to this mode of operation, unless memory limitations prevent running four separate jobs at once.

As everyone knows, raw processor power isn't the only measure of a computer's power. Thus the 64-node Columbia machine with 20% more processor power than the four-processor Cray-XMP/48 takes 18 μsec compared with de Forcrand's 6. Architecture and memory speed is also obviously important, and one would hope that a specialized machine could optimize these features for the problem it is particularly designed to solve.

How much computing power do we need? Suppose our next goal is to do a decent T_c scaling demonstration with dynamical quarks, and suppose with luck we could achieve this on lattice comparable to the ones used for the pure gluon phase transition. [3] Those calculations were done on the Cyber 205 and Columbia 16 node machine. Experience with current fermion algorithms suggests that we need at least 50 to 100 times as much power, depending on quark mass to get results with comparable statistics. Therefore, if we are lucky, we need a supercomputer with 20 to 40 GFlops. We see that with the new machines computing power is moving into the multi-GFlop range now, but more is probably needed, still.

9. Conclusions

Highlights of recent progress are these: (The question mark shows the need for considerable further work to settle the issue.)

- We are starting to guess at the value for T_c with dynamical quarks (?)
- The equation of state for quark matter shows substantial departures from ideal gas behavior, at least close to T_c (?)
- We see a large rise in the baryon suceptibility at T_c.
- There is a window in the $m - T$ phase diagram (?)
- Preliminary indications of the strength of the high temperature heavy quark-pair free energy would suggest in the Born-Oppenheimer approximation that the J/Ψ is unbound above T_c (?)
- In the chiral limit the screening spectrum of the plasma is consistent with a restoration of SU(N)×SU(N) chiral symmetry with parity doubling in the baryon sector.
- Is there gauge symmetry breaking at high temperature (??)
- Bigger computers are on the way.

In the following areas no progress has been made:

- Finite baryon density simulations
- Real time, finite temperature simulations

We may look forward to:

- Removing the (?) above with the help of more supercomputing power.

Acknowledgements

I would like to express my sincere appreciation to my colleagues in Japan for their warm hospitality and for lively discussions of physics during my sabbatical year.

Supercomputing Power of Some Existing and Planned Machines

Machine	GFlops	RAM	Pure SU(3) Size	Pure SU(3) Time/Link	Source
(General Purpose; A few, fast processors)					
Cyber 205(2)	0.40	32MB	$19^3 \times 14$	19μsec	Gottlieb et al [3]
HITAC S810/10	0.38	128MB	$16^3 \times 48$		
NEC SX-1	0.58	128MB		35μsec	
CRAY X-MP/48	0.84	64MB	$24^3 \times 48$	22μsec [a]	de Forcrand et al [24]
ETA-10E	3	1GB	$8^3 \times 64$	9μsec [b]	Berg et al [23]
NEC SX-2	1.3	252MB	16^4	13.5μsec	Osada [25]
CRAY 2	2				
CRAY YMP	3				
HITAC S820	3	512MB			
CRAY 3	10	1GW			
(Multiprocessor)					
QCD-PA-X	few	several GB			Iwasaki et al [26]
Columbia(16)	0.256		$16^3 \times 14$	140μsec	Christ et al [3]
INFN/APE(4)	0.256	64MB	$16^3 \times 32$	50μsec [c]	Parisi et al [27]
INFN/APE(16)	1	256MB			
ACPMAPS(16)	0.320	160MB			MacKenzie et al [28]
ACPMAPS(256)	5				
Columbia(64)	1	128MB	$24^3 \times 48$	18μsec	Deng [29]
Columbia(256)	4				
IBM GF-11(566)	11.3	1.13GB			Beetem et al [30]
(Array Processor)					
ST-100	0.1			105μsec	Gottlieb et al [3]
VP200	0.5			$\leq$ 20μsec	Deng [29]

a With only one of four processors in use. With all four, 6μsec.
b With only one of four processors in use
c Metropolis algorithm, 5 hits

References

[1] F. Karsch, "Lattice QCD at Finite Temperature: A Status Report", Sixth International Conference on "Ultrarelativistic Nucleus-Nucleus Collisions", 24–28 August, Nordkirchen, West Germany.

[2] M. Fukugita, "Lattice Chromodynamics with Dynamical Quarks", International Symposium "Field Theory on the Lattice", Seillac, France, 28 September – 2 October, 1987.

[3] A.D. Kennedy, J. Kuti, S. Meyer, and B.J. Pendelton, Phys. Rev. Lett. **54**, 87 (1985); S.A. Gottlieb, A.D. Kennedy, J. Kuti, S. Meyer, B.J. Pendelton, R. Sugar, and D. Toussaint, Phys. Rev. Lett. **55**, 1958 (1985); N. H. Christ and A.E. Terrano, Phys. Rev. Lett. **56**, 111 (1986).

[4] F. Karsch, J.B. Kogut, D.K. Sinclair and H.W. Wyld, Phys. Lett. **188B**, 353 (1987); E.V.E. Koracs, D.K. Sinclair, and J.B. Kogut, Phys. Rev. Lett. **58**, 751 (1987).

[5] S. Gottlieb, W. Liu, and R.L. Renken, R.L. Sugar and D. Toussaint, Phys. Rev. Lett. **59**, 1513 (1987).

[6] J. Kapusta, Nucl. Phys. B**148**, 461 (1979).

[7] U. Heller and F. Karsch, Nucl. Phys. B**251**, 254 (1985); Nucl. Phys. B**258**, 29 (1985).

[8] H.-Th. Elze, K. Kajantie, and J. Kapusta, University of Helsinki report, HU-TFT-88-1 (1988).

[9] S. Gottlieb, W. Liu, D. Toussaint, R.L. Renken, and R.L. Sugar, Phys. Rev. D**35**, 3972 (1987).

[10] S. Gottlieb, W. Liu, D. Toussaint, R.L. Renkin, and R.L. Sugar, Phys. Rev. Lett. **59**, 2247 (1987).

[11] C. Chen, C. DeTar, and T. DeGrand, Phys. Rev. D**37**, 247 (1988).

[12] M. Fukugita and A. Ukawa, Phys. Rev. Lett. **57**, 503 (1986); R. Gupta et al., Phys. Rev. Lett. **57**, 2621 (1986); J. Polonyi et al., Phys. Rev. Lett. **53**, 644 (1984); S. Gottlieb, W. Lin, D. Toussaint, R.L. Renken, and R.L. Sugar, Phys. Rev. D**35**, 3972 (1987); R.V. Gavai, J. Potvin, and S. Sanielevici, Phys. Rev. Lett. **58**, 2519 (1987).

[13] M. Fukugita and A. Ukawa, Phys. Rev. Lett. **60**, 178 (1988).

[14] T. Matsui and H. Satz, Phys. Lett. **178B**, 416 (1986).

[15] M. Faber, P. de Forcrand, H. Markum, M. Meinhart, and I. Stamatescu, Phys. Lett. **200B**, 378 (1988).

[16] A. Brussiere (NA38 Collaboration), *op. cit.* Ref. 1.

[17] O. Miyamura (1987, unpublished); M. Gyulassy et al., Lawrence Berkeley Laboratory report (1988); C. DeTar, Phys. Rev. D (1988, to be published).

[18] C. DeTar and J.B. Kogut, Phys. Rev. Lett. **59**, 399 (1987); Phys. Rev. D **36**, 2828 (1987).

[19] S. Gottlieb, W. Liu, D. Toussaint, R.L. Renken, and R. L. Sugar, Phys. Rev. Lett. **59**, 1881 (1987).

[20] S. Nadkarni, Phys. Rev. Lett. **60**, 491 (1988).

[21] J. Polonyi and H.W. Wyld, University of Illinois at Urbana-Champaign Report No. ILL-TH-85-23 (1985); J. Polonyi, in *Advances in Lattice Gauge Theory*, ed. D. Duke and J. Owens (World Scientific, Singapore, 1985).

[22] J.E. Mandula and M. Ogilvie, Phys. Lett. **201B**, 117 (1988).

[23] B. Berg, A. DeVoto, and C. Vohwinkel, Florida State University report, FSU-SCRI-87-56 (1987).

[24] P. de Forcrand, in *Lattice Gauge Theories, a Challenge in Large Scale Computing*, ed. B. Bunk et al., NATO Advanced Studies Institute Series B**140** (Plenum, New York, 1985).

[25] Y. Osada, private communication, (1987). (This algorithm is currently under development. I thank Yasuhiro Osada for providing his most recent figure.)

[26] Y. Iwasaki, T. Hoshino, T. Shirakawa, Y. Oyanagi, and T. Kawai, Tsukuba report UTHEP-176 (1987).

[27] G. Parisi in *Lattice Gauge Theory Using Parallel Processors*, ed. Xiaoyuan Li, Zhaoming Qiu, Hai-Cang Ren (Gordon and Breach, New York, 1987).

[28] P. MacKenzie et al., Fermilab report FERMILAB-Conf-214-T (1987).

[29] Y. Deng in *op. cit.*, Ref. 27.

[30] J. Beetem, M. Denneau, and D. Weingarten in *op. cit.*, Ref. 24.

Figure Captions

1. The deconfinement temperature T_d/Λ_L, [3] and the chiral symmetry restoration temperature T_c/Λ_L, Ref. [4] as a function of lattice size.

2. The chiral symmetry restoration temperature using the lattice nucleon for the mass scale, as a function of lattice size from Ref. 5. Upper points: T_d in quenched aproximation. Lower points with solid circles: T_c.

3. The energy density (open squares) and pressure (solid circles) of the quark plasma in units of T^4 as a function of gauge coupling $\beta = 6/g^2$ (which 9 increases with temperature) from Refs. 1,9. The dashed line gives the lattice corrected energy density to $O(\alpha_s^0)$ and the dot-dashed line, $O(\alpha_s^1)$.

4. Phase diagram for QCD with four quark flavors in quark mass vs gauge coupling. If evidence for a first order phase transition is reported, a solid line is shown. Otherwise a dotted line indicates the crossover region. Symbols for the central value distinguish various references [12] : Open circles (Gupta et al - exact algorithm), closed circles (Fukugita et al - Langevin algorithm), open triangles (Karsch et al and Kovacs et al - hybrid algorithm), closed

triangles (Gottlieb et al - hybrid algorithm), open squares (Gavai et al - Langevin algorithm).

5. Quark - antiquark free energy as a function of separation in the quark plasma at fixed gauge coupling β and varying quark mass. The top points correspond to the low temperature phase and the rest, the high temperature phase.
6. Screening masses in the chiral limit.

Fig.1

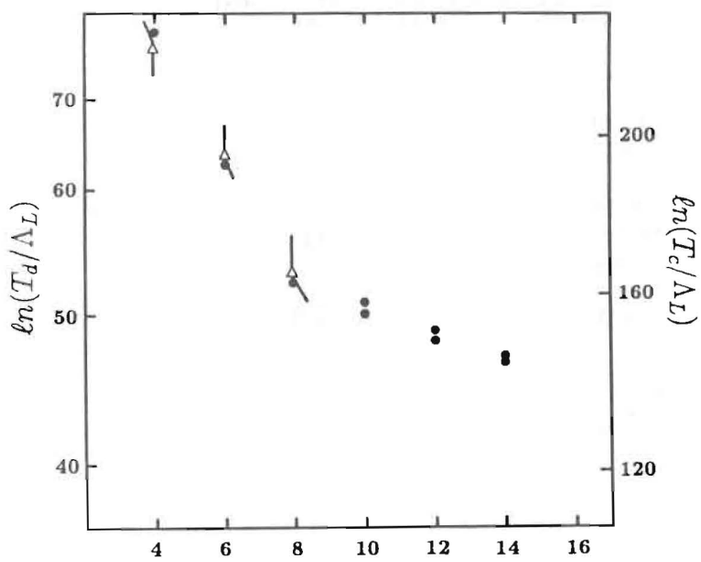

Fig.2

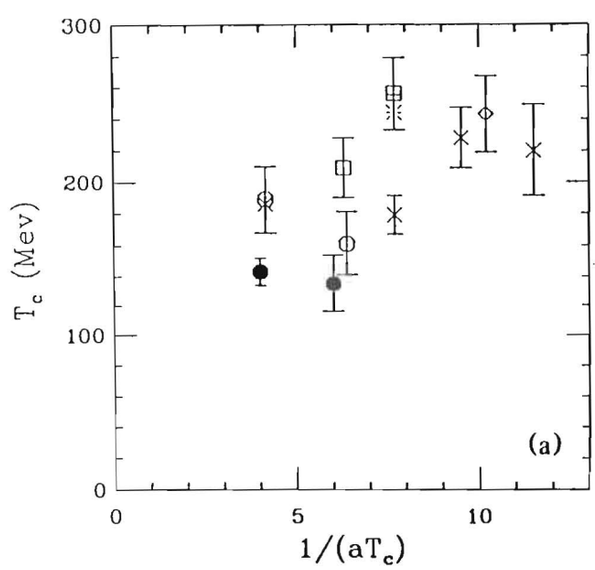

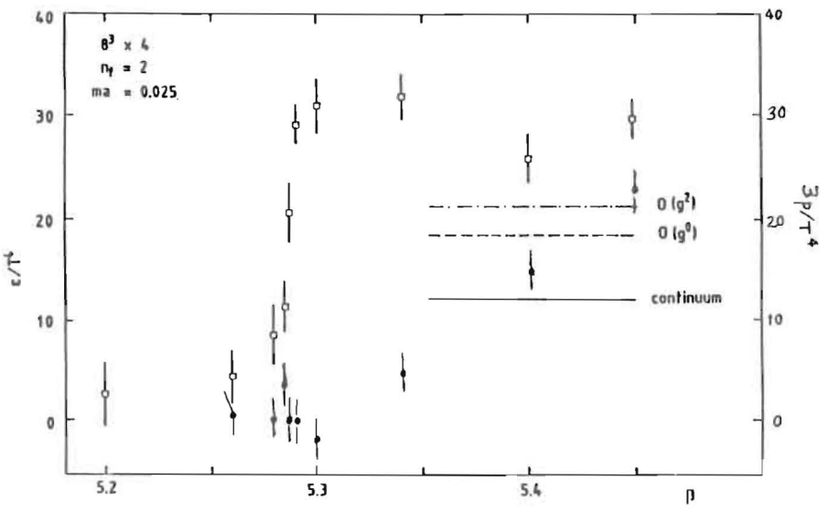

Fig.3

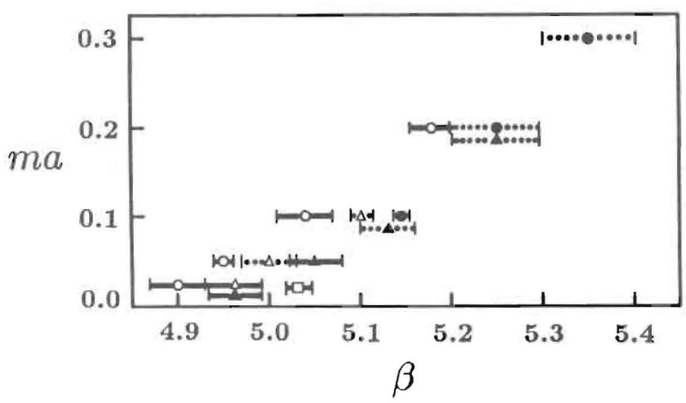

Fig.4

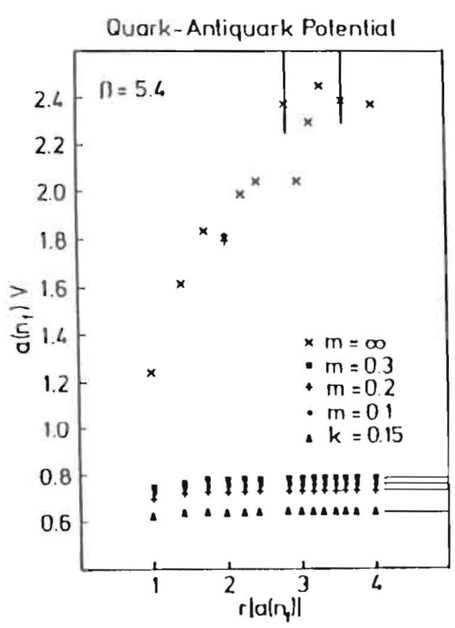

Fig.5

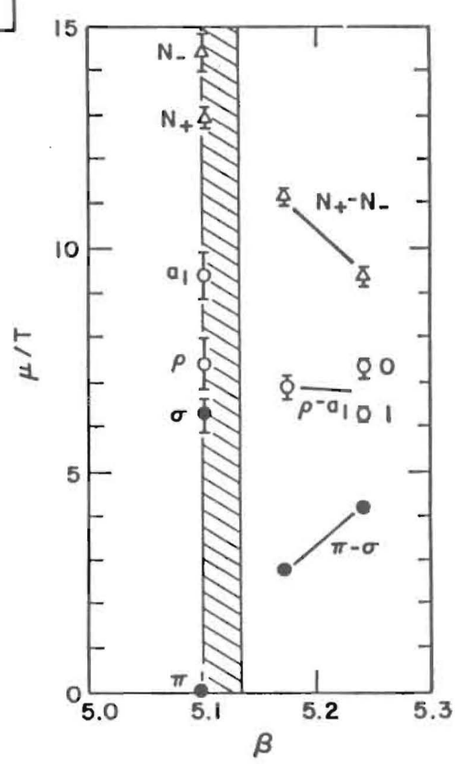

Fig.6

Hadrons at Finite Temperature

TEIJI KUNIHIRO

Department of Natural Sciences, Ryukoku University, Fukakusa,Kyoto 612

ABSTRACT

Character changes of pion and $\sigma-$meson associated with the chiral transition at finite temperature are examined on the basis of a QCD-motivated effective Lagrangian for the 2-flavour case. Brief discussions are also given on behaviours of scalar- and vector-mesons containing s-quarks and of the baryons at finite temperature.

1. Introduction

The world of strong interactions is characterized by some qualitative features such as confinement of colored quarks and gluons, spontaneous breaking of chiral(χ) symmetry, the chiral $U_A(1)$-anomaly, the OZI-rule and vector-meson dominance. The quantum chromodynamics (QCD) is now believed to be the fundamental theory of the strong interactions. It is very important that the confinement and chiral symmetry breaking(χSB) can be understood as phase transitions of the QCD vacuum. Recent studies based on effective theories of QCD[1,2,4,5,8] and the numerical simulations of the lattice QCD[10,11,12,13] have been revealing some characteristic features of the phase transitions. In the light of these development as well as the renormalization-group argument[15,43], the deconfined and chirally symmetric phase, the quark-gluon plasma(QGP) phase, was sure to be realized in the early universe, may exist in deep interior of the neutron stars if the central densities of the stars can be dense enough and also will be produced by the ultra-relativistic heavy ion collisions.

There have been active studies not only on the QGP itself but also the properties of hadronic matter at finite temperature(T) and/or the baryonic density or the chemical potential(μ).[14] Fundamental problems one shoud answer first in studying these systems are: what are the elementary excitations characterizing the system and how do they change their properties as T and/or μ are varied ? Answering these questions has been always the starting point to obtain the characteristic features of matter in condensed-matter physics and of nuclei in nuclear physics. In this talk, we concentrate on the $\chi-$ transition.†

Some years ago collective excitations in the Wigner phase above the critical temperature ($T_\chi \simeq 200$MeV) of χ-transition were examined[1]: It was found that

† It is also certainly important to examine how the confinement-deconfinement transition reflects in the excitations(hadrons) at high T. In this respect, J/Ψ at high T has been recently attracting much attention[18]. It would be also interesting to see how the qualitative features of the strong interactions other than the confinement and χSB (i.e.,the $U_A(1)$-anomaly, the OZI-rule and vector-meson dominance) change or persist under changes of the environment(temperature and/or the baryon density).

the color-singlet excitations, the counterpart of pion and σ meson in the QGP phase, exist as elementary modes as well as the liberated quarks and gluons near the critical point and they would soften as the system approaches the transition point. They correspond to the fluctuations of the order parameter $\langle\langle\bar{q}q\rangle\rangle$ and have small widths near T_χ if the χ-transition is of second or weak first order. T. Hatsuda and I have argued that they contribute to the cooling of a droplet of the QGP which will be formed in the intermediate stages of the relativistic heavy-ion collisions.

The elementary modes in the broken phase of χ-symmetry are well known; pion and σ-meson. Pion can be understood as the phase-fluctuation of the order parameter $\langle\langle\bar{q}q\rangle\rangle$ and is the well-known Nambu-Goldstone(NG) boson of the χSB. σ-meson is an amplitude fluctuation of the order parameter and have the mass $\sim 600MeV \sim 2M$, where M is the constituent-quark mass of the light quarks. One of the purposes of the present talk is to seek characteristic phenomena associated with the $\chi-$ trnsition, focusing our attention on the temperature dependense of the properties of the meson excitations, especially pion and σ-meson.[4,6,7]

Wait!, somebody may scream: Does such a light σ-meson exist, because the $\pi-\pi$ phase shift in $I = J = 0$-cahnnel shows attractive but no resonanse behaviour below the $K\bar{K}$ threshold ? Yes, we can believe the existence of σ. The reasoning of it is described as follows: First of all, we note that the very spontaneous breaking of χ-symmetry implies the σ-degree of freedom; $\langle\langle\bar{q}q\rangle\rangle \sim \sigma$ is the order parameter of the χSB and the σ-meson is nothing but the amplitude fluctuation of the order parameter as mentioned above. Therefore, it is natural that the lattice calculation of QCD yield the σ-meson with a rather small mass.[17] It may be said that the σ-meson is analogous to the Higgs mesons in thr Glashow-Weinberg-Salam theory. Furthermore, analyses of nuclear forces claims the need for the light iso-scalar scalar meson with mass 500$\sim$ 600 MeV.[19] As for the $\pi-\pi$ phase shift, we notice the width Γ of σ due to the process $\sigma \to \pi\pi$. The process gives a large width $\sim$ 450 MeV at T=0, in our calculation. The large mass can account for the absense of the clear σ-resonance below $\sim$1GeV.[20] Re-

cent analyses of the $\pi - \pi$ and γ-γ scatterings[21,22] seem to support the above picture.† We will show that the validity of the picture could be tested if the temperature of the system is raised: σ should appear as a sharp resonance at T$\neq$ 0 because the phase space for the decay $\sigma \rightarrow \pi\pi$ is suppresed.

Effective Lagrangian Approach: Indeed, it is desirable to investigate the $q\bar{q}$ collective modes starting from the continuum or lattice QCD. They are, however not so developed at present that one can deduce the dynamical aspects of the system reliably enough.‡ Therefore, we start with the following QCD-motivated effective Lagrangian of the Nambu-Jona-Lasinio (NJL) type[24,26,25], which reproduce the low-energy phenomena related with chiral symmetry at T=0[30,2,7,27]:

$$\mathcal{L} = \bar{q}(i\gamma \cdot \partial - \bar{m})q + g[(\bar{q}q)^2 + (\bar{q}i\gamma_5\tau q)^2], \tag{1.1}$$

where $\bar{m}$ is an averaged value of the current quark masse ($\bar{m} \simeq 5.5$ MeV). We assume the flavour $SU_f(2)-$ symmetry, then $m_u = m_d$. (1) can be regarded as an effective Lagrangian obtained by integrating out the long-range fluctuations of gluons.[28,29] There are some works which show that the Lagrangian of the NJL-type can be "derived" directly from QCD.[31,34,35,33] The Lagrangian is not renormalizable, hence a "cutoff" must be introduced. The "cutoff" in turn has a solid meaning in our case[36,2,7]: It is the energy scale separating the short-range asmptoticaly free and the long-range non-perturbative region. Thus the value of the cutoff can be determined from observables.

(1) has already been examined rather extensively for T=0[2,7]: The dynamical quark mass, the quark condensates in the vacuum and the properties of the NG-boson (π) have been found to be good agreement with the phenomenology and those obtained from a semi-phenomenological appproach such as the QCD sum- rule approach.[9]

† More extensive discussion on reality of σ-meson is given in Ref.[7].
‡ Nevertheless, see Ref. 23.

It is noteworthy that the phenomenological success of (1) mentioned above is of cource not a coincidence: Integrating out the quark fields, one gets a chiral Lagrangian including the Wess-Zumino-, Skyrme- and other higher derivative terms.[28,29,32] Such a chiral Lagrangian is known to well describe the low-energy hadron dynamics.

It should be noted that the confinement of quarks is not implemented in (1).† Nevertheless, it can be simulated by assuming that the colored quarks with constituent mass appears only in the internal lines. This treatment is justified if the gluons have the propagator of the form $1/q^4$.[38,39]

The Lagrangian has two free parameters, a momentum cutoff Λ and the couling constant g. They can be determined so as to reproduce the experimental values of the pion decay constant and the pion mass (at T=0). The results are

$$\Lambda = 631\, MeV \ and \ g = 0.214\, fm^2,$$

by which, phenomenologically reasonable values are obtained for the quark condensate ($\langle \bar{u}u \rangle \simeq (-250\, MeV)^3$), the quark-pion couploing constant ($G^2_{\pi q}/4\pi \simeq 1.$) and the constituent mas of u and d quarks ($M_u = M_d \simeq 335 MeV.$) Although, the coupling constants and cutoff may have T-dependence, we will assume that the T-dependence can be neglected.

† The fact that the theory without the confinement could describe the low energy phenomena related with chiral symmetry may imply that the quark condensates and the NG-bosons and the would be the NG-boson[5] are determined almost only by the dynamics contained in (1.1)and (5.1), and the confinement hardly affects these observables.[30,37,2] If this is the case, it is very likely that a deconfined but chirally broken phase exists in the phase diagram of QCD, and there low-enegy phenomena related with chiral symmetry would not be so changed from those at $T = 0$. The results in Ref. [1] might be seen as a description of such a phase. The above picture has been recently argued vigorously by Asakawa and Yazaki[42].

2. Determination of the equilibium state: dynamical quark mass and the qurk condensates

The temperature-dependent quark mass $M(T)$ of the quarks are determined from the self-consistency condition (SCC) or the Dyson equation in the finite-temperature Hartree-Fock theory,

$$M(T) = \bar{m} + M_D(T), \tag{2.1}$$

where $M_D(T) = -2g\langle\langle\bar{q}q\rangle\rangle$ is the dinamical quark mass and $\langle\langle O\rangle\rangle$ denotes the thermal average of the operator O;

$$\langle\langle O\rangle\rangle = \mathrm{Tr}\,(e^{-\beta H}O)/\,\mathrm{Tr}\,(e^{-\beta H}). \tag{2.2}$$

The r.h.s. of eq.(2.1)can be nicely evaluated with use of the temperature Green's function $\mathcal{G}_0(\tau, \mathbf{x})$;

$$\langle\langle\bar{q}q\rangle\rangle = tr\mathcal{G}_0(0+, \mathbf{x}) \tag{2.3}$$

Here tr denotes the trace operation with respect to the color, flavor and spin indices. The Fourier transform of $\mathcal{G}_0(\tau, \mathbf{x})$ reads as

$$\mathcal{G}_0(p^0, \mathbf{p}) = [\not{p} - M(T)]^{-1}, \tag{2.4)0}$$

with $p^\mu = (i\nu_n^F, \mathbf{p})$ and $\nu_n^F = (2n+1)\pi T$ being the Matsubara frequency for fermions. It easily sean that the SCC (eq. (2.1)) is reduced to the " gap equation",

$$1 - \bar{m}/M = 2gN_CN_f/\pi^2 \cdot \int_0^\Lambda d|\mathbf{p}|\mathbf{p}^2 f(E)/E, \tag{2.5}$$

where $E = \sqrt{M^2 + \mathbf{p}^2}$ and $f(E)$ is given in terms of the quark and anti-quark distribution function $n(E) = (\exp(\beta E) + 1)^{-1}$;

$$f(E) = 1 - 2n(E). \tag{2.6}$$

Here, the following remarks are in order: One can see that the integral in eq. (2.5)becomes small as T increases if $M(T)$ is fixed, because $f(E) < 1.$ for $T \neq 0$.

The mean-field approximation of the NJL-model which we have adopted leads to a typical second order chiral transition at finite temperature in the case of $\bar{m} = 0$.[43,2] For $\bar{m} \neq 0$, the transition turns to a crossover one and $\langle\langle\bar{q}q\rangle\rangle$never vanishes.[1,7] The numerical simulations of the lattice QCD suggest that the transition is of first order for light quarks.[10,11,12,13] Nevertheless, it is noteworthy that the gross feature of the T-dependence of the quark condensates of ours are very similar to those in the lattice calculations except just near the critical point.[7] Therefore, one can be safely based on our results to discuss the chiral transition at $T = 0$.

3. Meson Excitations

We are now in a position to investigate meson excitations at $T \neq 0$. Information on meson excitations is contained in the retarded Green's function[40,44];

$$\Pi^R_\alpha(\omega, \mathbf{q}) = \mathcal{F}\theta(T)\langle\langle[\bar{q}(t,\mathbf{x})\Gamma_\alpha q(t,\mathbf{x}), \bar{q}(0,\mathbf{0})\Gamma_\alpha q(0,\ 0)]\rangle\rangle. \tag{3.1}$$

Here $\mathcal{F}$ denotes the Fourier transformation and Γ_α is the spin$\otimes$flavor-matrix specifying the meson α;

$$\begin{aligned} \Gamma_\alpha &= 1 && \text{for } \sigma - \text{meson } (\alpha = \sigma), \\ &= i\gamma_5\tau && \text{for pion } (\alpha = \pi) \end{aligned}$$

Owing to the Abrikosov-Gor'kov-Dzyaloshinskii-Fradkin theorem[40,44], the retarded Green's function can be obtained as an analytic continuation of the temperature Green's function;

$$\mathcal{T}\!\!\mathcal{L}_\alpha(\omega_n^B, \mathbf{q}) = \mathcal{F}\langle\langle T_\tau \bar{q}(\tau,\mathbf{x})\Gamma_\alpha q(\tau,\mathbf{x})\bar{q}(0,\mathbf{0})\Gamma_\alpha q(0,\mathbf{0})\rangle\rangle, \tag{3.2}$$

where $q(\tau, \mathbf{x})$ denotes the imaginary time operator and $\omega_n^B = 2\pi nT$ is the Matsubara frequency for bosons. A simple diagramatic expansion is possible for

$\Pi_\alpha(\omega_n^B, \vec{q})$ and the ring approximation for it is given as follows;

$$\begin{aligned} \Pi_\alpha(\omega_n^B, \mathbf{q}) &= \Pi_\alpha^0(\omega_n^B, \mathbf{q})\mathcal{D}_\alpha(\omega_n^B, \mathbf{q}), \\ \mathcal{D}_\alpha^{-1}(\omega_n^B, \mathbf{q}) &= 1 - 2g\, \Pi_\alpha^0(\omega_n^B, \mathbf{q}), \end{aligned} \tag{3.3}$$

where Π_α^0 is the lowest order of Π_α . Then the dispersion relation of the meson α is obtained as a zero of the inverse of the propagator $D_\alpha(\omega, \mathbf{q})$ which is given by the analytic continuation of $\mathcal{D}_\alpha(\omega_n^B, \mathbf{q})$:

$$\begin{aligned} 0 &= 1 - 2g\Pi_\alpha^{R(0)}(\omega, \mathbf{q}), \\ &= [D_\alpha(\omega, \mathbf{q})]^{-1}, \end{aligned} \tag{3.4}$$

where $\Pi_\alpha^{R(0)}$ is expressed as,

$$\begin{aligned} \Pi_\alpha^{R(0)}(\omega, \mathbf{q}) = -\mathrm{Tr} \int d^4p \tanh \frac{p^0}{2T} \Gamma_\alpha [G^R(p^0 + \omega, \mathbf{p} + \mathbf{q}) \Gamma_\alpha \mathrm{Im} G^R(p^0, \mathbf{p}) \\ + \mathrm{Im} G^R(p^0, \mathbf{p}) \Gamma_\alpha G^R(p^0 - \omega, \mathbf{p} - \mathbf{q})], \end{aligned} \tag{3.5}$$

with $G^R(G^A = (G^R)^*)$ being the retarded (advanced) Green's function;

$$G^R(p^0, \vec{p}) = [\not{p} - M(T) + i\eta \cdot sgn(p^0)]^{-1} \tag{3.6}$$

where $p^\mu = (p^0, \mathbf{p})$ and $\eta > 0$. It should be noticed that there arises an imaginary part in $\Pi_\alpha^{R(0)}$ due to the coupling to $q\bar{q}$ continuum in our model. In the confined phase, the colored quarks are confined so that the continuum is absent in reality. The confinement is originating from othr mechanism than those built in thr NJL model. Therefore we will discard the imaginary part as artifacts due to the short-comings of the model. When one consider colore-singlet excitations in the deconfined phase, it is necessary to take into consideration the width due to the existence of the continuum.[1]

The final expresseions for the dispersion equations of $\sigma-$meson and pion are the following:

$$0 = [D_\sigma(m_\sigma, 0)]^{-1} = 1 - (2gN_cN_f/\pi^2)\int_0^\Lambda \mathbf{p}^2 d|\mathbf{p}|\frac{f(E)}{E}[1 - \frac{(m_\sigma^2 - 4M^2)}{(m_\sigma^2 - 4E^2)}]$$

$$0 = [D_\pi(m_\pi, 0)]^{-1} = 1 - (2gN_cN_f/\pi^2)\int_0^\Lambda \mathbf{p}^2 d|\mathbf{p}|\frac{f(E)}{E}[1 - \frac{m_\pi^2}{(m_\pi^2 - 4E^2)}]$$

(3.7).

In general, the thermal factor $f(E)$ decreases as T goes high. Thus temperature tends to reduces the collectiveness of the meson excitations, and increases the meson masses provided that the quark mass M were independent of T. Since M(T) is actually dependent on T because of the self-consistency condition ((2.1)) on it, however, m_π and m_σ does not show such a simple behavior. The numerical calculation shows the following[6,7]: Below T_χ, the pion mass $m_\pi(T)$ has only a small T-dependence and $m_\sigma(T)$ becomes small considerably as T is raised. A remarkable point is that differnce between m_σ and $2m_\pi$ decreases as T goes high and vanish at a temperature lower than T_χ. The significance of this feature will be clear soon.

4. T-dependence of the coupling constants and the width of σ-meson

In this subsection, we calculate the following physical quantities related with pion and $\sigma-$meson; the meson-quark coupling constant $G_{\alpha q}$, the pion decay constant f_π, the $\sigma - \pi - \pi$ coupling constant $\lambda_{\sigma\pi\pi}$ and the decay width (Γ_σ) of σ-meson due to the process $\sigma \to \pi\pi$.

By comparing the exchange of elementary bosons between quarks and the exchange of $q - \bar{q}$ collective modes having the same quantum numbers, one can

extract the meson-quark coupling constant;

$$G^2_{\alpha q}(\omega^2;T) = 2g(\omega^2 - m^2_\alpha)D_\alpha(\omega,\mathbf{0};T). \tag{4.1}$$

The explicit form of $G_{\pi q}(T) \equiv G_{\pi q}(\omega^2 = 0;T)$, for example, is,

$$G^2_{\pi q}(T) = 2gm^2_\pi[1 - (2gN_cN_f/\pi^2)\int_0^\Lambda \mathbf{p}^2 d|\mathbf{p}|\frac{f(E)}{E}]^{-1}, \tag{4.2}$$

where m_π is the solution of eq.(3.7). We give here also the on-shell coupling constant $G^{on}_{\pi q}(T) \equiv G_{\pi q}(\omega^2 = m^2_\pi;T)$ which is given in terms of the residue of the propagator;

$$\begin{aligned}(G^{on}_{\pi q}(T))^2 &= 2g[\frac{d}{d\omega^2}D^{-1}_\pi|_{\omega=m_\pi}]^{-1}, \\ &= \frac{4\pi^2}{N_CN_f}[\mathrm{Pf}\int_0^\Lambda \mathbf{p}^2 d|\mathbf{p}|\frac{f(E)}{E}(\frac{E}{(E^2 - m^2_\pi/4)})^2]^{-1},\end{aligned} \tag{4.3}$$

where Pf denotes the finite part.

The pion decay constant $f_\pi(T)$ is given as

$$f_\pi(T) = G^{on}_{\pi q}M(N_CN_f/4\pi^2)\mathrm{Pf}\int_0^\Lambda \mathbf{p}^2 d|\mathbf{p}|\frac{f(E)}{E}\frac{1}{(E^2 - m^2_\pi/4)}. \tag{4.4}$$

The chiral perturbation, in which $\bar{m}/\Lambda$is supposed to be small compared with the total mass $M(T)/\Lambda$ gives the current algebra relations such as the Goldberger-Treiman (GT) and the Gell-Mann-Oakes-Renner relations at $T \neq 0$;

$$f_\pi(T)G_{\pi q} = M(T), \tag{4.5}$$

$$f^2_\pi(T)m^2_\pi = -\bar{m}\langle\langle\bar{q}q\rangle\rangle. \tag{4.6}$$

Although these relations hold quite well at $T = 0$, of course, however tend to loose the validity as T goes high since $M(T)$ becomes small and approaches $\bar{m}$ as T rises[46].

The $\sigma-\pi-\pi$ coupling constant $\lambda_{\sigma\pi\pi}$ is defined by the diagram shown in Fig.8 in Ref. 7, where all external momenta are set to be 0. The resulting expression for $\lambda_{\sigma\pi\pi}$ is

$$\lambda_{\sigma\pi\pi} = -2N_C N_f G_{\sigma q} G_{\pi q}^2 M \frac{\partial}{\partial M^2}[\int \frac{d^3p}{(2\pi)^3}\frac{f(E)}{E}]. \tag{4.7}$$

The T-dependences of $G_{\pi q}(T)$, $f_\pi(T)$ and $\lambda_{\sigma\pi\pi}$ are shown in Ref. 4,6and 7. They all gradually decrease as T rises, which implies that the interactions of pion with other hadrons and leptons become weak as the system get heated. However, there is an exception. The electromagnetic process $\pi_0 \to 2\gamma$ gives the width $\Gamma_{\pi_0\to 2\gamma}$ which increases as T goes high[45,46]: Since the axial anomaly at $T \neq 0$ is the same as that at $T = 0$ [47], $\Gamma_{\pi_0\to 2\gamma}$ at $T \neq 0$ may be evaluated with the use of the formula at $T = 0$[48] as

$$\Gamma_{\pi_0\to 2\gamma} = \alpha^2 m_\pi^3/6\pi^3 \cdot (G_{\pi q}^{on}/M(T))^2,$$

where it should be noted that the GT-relation eq.(4.5)has not been used because the validity of it is losed at high temerature as mentioned before.† Inserting the T-dependences of m_π, $G_{\pi q}^{on}$ and $M(T)$ obtained above, we see that $\Gamma_{\pi_0\to 2\gamma}$ varies roughly as $8eV \to 40eV$ when $T = 0 \to 200MeV$.

Finally, let us calculate the width of σ-meson. The width is related with the imaginary part of the σ-propagator;

$$\Gamma_\sigma = \mathrm{Im}\Sigma(m_\sigma, 0)/2m_\sigma.$$

Of various self-energy diagrams in the one-loop order, only the pion loop gives the imaginary part which does not vanish so long as $m_\sigma > 2m_\pi$. Other diagrams such as σ-loop(s) contribute only to the real part of the self-energy; we neglect

† A thernal distribution function of photon would be multiplied to the above formula if we assume that photons are in thermal equilibrium. The thermal factor tends to further increase the width as T is raised.

them because of the large mass of σ-meson. Using the thermal Green's functions for bosons, we get

$$\Gamma_\sigma(T) = (3\lambda^2_{\sigma\pi\pi}/16\pi m_\sigma) \cdot \sqrt{1 - 4m_\pi^2/m_\sigma^2} \cdot (1 + 2/[\exp(m_\sigma/2T) - 1]).$$

Here, we note that as T is increased, both the coupling constant $\lambda_{\sigma\pi\pi}$ and the phase- space factor $\sqrt{1 - 4m_\pi^2/m_\sigma^2}$ become large. Thus, the T-dependence of $\Gamma_\sigma(T)$ can not be simply imagined without an explicit computation. Then the numerical computation shows the following: At small temperatures lower than, say, 80 MeV, $\Gamma_\sigma(T)$ hardly decreases as T is increased but at Temperatures higher than that temperature it does decreases considerably as T goes high and then vanishes at the temperature $T = 197$ MeV $\equiv T_\sigma$ where $m_\sigma = 2m_\pi$. At the temperatures higher than T_σ, σ-meson can not decay through the process $\sigma \to 2\pi$; it can decay only through the electromagnetic process $\sigma \to 2\gamma$.

The smallness of $\Gamma_\sigma(T)$ at high temperatures implies that σ-meson, which has a large width due to the coupling with 2π at $T = 0$, appears as an elementary excitation with a very small width, closely before the chiral transition occurs. Since the couplings of the mesons with matter becomes weak at high temperatures as we have seen for pion as an example, the appearance of a long-lived σ-meson might be used as a signature of the formation of the hadronic matter at high temperature and as a precursory phenomenon of the chiral transition. Therefore, it would be very interesting to mesure the correlations of 2γ's and and their invariant masses in experiment of relativistic heavy ion collisions; there might come a bump in the cross sections in the region of the invariant mass $\simeq 2m_\pi$.

5. Discussion

So far, we have confined ourselves to the 2-flavor case ($N_f = 2$). In this case, the Lagrangian we have used is essentially equivalent to the old NJL model. When the s-quark is taken into account, the effective Lagrangian we should use to describe the quark condensates and the scalar (pseudo-scalar) mesons takes the following form;

$$\mathcal{L} = \bar{q}(i\gamma\cdot\partial - \mathbf{m})q + \frac{g_S}{2}\sum_{a=0}^{8}[(\bar{q}\lambda_a q)^2 + (\bar{q}i\lambda_a\gamma_5 q)^2] + g_D[\det\bar{q}_i(1-\gamma_5)q_j + h.c.], \quad (5.1)$$

where $\mathbf{m} = \mathrm{diag}(m_u, m_d, m_s)$ with $m_i\,(i = u, d, s)$ being the current quark mass, $i, j(= 1, 2, \ldots, N_f)$ are flavor indices, λ^a are the generators of the flavor $U(N_f)$ group with $\lambda^0 = \sqrt{2/N_f}\cdot\mathbf{1}$ and the color indices are suppresed. Apart from the last term (anomaly term), which breaks the $U_A(1)$ symmetry[31]† , the Lagrangian is invariant under $U_L(N_f)\otimes U_R(N_f)$ when m_i's are neglected.

The Lagrangian has already been examined rather extensively for T=0[5]: The dynamical quark mass, the quark condensates in the vacuum and the properties of the NG-bosons (π, K, η)and the would-be NG boson (η') have been found to be in good agreement with the phenomenology and those obtained from a semi-phenomenological appproach such as the QCD sum- rule approach. Thus the $U_A(1)$ problem is resolved in this Lagrangian. The mixing angle between the η_0- and η_8-mesons has been found to be about 20°, though the angle is not definitely detemined from the solutions of the dispersion equations[51]. Furtheremore, the Lagrangian has been found to give a good description of the radiative meson decays[49,50].

It would be very interesting to apply the Lagrangian to the $T \neq 0$case. Especially, it would be intriguing to see how the degeneracy between the η- and

† Although there exists the anomaly term in the $N_f = 2$-case, too, the term does not change the physics as far as σ-meson and pion are concerned.

η'-mesons would be restored,i.e., how the $U_A(1)$-symmetry would be restored. In this respect, it may be more realistic to make g_D have a T-dependence as the instanton-calculation might give.

We have extensively discussed on the scalar mesons so far. The vector mesons can also be examined using the 4-fermi interaction of the NJL type;

$$\mathcal{L}_V = g_V \sum_{a=0}^{8} (\bar{q}\lambda_a \gamma_\mu q)^2 + g_A \sum_{a=0}^{8} (\bar{q}\lambda_a \gamma_\mu \gamma_5 q)^2. \tag{5.2}$$

A vector type interaction arises as a Fock term of the scalar type interactions given in (5.1). Ebert and Reinhard[32] have, however, shown that the introduction of the $\mathcal{L}_V$ is necessary for description of the vector meson at $T = 0$.

It is easily shown using $\mathcal{L}_V$ that if we neglect the scalar-vector couplings, the mixing between ω_0- and ω_8-mesons are the ideal mixing and the resulting physical ω-meson is degenerate with the ρ-meson even at $T \neq 0$ [46]. It would be intriguing to see how the scalar-vector couplings affect the mixing between the ω_0 and ω_8 and the mass degeneracy between the ω- and ρ-mesons are lifted at finite temperature as well as at $T = 0$. It is very likely that thermal effects make the vector mesons heavier. If this is the case, the coupling between the vector mesons and photons would be supressed in the systems at high temperature like the QGP.

If we assume that some relations which hold at $T = 0$ keep their validity, we can say more about hadrons at $T \neq 0$[52]. Ioffe have given an interesting relation between the nucleon- and $\Delta-$ masses and the quark condensate[54];

$$M_N = [-2(2\pi)^2 \langle \bar{q}q \rangle]^{1/3},$$
$$M_\Delta = 1.4 M_N.$$

If we assume the relations hold even at $T \neq 0$, we see that as T is raised, these baryons become lighter, because the quark condensate decreases with increasing

temparature. Similarly, assuming that KSRF relation [53] holds at finite temperature, we can say about the T-dependence of the ρ- and ω-mesons and their coupling constants with nucleon. These arguments are very interesting, however it should be noticed that it remains as a fundamental problem to examine how these relations which are known to hold at $T = 0$ persit or change at finite temperature.

ACKNOWLEDGMENTS

The talk given here is based on the works (published or unpublished) in collaboration with T. Hatsuda, who is now in State University of New York at Stony Brook and had been busy for preparing the travel to Stony Brook and furtheremore his marriage (!) in March, 1988. He also helped me to prepare the talk with some advices. I would like to express my sincere thanks and say "Congratulation !" to him.

REFERENCES

1. T. Hatsuda and T. Kunihiro, Phys.Rev.Lett. 55(1985)158.
2. T. Hatsuda and T. Kunihiro, Prog.Theor.Phys. 74(1985)765.
3. T. Hatsuda and T. Kunihiro, Phys. Lett. B185(1987)304.
4. T. Hatsuda and T. Kunihiro, Phys. Lett.B198(1987)126.
5. T. Kunihiro and T. Hatsuda,Phys. Lett.B(1988),in press.
6. T. Hatsuda and T. Kunihiro,in *Nuclear Phase Trnsitions and Heavy Ion Reactions*,pp.73-82,edited by T.T.S.Kuo, D.Strottman and S.S. Wu (World Scientific,1987).
7. T. Hatsuda and T. Kunihiro,Prog. Theor. Phys.supple.91(1987)284.
8. S. Midorikawa, H. So and S. Yoshimoto, Z. Phys.C 34(1987)307.
9. L. J. Reinders, H. Rubinstein and S. Yazaki,Phys. Rep.127(1985)1.
10. M.Fukugita, S.Ohta,Y.Oyanagi and A.Ukawa,Phys. Rev. Lett.58(1987)2515.
11. S.Gottliev, W.Liu,D.Toussaint,R.L. Renken and R.L. Sugar, Phys. Rev. Lett. 58(1987)3972.
12. R.V. Gavai,J.Potvin and S. Sanielevici,Phys. Rev. Lett.58(1987)2519.
13. E.V.E. Kovacs,D.K. Sinclair and J.B. Kogut,Phys. Rev. Lett.58(1987)751.
14. As a review article; J.Cleymans,R.G.Gavai and E. Suhonen,Phys. Rep. 130(1986)217.
15. J.C. Collins and M.J. Perry, Phys. Rev. Lett.34(1975)1353.
16. A.B. Kisslinger and P.D. Morley, Phys. Rev.D13(1976)2771.
17. G.W. Klicup, S.R. Sharpe, R. Gupta, G. Guralnik, A. Patel and T. Warnock, Phys. Lett. B164(1985),347.

18. T. Hashimoto, O. Miyamura, K. Hirose and T. Kanki, Phys. Rev. Lett.57 (1986) 2123; T. Matsui and H. Satz, Phys. Lett.B(1986) 416.

19. J.W. Durso, A.D.Jackson and B.J. Verwest, Nucl. Phys.A345(1980)471.

20. J.L. Basdevant and B.W. Lee,Phys. Rev. D2(1970)1680.

21. E. van Beveren, T.A. Rijken, K. Metzger, C. Dullemond, G.Rupp and J.E. Ribeiro, Z. Phys. C30(1986)615.

22. G. Mennesier, Z. Phys. C16(1983)241.

23. C. DeTar, talk presented in this meeting.

24. Y. Nambu and G. Jono-Lasinio, Phys. Rev. 122(1961)345; 124(1961)246.

25. T. Eguchi and H. Sugawara, Phys. Rev. D10(1974)4257.

26. T. Kunihiro and T. Hatsuda, Prog. Theor. Phys.71(1984)1332.

27. M.K. Volkov, Ann. Phys.(N.Y.)157(1984)282.

28. A. Dhar and S.R. Wadia, Phys. Rev. Lett.52(1984)959.

29. A. Dhar, R. Shankar and S.R. Wadia, Phys. Rev. D(1985)3256.

30. T. Goldman and R.W. Haymaker, Phys. Rev. D24(1981)724.

31. G. 't Hooft,Phys. Rev. D14(1976)3432;D18(1978)2199(E); Phys. Rep. 142 (1986) 357.

32. D. Ebert and H. Reinhardt, Nucl. Phys. B271(1986)188.

33. R. Ball,*Proceedings of the Workshop on "Skyrmions and Anomalies"*, Mogilany,Poland,1987.

34. N. Kawamoto and J. Smit, Nucl. Phys. B192(1981)100.

35. I. Ichinose, Phys. Lett.B135(1984)148.

36. T. Hatsuda and T. Kunihiro,Phys. Lett.B145(1984)7.

37. A. Manohar and H. Georgi, Nucl. Phys. B234(1984)189.

38. H. Pagels, Phys. Rev. D14(1976)2747; D15(1977)2991.

39. J.M. Cornwall, Phys. Rev. D22(1980)1452.

40. A.A. Abrikosov, L.P. Gor'kov and I.E. Dzyaloshinskii, *Method of Quantum Field Theory in Statistical Physics*, (Prentice-Hall, Engelwood Cliffs, N.J.,1963).

41. A. Suzuki and R.K. Bhaduri, Phys. Lett.B125(1983)347, and references therein.

42. M. Asakawa, talk given in this meeting(1988).

43. S. Kawati and H. Miyata, Phys. Rev. D23(1981)3010.

44. A. Fetter and J. Walecka, *Quantum theory of many-particle systems*, (Mcgraw - Hill, N.Y., 1971).

45. O. Miyamura, private communication to T. Hatsuda,1987.

46. T. Hatsuda and T. Kunihiro, unpublished,1987.

47. H. Itoyama and A.H. Mueller, Nucl. Phys. B218(1983)349.

48. C. Itzykson and J.-B. Zuber, *Quantum Field Theory* (McGraw-Hill, 1980).

49. L.-H. Chan, Phys. Rev. Lett.39(1977)1124.

50. D.W. Mckay and H.J. Munczek, Phys. Rev. D30(1984)1825; ibid. D32 (1985) 266.

51. T. Kunihiro, unpublished

52. T. Hatsuda, private communucation.

53. K. Kawarabayashi and M. Suzuki, Phys. Rev. Lett.16(1966)255; Riazudin and Fayyazuddin, Phys. Rev. 147(1966) 1071.

54. B.L. Ioffe, Nucl. Phys. B188(1981)317; (E)B191(1981)591.

Hadron-Quark Phase Transition and An Excluded Volume Effect

Hiroaki KOUNO and Fujio TAKAGI

Department of Physics, Tohoku University
Sendai, 980 Japan

I. Introduction

Quantum chromodynamics (QCD) predicts two kinds of phase transition at high temperature or high baryon number density, one from the quark confining hadronic phase to the deconfined quark-gluon phase and another from the spontaneously broken chiral symmetry phase to the chiral symmetry restoring phase. At present, Monte Carlo lattice QCD calculation provides most reliable results on the properties of these phase transitions. However, a more phenomenological approach is also necessary because the Monte Carlo lattice QCD has many difficulties including the problem on the treatment of the chemical potential. Here, we start with an independent many phase model proposed by Cleymans et al.[1),2),3)] The following three phases are prepared independently and the critical curve for a transition between two of them is evaluated by using the Gibbs criteria:(i)the hadronic phase (H phase) where quarks and gluons are confined in color singlet hadrons and the chiral symmetry is broken spontaneously;(ii)the constituent quark phase (C phase)

where constituent quarks are deconfined while the chiral symmetry is still broken spontaneously so that there are pions also;(iii)the quark-gluon phase (q-g phase) where massless quarks and gluons are deconfined and the chiral symmetry is unbroken.

II.Quark deconfining phase with a constant vacuum energy

The q-g phase is described as a relativistic ideal gas of massless quarks and gluons with N_f(the number of the flavors) = 2 and N_c(the number of colors) = 3. The energy density, the pressure and the net baryon number density are given respectively by

$$\varepsilon_q = 37\pi^2T^4/30 + 3\mu_q^2T^2 + 3\mu_q^4/(2\pi^2) + B, \tag{2.1}$$

$$p_q = 37\pi^2T^4/90 + \mu_q^2T^2 + \mu_q^4/(2\pi^2) - B, \tag{2.2}$$

and

$$n_q = 2\mu_qT^2/3 + 2\mu_q^3/(3\pi^2), \tag{2.3}$$

where T is the temperature, B is the bag constant and μ_q is the baryonic chemical potential per quark. The q-g phase can be physical only when $p_q \geqslant 0$. The T-μ curve determined by the condition $p_q = 0$ gives the zeroth order approximation of the critical curve for the quark deconfining phase transition. See Fig.1 of the next section.

III.Pathology of point particle approximation for nucleons

If one assumes that the H-phase is described by a gas of free point-like nucleons (N), antinucleons ($\bar{N}$) and pions (π), pathology emerges.[1),2)] We have calculated the critical curve in the T-μ plane for various values of B. See Fig.1. At a fixed μ,

Fig.1

the q-g phase is always realized at sufficiently high T. This is natural. On the other hand, the H-phase is realized at sufficiently large μ if T is fixed. This is very unnatural.

IV.Repulsive interactions and an excluded volume effect

Cleymans et. al. have taken into account the repulsive interaction between two nucleons as an excluded volume effect in order to avoid the pathology mentioned in the preceding section.[2)] However, they have only considered the difference between the volume occupied by nucleons and the one occupied by antinucleons. Furthermore, they have applied the excluded volume effect to N, $\bar{N}$ and π on an equal footing. The net baryon number density n_h, the energy density ε_h and the pressure p_h thus take the following form in their model (let it call model I) for a system with nonnegative baryon number density;

$$n_h = n^0/(1 + n^0 V_N), \tag{4.1a}$$

$$\varepsilon_h = (\varepsilon_N^0 + \varepsilon_{\bar{N}}^0 + \varepsilon_\pi^0)/(1 + n^0 V_N), \tag{4.1b}$$

$$p_h = (p_N^0 + p_{\bar{N}}^0 + p_\pi^0)/(1 + n^0 V_N), \tag{4.1c}$$

where n^0 is the net baryon number density i.e., the baryon number density n_N^0 minus the antibaryon number density $n_{\bar{N}}^0$, and $V_N = 4\pi R^3/3$ with R being the hard core (?) radius of a nucleon. All the quantities with the superscript 0 are calculated in the free (point) particle approximation, e.g.,

$$n_N^0 = \frac{2}{\pi^2} \int_0^\infty dk \frac{k^2}{\exp\{(E(k) - \mu)/T\} + 1},$$

where μ is the baryon chemical potential of a nucleon and $E(k) = \sqrt{k^2 + m^2}$. We take R = 0.8 fm in the following calculations.

There are strong repulsive interactions only between a pair of nucleons or a pair of antinucleons. A pion would not feel a strong repulsive force from another pion, nucleon or antinucleon. Therefore, for example, the effectively available volume for a nucleon is the true geometrical volume minus the volume occupied by nucleons. The excluded volume effect would be absent for a pion at this level of the approximation. Thus, we propose a modified model (model II) which is characterized by the following formulae;

$$n_h = \frac{n_N^0}{1 + n_N^0 V_N} - \frac{n_{\bar{N}}^0}{1 + n_{\bar{N}}^0 V_N}, \tag{4.2a}$$

$$\varepsilon_h = \frac{\varepsilon_N^0}{1 + n_N^0 V_N} + \frac{\varepsilon_{\bar{N}}^0}{1 + n_{\bar{N}}^0 V_N} + \varepsilon_\pi^0, \tag{4.2b}$$

$$p_h = \frac{p_N^0}{1 + n_N^0 v_N} + \frac{p_{\bar{N}}^0}{1 + n_{\bar{N}}^0 v_N} + p_\pi^0 . \qquad (4.2c)$$

V. Quark deconfining phase transition

The critical curve between two phases is determined by the condition of equal pressure and equal chemical potential at an equal temperature: A first order phase transition is predicted between H and q-g phases. The phase diagram in the T-μ plane is shown in Fig.2, where the zero pressure line determined by the condition $p_q = 0$ is also shown. For $B^{1/4} = 200$ MeV,

---

Fig.2

---

the critical temperature at $\mu = 0$ is 143 MeV while the critical chemical potential at $T = 0$ is 1360 MeV which gives the critical baryon number density 0.44 fm^{-3} on the H-phase side. There is also a gap in the energy density along the critical curve. It ranges from 0.88 to 1.04 GeV/fm^3 on the q-g phase side and from 0.056 to 0.53 GeV/fm^3 on the H-phase side.

VII. Possible realization of the constituent quark phase

The C-phase is characterized by a massive constituent quark Q with mass $m_Q = m_N/3$ and a pion as the Nambu-Goldstone boson. Since constituent quarks are deconfined in this phase, the vacuum energy density B_Q is supposed to be positive. This bag constant B_Q is not necessarily equal to the original bag constant B. The C-phase can be realized as an intermediate phase that separates the H-phase and the q-g phase if B is large and B_Q is not too large. See Fig.3.

Fig.3

Monte Carlo lattice QCD suggests that both the deconfining transition and the chiral symmetry restoring transition take place at the same critical temperature at least when $\mu = 0$. In the model II, the C-phase cannot be realized at $\mu = 0$ if B_Q is sufficiently large and B is not too large.

VII. Conclusion

The results given in sections IV, V, VI are summarized as follows:(i) the excluded volume effect is crucial to reproduce a natural phase diagram;(ii) it is easier to realize the C-phase in the high T, small μ region than in the low T, large μ region provided B is large and B_Q is not too large;(iii) a favourable value of the bag constant is $B^{1/4} \sim 200$ MeV since it gives a reasonable value for the critical temperature at $\mu = 0$ and also for the baryon number density in the H-phase at the critical chemical potential with $T = 0$. Other interesting results: (iv) the stability of the normal nuclear matter gives the lower bounds 156 MeV $< B^{1/4}$, $0 < B_Q$;(V) for a positive B_Q and any μ, the C-phase cannot be realized at $T = 0$ if $B^{1/4} < 215$ MeV.

The difference between the model I and the model II for the H-phase is small as long as the critical region and the H-phase inside it are concerned. It becomes significant when T and/or μ is so large that the system would be in the q-g phase far from the critical curve.

References

1) J. Cleymans, R. V. Gavai and E. Suhonen, Phys. Rep. 130 (1986),217.

2) J. Cleymans, K. Redlich, H. Satz and E. Suhonen, Z. Phys. C33 (1986),151.

3) J. Cleymans and E. Suhonen, Z. Phys. C37 (1987),51.

Figure captions

Fig.1. The critical curves that separate the H and the q-g phases for a free (point-like) hadron model with various values of the bag constant.

Fig.2. The critical curves for H-(q-g) transition are shown by solid lines for two choices of the bag constant. Here, the H-phase is described by the model II where the excluded volume effect is taken into account. For comparison, the corresponding zero pressure lines are shown by the dashed curves.

Fig.3. An example of the phase diagram for model II with three phases.

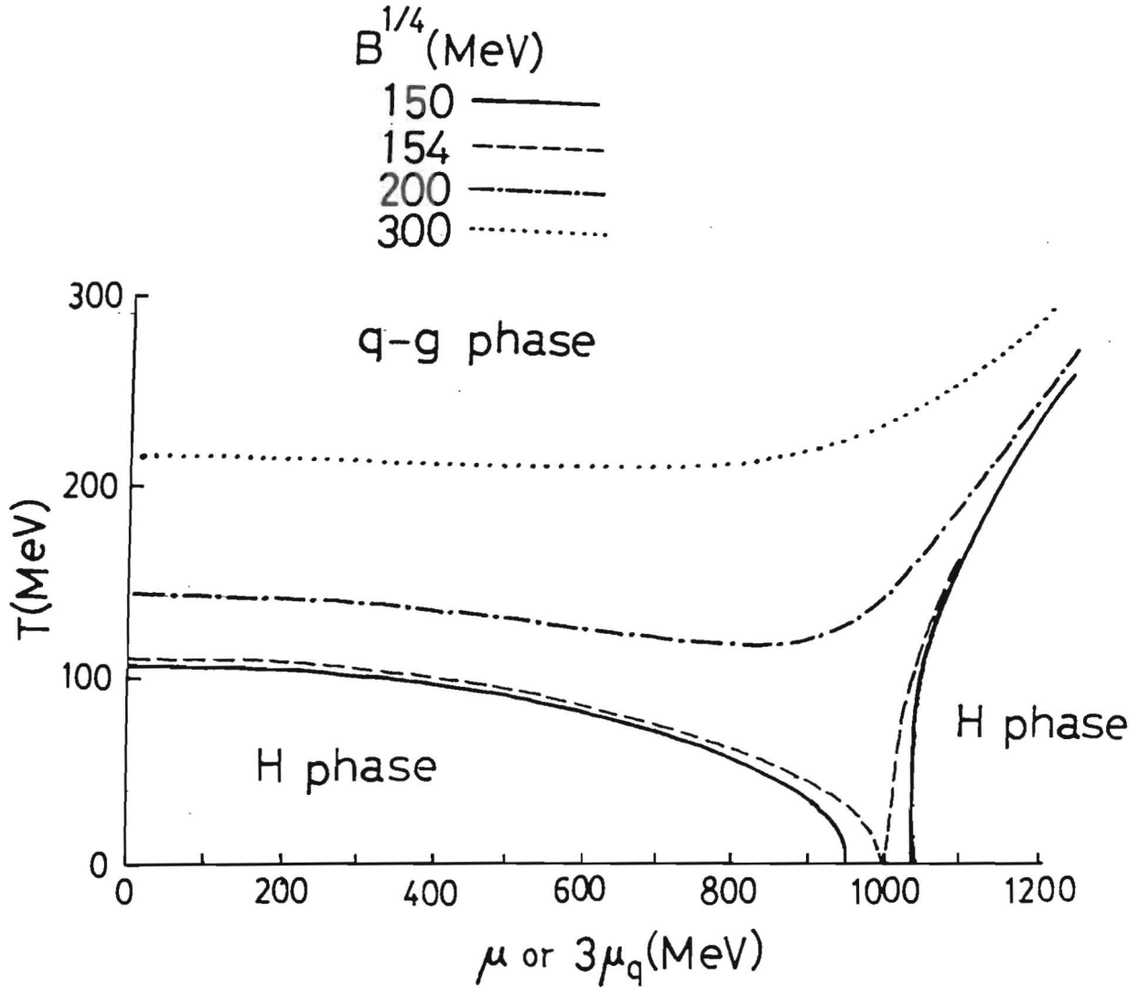
B^1/4 (MeV)
150
154
200
300
q-g phase
H phase
H phase
T(MeV)
300
200
100
0
0
200
400
600
800
1000
1200
μ or 3μq(MeV)

Fig. 1

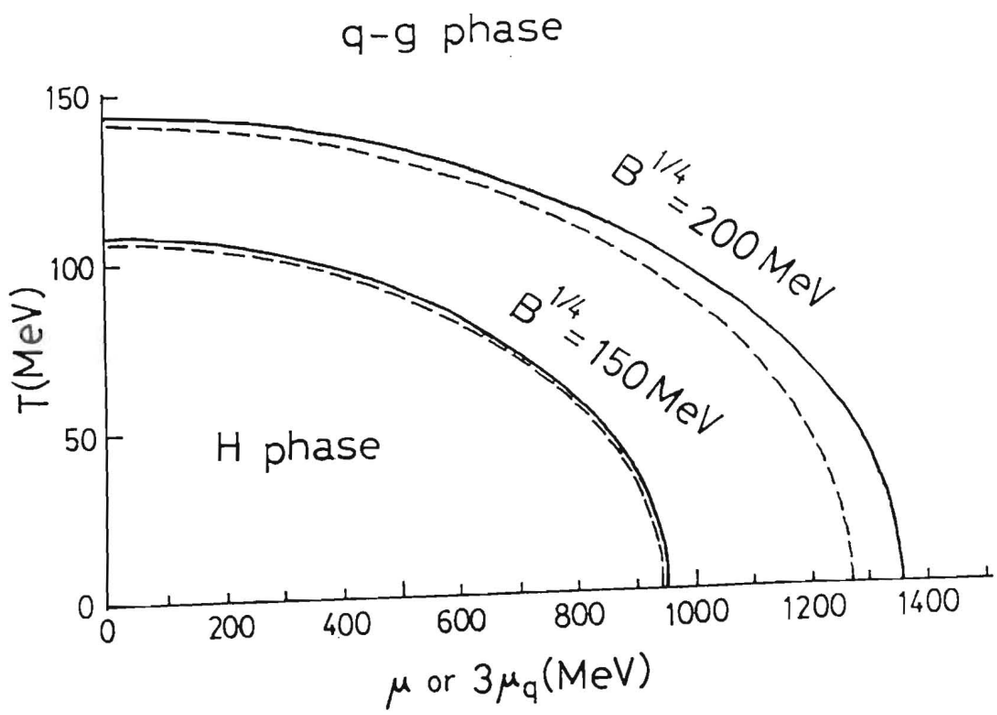
q-g phase
150
100
50
0
T(MeV)
$B^{1/4}$ = 200 MeV
$B^{1/4}$ = 150 MeV
H phase
0
200
400
600
800
1000
1200
1400
μ or $3\mu_q$(MeV)

Fig. 2

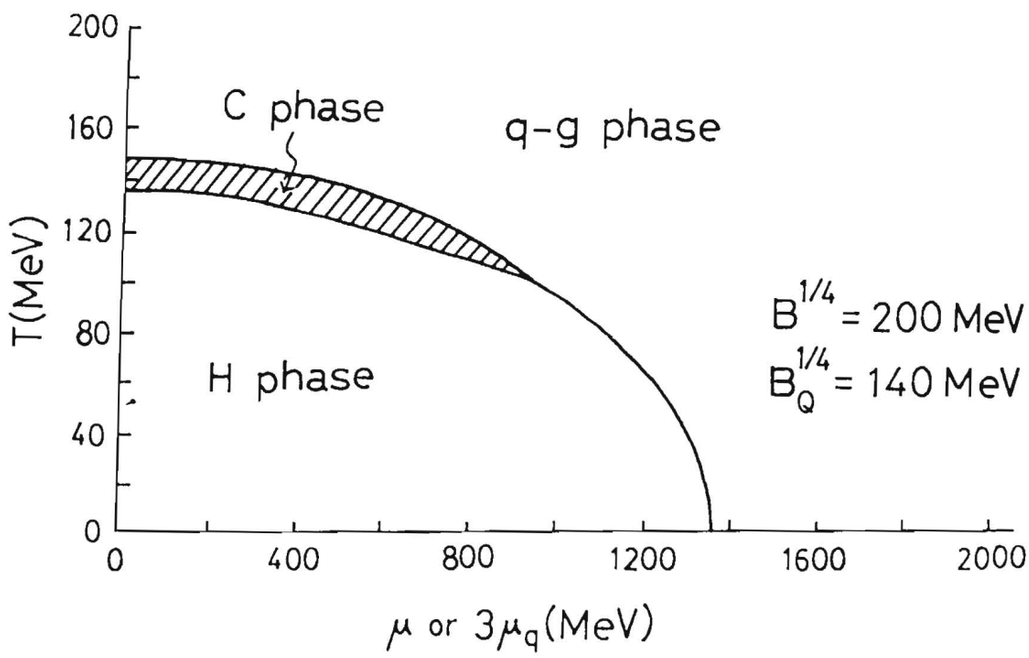
200
160
120
80
40
0
T(MeV)
C phase
q-g phase
H phase
$B^{1/4}$ = 200 MeV
$B_Q^{1/4}$ = 140 MeV
0
400
800
1200
1600
2000
μ or $3\mu_q$(MeV)

Fig. 3

HIGH ENERGY PARTICLE/NUCLEAR ASTROPHYSICS WITH EMULSION CHAMBERS

Yoshiyuki Takahashi

Department of Physics
University of Alabama in Huntsville,
Huntsville, AL.35899, USA

and

ES62, Space Science Laboratory,
NASA/Marshall Space Flight Center, Huntsville, AL.35812, USA

ABSTRACT

Several selected issues of high energy cosmic ray astrophysics with regard to the origin of high energy nuclei are presented. Relevant observational advancement achieved in the past decade by HEAO-3 satellite, CRNE SPACELAB-2 experiment, and the balloon-borne JACEE emulsion chambers are summarized. Significant problems engendered from these observations rendered some new expectations. Observability of high energy nuclei from explosive nucleo-synthesis with pulsar-acceleration has come into our scope of view more seriously than before. Further observations of high energy nuclei are demanding innovative, and large-scale detectors in space, for which a few examples of planned observations are introduced with an emphasis on the use of advanced emulsion chamber technology. New techniques in determining very high primary energies are discussed. In particular, efforts which include charge (and energy) mesurements with transition radiation detection, and isotopic evaluation via heavy-ion interactions, are explained. Finally, a concept of a Super-JACEE experiment, dedicated for heavy-ion studies in space, is briefly presented.

A talk presented at the KEK Workshop on Quark-Gluon Plasma,
National Laboratory for High Energy Physics, Tsukuba, Japan,
February 18 - 20, 1988

1. High Energy Cosmic Particles and Nuclei

To our best knowledge through observations from the earth, the cosmic rays are composed of those elements similar to solar abundances, except for light-nuclei, sub-iron nuclei, and trans-actinides (Fig. 1, Meyer et al., 1974). Light and sub-iron nuclei are substantially more enhanced in the cosmic rays as a result of fragmentation of heavier nuclei through the collision processes in the galaxy, while actinides and very heavy elements may eventually reveal r- or s-processes in the explosive nucleo-synthesis in the supernova explosion (Fig. 2, Waddington et al., and Fowler et al., 1985). Most available data upto 100 GeV/amu regime can be consistently understood, to the first order, by simple models such as "nested leaky-box" or "leaky box" in which solar abundance nuclei are produced, and propagate through some energy-dependent paths with or without truncated path length distributions. Nevertheless, it has been noticed that isotopic abundances of some elements such as ^{22}Ne, ^{25,26}Mg, and ^{29,30}Si (Fig. 3, Webber et al., 1985) are not simply expalined within these framework, but may require sources from Wolf-Rayet stars and others. (see most recent summary, J. P. Meyer, 1985).

Fig. 1 Cosmic (solid lines) and solar (dashed lines) abundances (Meyer et al., 1974).

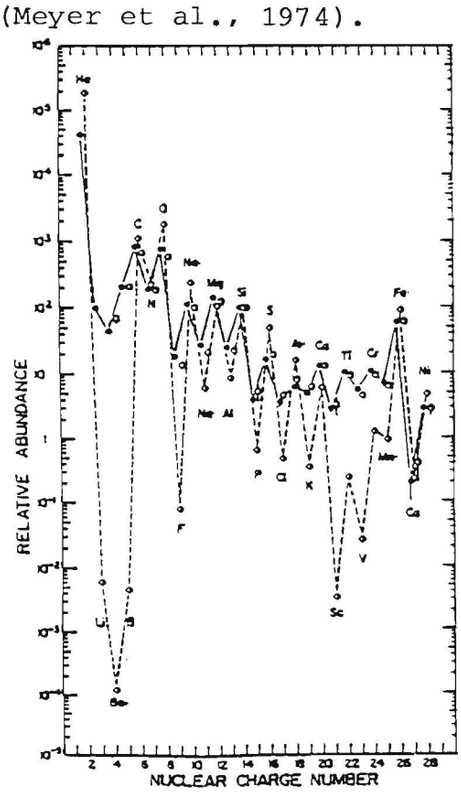

Fig. 2 Abundances of very heavy nuclei observed by HEAO-3C and Ariel-6 satellittes.

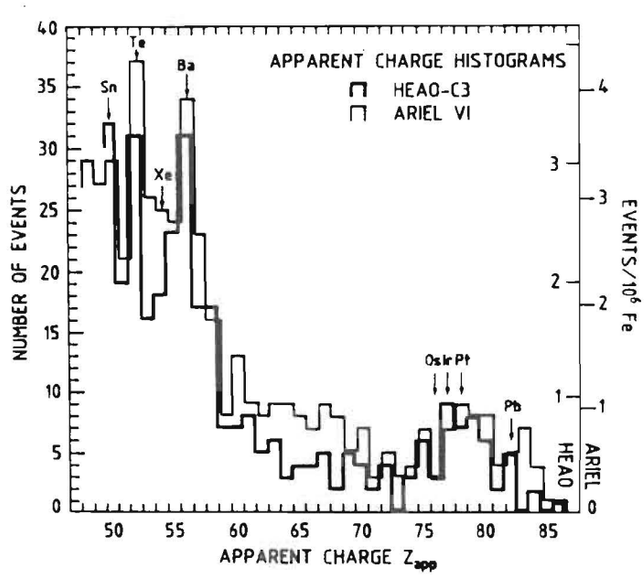

Fig. 3. Isotopic distribution of low-energy cosmic ray nuclei.

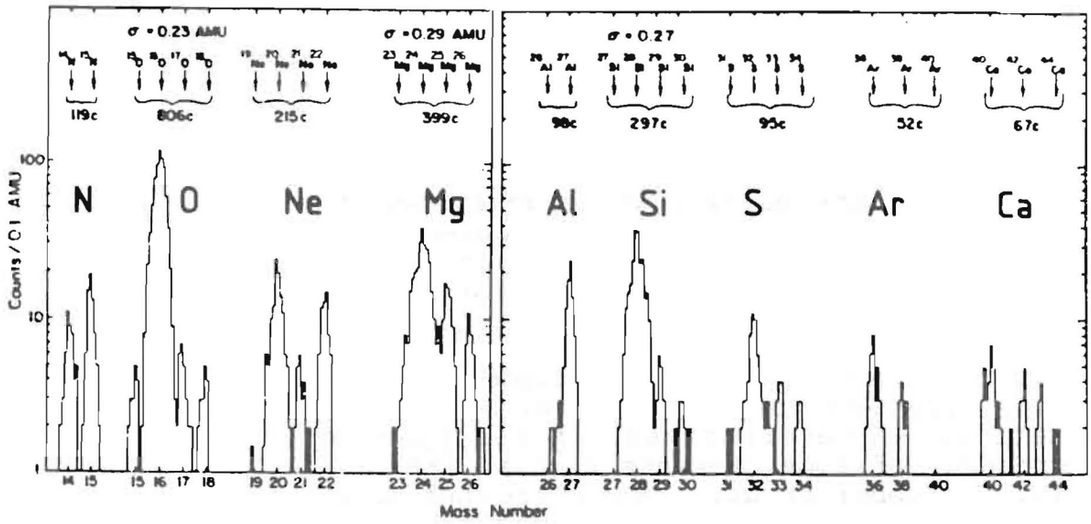

While these low energy particles and nuclei are understood as above, for which both interstellar and supernova shock accelerations successfully account for their energy spectra at least to the first order approximation, the high energy phenomena have been least understood both experimentally and theoretically. Limitations of observation are due to instrumental incapabilities of measuring very high energy nuclei, and also, due to the very small flux of these particles compared with available exposure factors of most experiments. Theoretically, shock acceleration has been known incapable of accelerating particles above 10 TeV/amu, and other alternative acceleration mechanisms have been much less clearly established.

Until the last decade practically no experiments have approached the high energy region beyond 100 GeV/amu, while the interest of origin of cosmic ray nuclei in high energy astrophysics and discussions of new observations were shifting inexorably to higher energies. New-generation experiments of elemental abundances and energy spectra of cosmic rays have extended observation in the past decade up to about 1 TeV/amu. These landmark measurements have been made by (1) HEAO-3 (C2: French-Danish Collaboration, Juliusson et al., 1983; C3: Washington-Caltech-Minnesota, Binns et al., 1988), (2) Spacelab-2 (CRNE: University of Chicago, Grunsfield et al., 1988), and (3) the JACEE balloon flights (The Japanese-American-Cooperative-Emulsion-Experiments, Burnett et al., 1988). They have generally confirmed overall consistency of elemental composition, similar to solar abundances, with energy dependent-path length for propagation consistent with that in GeV - 10 GeV regime.

Nevertheless, several new, unexpected results have been also obtained, e.g., Ar/Fe and Ca/Fe enhancements at above 500 GeV/amu (HEAO 3-C in Fig. 4 and JACEE in Fig. 5), steeper spectral index in Si-spectrum (CRNE, Fig. 6), and a flatter He spectrum than that of hydrogen (JACEE, Fig. 7).

Fig. 4. HEAO-3 (C3) results.

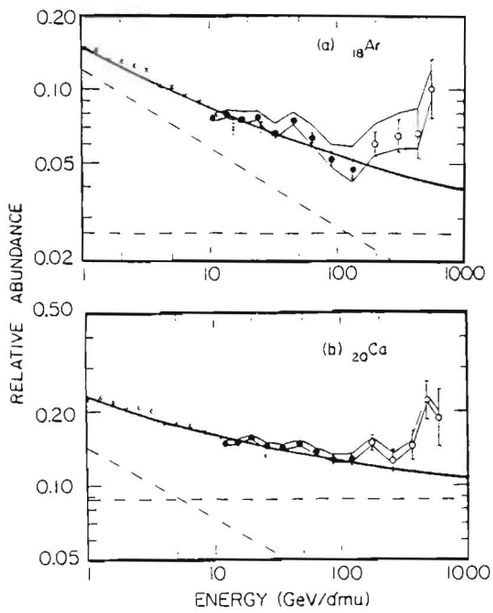

Fig. 5. JACEE data having Ca overabundance above TeV/amu.

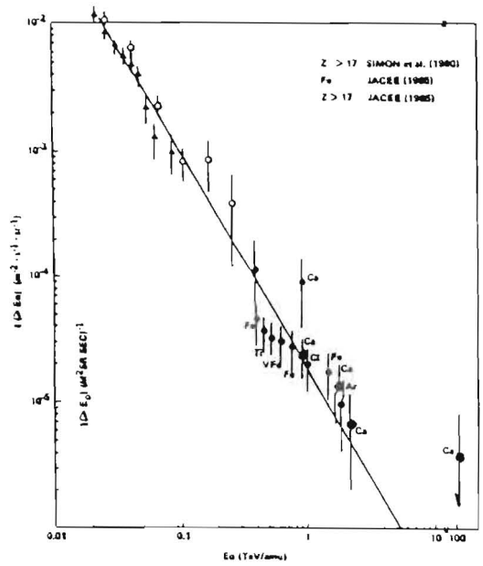

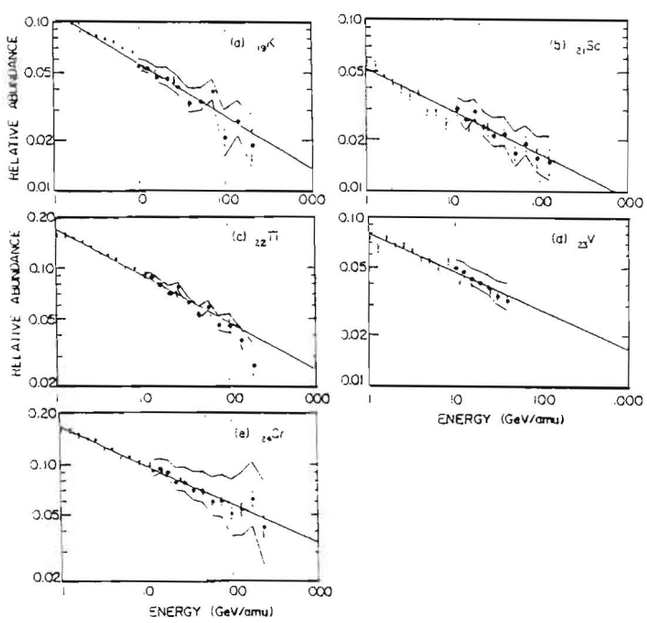

Fig. 6. CRNE results.

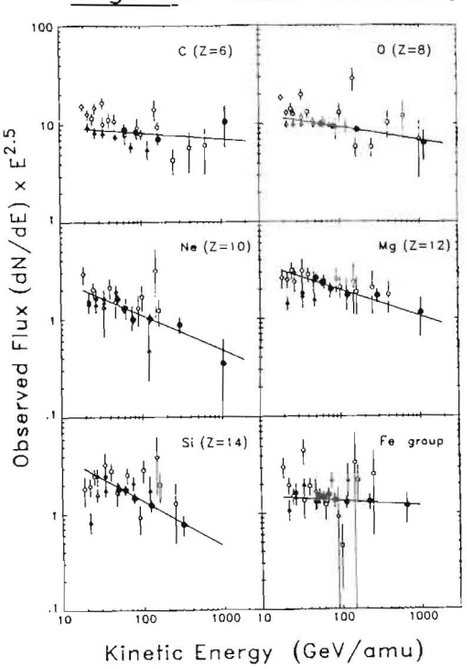

Fig. 7. He/p ratio by JACEE

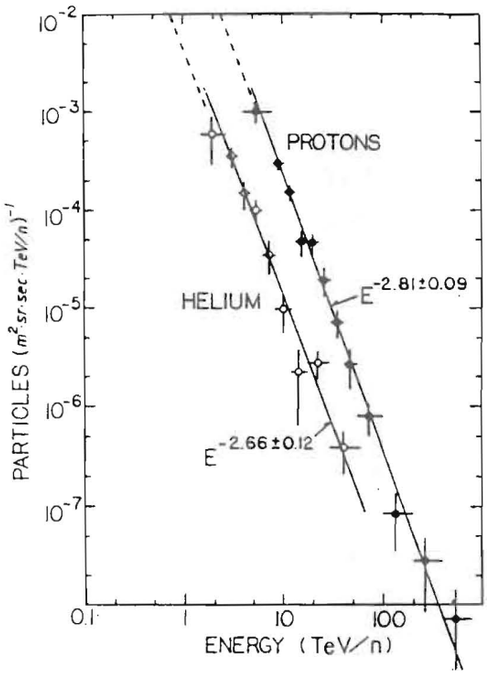

Fig. 8. Distortion of energy spectra of pulsar components due to x-rays.

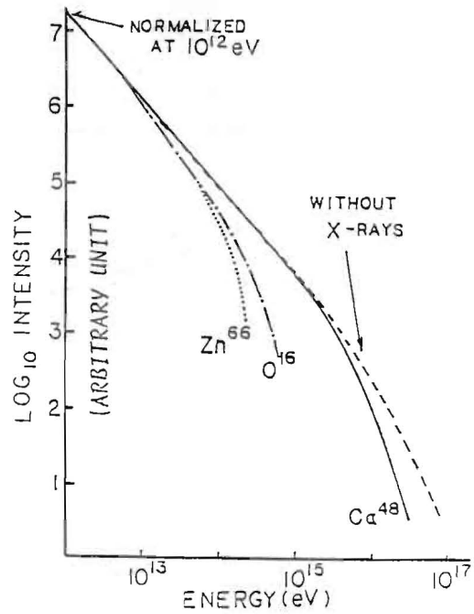

These new results necessarily require, for confirmation, advanced observations in the coming decade at much higher energies with a well-calibrated detection system. To these new scope of cosmic ray nuclei several theoretical suggestions are offered. For instance, pulsar components are re-examined from such a viewpoint that the vicinity of a pulsar should have boundary conditions inherent in the nuclear statistical equilibrium (NSE) or explosive nucleo-synthesis in the type-II supernovae; in which elemental abundances are significantly different from solar-abundances or those from type-I supernovae. Most prominenent nuclei are neutron-rich nuclei such as ^{66}Zn and ^{48}Ca (strong shock), and medium-heavy nuclei ranging from sulphur to calcium (weak shock), depending on the type of shocks for the cause of SN-II explosions (Hartman and Wooseley, 1985; Takahashi et al., 1986). Whether these "ideal" pulsar-components, different from other major components at low energies, should be observable or not are still unclear, partly because "milking" due to x-ray collision with accelerated nuclei, and uncertainity of acceleration itself. For the former process it is known that different nuclear potential in (gamma,alpha) reactions would play a substantial role in distorting elemental abundances and energy spectra between those with and without "hot" circumstellar x-rays in the vicinity of a pulsar (Fig. 8). This nuclear "milking", however, would partly produce helium overabundance at 10^{13-14}eV/amu regime relative to protons (Fig. 7, Takahashi, 1987), as a direct consequence of (gamma-alpha) photo-nuclear dissociation,

while (gamma, n) or (gamma,p) processes would affect "milking" at somewhat higher energies for most nuclei. All of these new problems, inspiring high energy observations, are possibly very much related to details of supernova explosions and/or other unknown mechanism, and advancement of higher energy observations is anticipated to reveal some of hitherto unclarified, local-energetics of the galactic activity.

2. Qualification of Detectors for High Energy Observations

The first or fundamental qualification for any experiments is energy and charge measuring capability within a limited space-flight configuration. Familiar detectors at low energies such as ionization detectors, Cerenkov counters, transition radiation telescope, would disqualify at energies above 50, 500, and 5000 GeV/amu, respectively, unless some drastic breakthroughs are made. The ordinary, one-dimensional, total-absorption-type calorimeter, would measure energies upto 100 TeV (considering its finite radiation length of about 30 - 40 r. l. at best); however, it would disqualify for most space flight experiments due to its monstrous weight.

The JACEE balloon flight experiments using emulsion chambers (Fig. 9) have demonstrated excellent capability of measuring energy and charge of high energy cosmic ray particles even beyond 100 TeV/amu. Using a visual or photometric electron-sampling method within a small-radius and its lateral scaling law, this calorimetric technique was founded in the late 1950's to early 60's by the three-dimensional electro-magnetic shower theory (Nishimura, 1964), and in the late 1970's, by 300 GeV electron calibration experiments (Dake et al., 1977; Hotta et al., 1980). In addition to this already-proven technique, a use of the direct electron-pair production method has been investigated and calibrated in recent years (Takahashi et al., 1985; Derrickson et al., 1988; Eby, 1988). It is hoped that these works provide upon further refinement of the cross section, another energy measuring technique, for high energy heavy nuclei, even upto 10,000 TeV/amu, within a few cm-thick nuclear emulsions.

Extension of the composition measurements to the spectral bend at 10^{15} eV is of critical importance in the understanding of cosmic ray accceleration and confinement in the galaxy, but would require a successful balloon flight program of at least for another several decades. Light-weight, and economical detectors, (emulsion chambers), may realize these high energy experiments on a longer exposure facility in space, since it has a large dynamic range of performance in measuring the energy and the charge of cosmic ray particles.

It should be also considered that the emulsion chamber measurements by JACEE of heavy ion interactions at above 1 TeV/amu remain the only source of high energy data for exploring a possible phase change of nuclear matter. After exploratory high energy heavy-ion experiments with the CERN SPS we learned that the energy density achievable with 200 GeV/amu beams falls short of several GeV/fm^3, while high energy cosmic ray events have exhibited even higher densities. Some illuminating collective effects, including high transverse momentum, being demonstrated in the JACEE cosmic ray events, may be confirmed by planned heavy-ion colliders (RHIC) within 10 years, but nuclear and particle physics at higher energies and higher particle densities inevitably require minute track detectors (as good as emulsion chambers), which demand further use of cosmic rays and emulsion chambers. The projected balloon-borne magnet spectrometer facility, and ASTROMAG, will provide excellent opportunities to perform most-detailed and confirmative experiments of heavy-ion interactions with magnetic emulsion chambers (MAGIC detector, described later; also Iyono, this volume). These emulsion chamber experiments may promise a maximum return from space, since they are capable to produce data in both fore-front astrophysics and nuclear/particle physics.

Well-calibrated emulsion chambers with various physical capabilities, if prepared with sufficient preparatory investigations, will meet requirements for advanced observations of particles and nuclei in space at these high energies, as pointed out in recent workshops of the use of space facility for cosmic ray physics. The cited workshops are:

The Workshop on Cosmic Ray and Gamma-Ray Experiments for the Space Station Era, LSU, Baton Rouge, October 1984; Proceedings published by LSU Press, Eds. W. V. Jones and J. P. Wefel, 1985,

and

The Workshop on Scientific Uses of the Space Station, UCSD, San Diego, August 1985; Proceedings published by Washington University, Ed. J. Klarman, 1986.

At least a dozen papers at these workshops discussed the application and advantages of emulsion detectors. In 1985 the NASA Cosmic Ray Working Group issued a report which endorsed as a major element of its recommendations the development of "a programmatic plan to measure the spectra of cosmic rays at high energies". Two candidate approaches are calorimeters (the HESS Array - Ormes and Streitmatter, 1985) and Large area passive arrays including emulsions (Takahashi and Gregory, 1985). In the latest (1988) report of the same Working Group recommends CRNE on Station. (An optional use of emulsion chambers with CRNE has been informally discussed by University of Chicago team and the present author.)

3. State of the Art of Emulsion Techniques

Nuclear track emulsions have been used in cosmic ray research for 50 years and have been the detection medium for many major landmarks in both particle/nuclear physics and cosmic ray astrophysics. Some of these are

(1) the first demonstration of existence of π-meson (Lattes et al., 1947);
(2) the discovery of heavy and high charge elements in the cosmic radiation (Freier et al., 1948; Bradt and Peters, 1948);
(3) one of the first measurements of the low energy cosmic ray helium spectrum (Fowler et al., 1957);
(4) confirmation of trans-iron nuclei in the cosmic rays (Fowler et al., 1967);
(5) discovery of charmed particles (Niu et al., 1971);
(6) observation of electron spectrum to the highest energy region (Nishimura et al., 1980);
(7) observation of secondary particle multiplicities exceeding 1,000 and first information in search of new state of matter (quark-gluon plasma) in nucleus -nucleus interactions above 1 TeV/amu (JACEE 1983(a), 1984(a), 1986(b));
(8) the first direct measurement of chemical composition of cosmic rays at 10^{14} eV (JACEE 1983(b), 1984(b)).

As noted by this brief list, the use of photographic emulsions has not only been remarkably sustained over many decades but continues to be a powerful technique. The JACEE results listed above, and other landmarks, were obtained with use of emulsion stacks or emulsion chambers flown on high altitude balloons. Such chambers, which consist of stacks of nuclear-track emulsions, heavy metal plates and other etchable detector materials, were originally devised by Kaplon et al. (1952) for the study of nuclear effect of the interaction and cosmic ray energy spectra. The technique has been improved and rejuvenated for much higher energy studies by several groups, most recently by the JACEE collaboration (JACEE, 1986a).

In spite of the tremendous strides made in electronic detector technology during the same historical period, emulsion chambers still find unique application. One reason is their high spatial resolution, and ability to record multiple tracks from interactions in full detail. It should be also emphasized that emulsions record most natural phenomena without pre-selection or prejudice, and hence, often provide an opportunity for revelation of hitherto-undiscovered phenomena or priciples in physics. This character, though a weak point for quick data retrieval, has endowed, and will continue to assign, emulsions a role of "unmasked watcher or guide" in observations of such natural phenomena as cosmic rays.

4. Need for Further Technical Work in Emulsion Chamber Technology

1). Average Isotopic-Mass Evaluation via Heavy-Ion Interactions

Detectors that have a variety of unique capabilities are most desired to maximize the scientific return from valuable space experiments. Further research into emulsion chamber techniques, in addition to the existing energy measuring methods, would be prudent. Several important new technical feasibility of those described above are recently demonstrated from preliminary efforts (Takahashi et al., Spring Meeting of American Physical Society, Baltimore, 4/18-22, 1988). So far the isotopic distribution measurement of element above 1 GeV has been technically prohibitive, not to speak of above 1 TeV/amu. If we continue further to elaborate understanding of nucleus-nuclus collisions with existing and future data, the mass evaluation, at least for those Ar (36 and 40) and Ca (40 and 48) nuclei, would become possible, although the technique is still far from being able to give a mass assignment for individual nuclei. In particular, the statistical, isotopic evaluation for nuclei like Ar and Ca is considered important in probing possible SN type-II origin of high energy nuclei (Hartman, Woosley and El Eid, 1985; Takahashi et al., 1986). Very accurate atomic mass number dependence of central rapidity-density must be established for this. Fig. 11 illustrates present summary of the inclusive rapidity density data as a function of the atomic mass number. Empirically, it can be best understood as $B^{0.45 \pm 0.05}$ for the data from the JACEE-III experiments (Burnett etal., 1987) and the CERN ^{16}O (200 GeV) experiments (Jain, 1987; Hayashi et al, 1988; Iyono, this volume).

2). Long-Range Delta-Rays and Transition Radiation

Examination of long-range delta-rays would potentially allow measurement of transition radiation-Compton process in long-range delta-rays above about 20 keV: Nuclear emulsion is found to be an efficient transition radiator, having numerous microscopic interfaces of different plasma frequencies (silver-halide crystals and gellatine). It is also conceived that emulsion itself works as an excellent detector of them, since these x-rays, shortly after emission off the nuclear track, give rise to electrons by subsequent Compton scattering, which leave track records similar to long-range delta-rays (Takahashi et al., 1988). If this process is confirmed as a cause of the known anomaly in long-range delta-rays (Kim, 1967; Takahashi, 1985; Takahashi et al., 1988(b)), it will let the transition radiation process be calibrated for cosmic ray observations. Coupled with the ongoing exploration of a direct electron-pair technique, and a

method to evaluate isotopic abundances of heavy nuclei, these new techniques may enrich the world of high energy cosmic ray nuclei studies in future space-flight exploration.

3). Minute Tracking Technology

In addition to these techniques, a very fine tracking method in the magnetic field has been recently demonstrated in the CERN EMU05 emulsion chamber experiments for a heavy-ion interaction study (Takahashi et al., 1988). The new emulsion chamber called as MAGIC (Magnetic-Interferometric-Emulsion-Chamber), uses very thin emulsion films (50 micron emulsions on 70 micron thick polystylene) in a magnetic, tracking telescope (Fig. 10), designed to measure isospin-correlations and momentum distributions. (A similar idea, but with different configuration and objectives, has been independently considered by several other people for study at much low energies (Hayashino, 1987)). The MAGIC detector allows the most detailed observation of tracks emanating from high energy interactions. For the first time in the long emulsion history, a successful use of magnetic field for charge-sign and momentum measurement is finally realized (Takahashi et al., 1988(a); Hayashi et al., 1988; Tabuki et al., 1988). Isospin correlations, particle momenta, emission angles, have been accurately measured for all the individual tracks in very high-multiplicity (more than 500) events. Capability of particle identification among electrons, muons, pions, kaons, protons, Sigma-, Xi-, and Omega-hyperons, is demonstrated as a realistic, and fruitful work. We plan to examine methods of particle tracking and ionization measurements further in magnetic field with emulsion chambers so that information on momentum distribution, particle composition, and isospin distribution could be studied in very high energy, heavy nucleus interactions in a future magnet facility (e.g., Astromag). In particular, we try to develop a semi-automatic method of ionization measurements by applying electron microscopy for steep tracks. A fundamental relationship of the grain density vs. momentum for "silver-halide crystals in a magnetic field" is hitherto unclarified, and must be studied both experimentally and theoretically.

Application of these techniques would be conceived in Super-JACEE experiments, which utilize superconducting magnet and emulsion chamber in space. Very high energy densities in heavy-ion interactions above several TeV/amu could be achieved in JACEE-type experiments with the most detailed data including charge-sign and momentum assignments of individual charged tracks. The best confirmation of high P_T measurements would be possible by such an experiment, while the previous JACEE experiments are limited to measure P_T of photons.

The minute tracking technology not only provides unique nuclear collision data, but also can benefit particle/nuclear astrophysics program in future by allowing examination of other single individual cosmic ray tracks; an application of which in Astromag program may open a window in quest of presently-undiscovered, astrophysical objects such as stable and neutral H-particles (Lambda-Lambda bound state), and other strange matter, which are presumably remnants of the materialization in the big-bang. Candidates may be observed in neutral primaries which are producing more particles and strange particles than protons at equivalent energy.

For further technological advancement of emulsion methods, various calibration work are remaining. One can achieve a part of them by analyzing various nuclear emulsions exposed in previous balloon flight experiments and accelerator exposures. These can cover wide energy region, and will provide substantial calibration of emulsion techniques for future space flight experiments. Thus, major efforts will be devoted to the analysis of nuclear tracks in available emulsions. However, three new calibration experiments will be also performed in the present efforts, which are:

(1). 180 GeV/amu Pb-beam (1991) and 12 GeV/amu Au-beam (1990) for calibrating Z^2-scaling of cross sections for direct-electron production and transition radiation;

(2). 10 - 500 GeV muons for delta-ray range spectrum measurement and highest-Lorentz factor calibration of direct electron-pair production, by using accelerators at Brookhaven National Laboratoty and Fermilab;

(3). Ionization calibration in the magnetic field, using some available accelerator that can vary the velocity of the beam particle 0.05c to 0.999c. (KEK PS may be a useful machine).

Several other technical considerations are due. In particular, investiment in advancement of video-memory analysis is most important, not particularly for the quality of the data, but for the speed of the analysis. When we review the degree of such investiment in emulsion technology, we are surprised to learn how small effort has been made in the whole emulsion laboratories. Labor-intensiveness of emulsion works have been criticized for its slow analysis and also for its unaccessibility by less-experienced scientists. Since space-flight missions demand a bank of retrieved data in standardized form as well as permanent storage of original emulsions, it is urgent to lay-out a plan of advanced video-analysis.

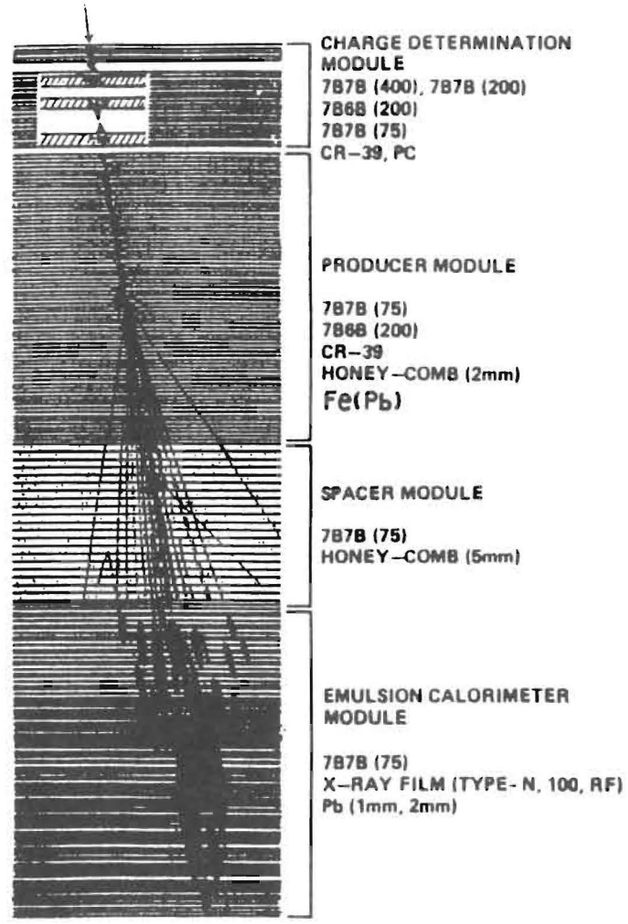

Fig. 9

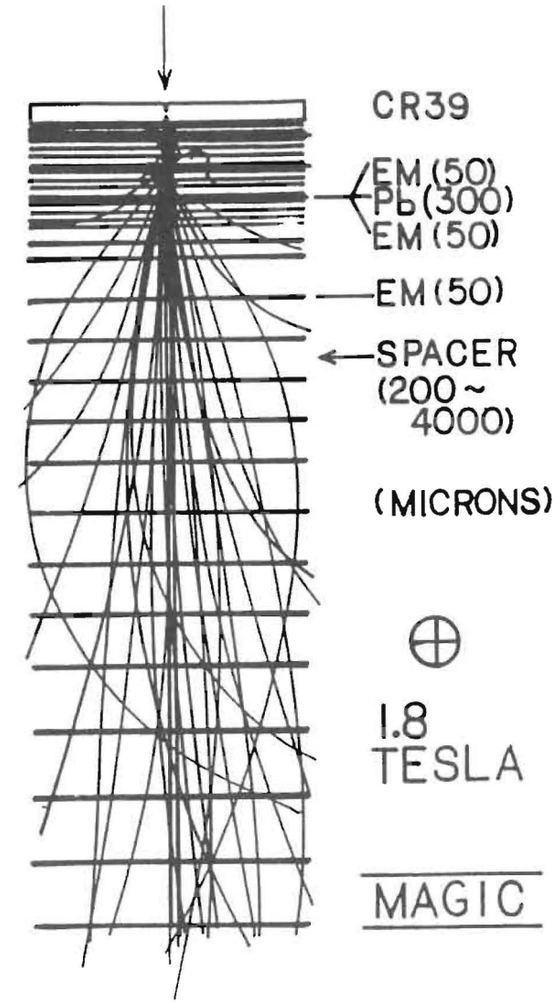

Fig. 10

Fig. 9. JACEE emulsion chamber

Fig. 10. MAGIC chamber

5. Current State of the Art.

Which emulsion detectors (MAGIC or JACEE-type) are used will depend on what should be measured. For measurements of long-range delta-rays and direct electron-pairs, the JACEE-type is preferentially adopted; and for the central rapidity density measurements and secondary tracking in nuclear collisions, the MAGIC-type is more advantageous.

Scanning and measurements have been performed with a microscope - TV - digitized computer, with objectives magnification of 20 - 100 x. Any existing microscope facilities will be used for these measurements, but it is very desirable to have at least a digitized microscope and a desk-top computer (with hard disc of 40 MB).

5-1. Delta-Ray Measurements

With the highest magnification (100 x 10 x 1.7) transversal range of individual delta-rays can be registered when it is longer than 1/5 unit of a reticle (1.0 micron). Measurements on tracks of accelerator nuclei are performed until the total number of delta-rays reaches 20,000. Fig. 12 shows some examples, with statistics of about 5,000 obtained in the preliminary measurements. Some comparable cosmic ray track data are shown in Fig. 13. A range-spectrum calculated for knock-on, and for TR + Compton component, taking account of the size distribution of silver-halide crystal and gelatine interfaces, is given in Fig. 14a, for comparisons with the preliminary accelerator data, and Kim's unpublished proton data (Kim, 1965) (Fig. 14b). To speed up the measurements, application of CCD-TV video-analysis with multiple frame-grabber-memory is useful which store optical density along the track, and allow an integral digital image analysis of delta-rays.

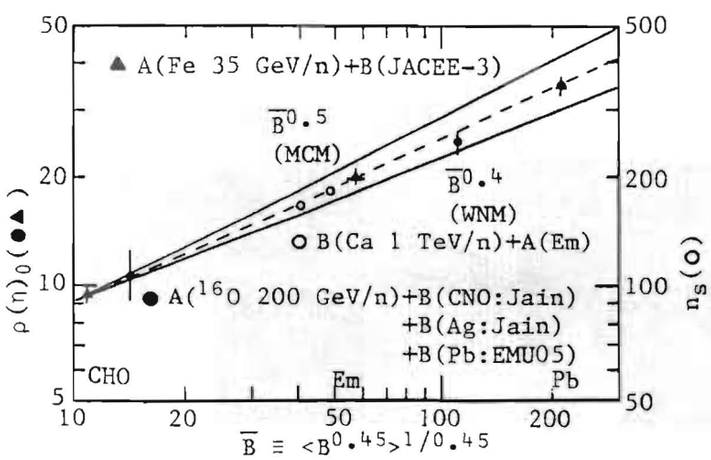

Fig. 11 Empirical atomic-mass-number dependence of the central rapidity-density in nucleus (A) + nucleus (B) collisions.

Fig. 12 Range spectra of delta-rays from nuclei at 2, 60, and 200 GeV/amu.

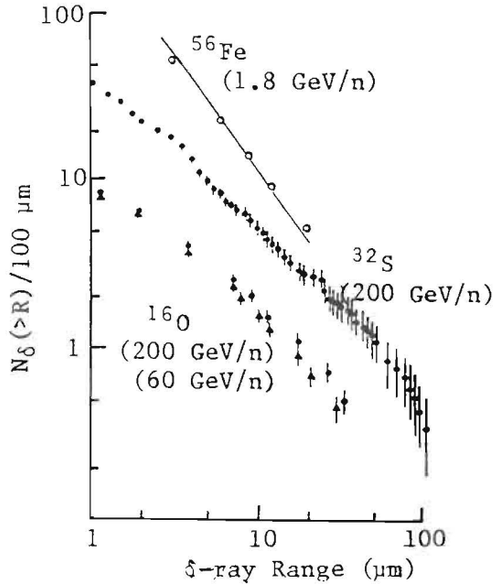

Fig. 13. Range spectra of delta-rays from high energy cosmic ray nuclei above 1 TeV.

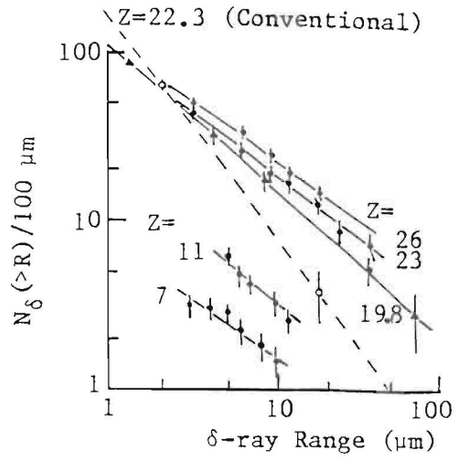

Fig. 14a. X-ray and electron energy spectra due to Transition Radiation and subsequent Compton scattering.

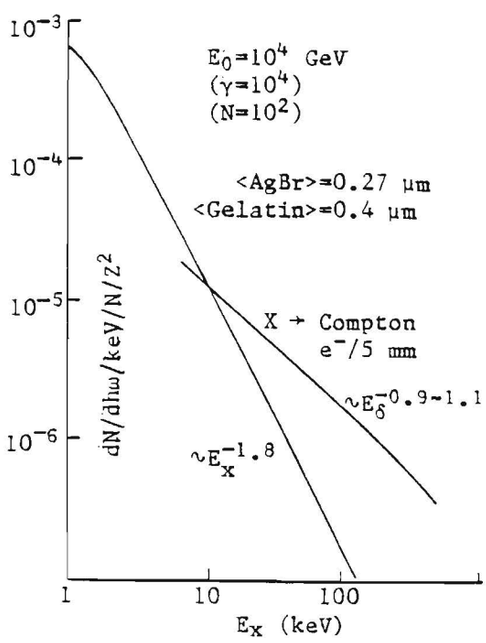

Fig. 14b. Anomalous delta-rays in high energy proton tracks.

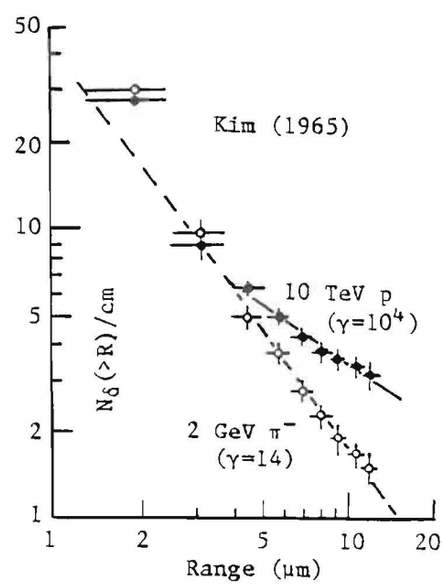

5-2. Direct electron pairs

Pairs are registered during the along-the-track scanning with the highest magnification of microscope. Scanning of available tracks for high energy cosmic ray nuclei in the balloon-borne emulsions is usually limited to several mm, and statistics of pairs is not sufficient for primary energy determination. Either JACEE-type or MAGIC-type emulsion chambers have to install thick emulsions so that several cm of track lengths for each events could be secured. In accelerator emulsions we continue scanning and registration until 1,000 pairs are registered (corresponding to the resulting statistical error of cross section to about 3 %). This will provide a calibration cross section of pair-production, necessary basis for cosmic ray energy determination by the direct electron-pair method.

Figs. 15a and 15b illustrate the present status of available cross section data and calculational data, respectively. It is understood at this stage that the suppression of cross section at low Lorentz Factors is observed, and a theory consistent with these data predicts asymptotic release from this suppression at Lorentz Factor higher than 10^4. Muons, unlike electrons, do not significantly contaminate the e-pair data with bremsstrahlung-oriented, external e-pair production. The muon beam at the highest energy (500 GeV) is crucial in establishing unambiguous cross section data at high Lorentz factor (5000). Electrons, though providing much higher Lorentz factors, are very ambiguous for this study due to its large cross section of bremsstrahlung and external conversion.

Fig. 15a. Available data.

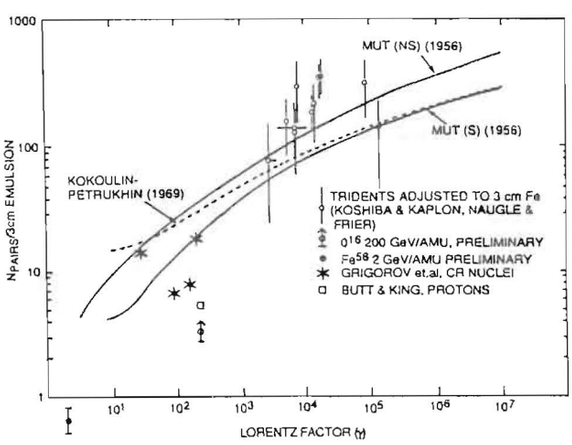

Fig. 15b. Calculations.

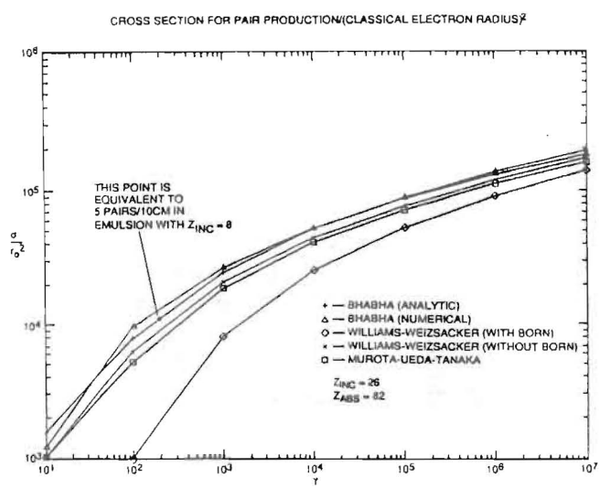

5-3. Central rapidity density, tracking and dE/dx.

Secondary tracks in the JACEE cosmic ray events have been measured in emulsion plates located immediately downstream the interaction vertex. Fig. 11 shows the atomic mass number dependences of central rapidity density observed with cosmic rays (JACEE, 1987a) and with accelerator Oxygen beams (Jain et al., 1988; Takahashi et al., 1988a). Open circles in this figure illustrate an expected difference of the rapidity density for ^{40}Ca and ^{48}Ca.

Much detailed, nuclear interaction data in accelerator emulsions, are obtained during tracking procedure at almost every available layer (typically 15 layers) of the MAGIC detector. Tracking accuracies are 2.0 micron in the longitudinal coordinate (z), and 0.7 microns in the transverse coordinates (x, y) for Oxygen events with the microscope we have been using. The momentum measurements of charged tracks in a Magnetic field of 1.8 Tesla show accuracies to (1.5 + P/3 GeV/c)% for 15-layers of MAGIC telescope (Fig. 16). Space application with 1.3 - 1.0 Tesla super-conducting magnet (such as Astromag) may be slightly poorer in momentum measurements.

Fig. 17 shows pseudo-rapidity distribution of different charge-signs (+, -) in an event of ^{32}S (200 GeV/amu) + Pb (Takahashi et al., 1988a).

Fig. 16. Momentum resolution.

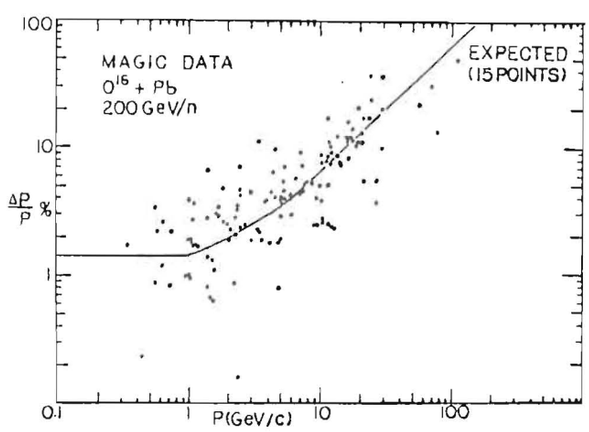

Fig. 17. Pseudo-rapidities of positive and negative tracks.

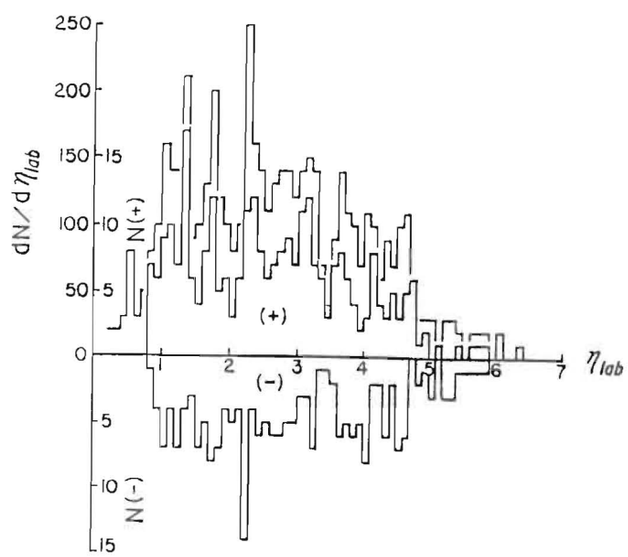

The ionization measurements (grain counting) are made for large angle tracks (dip angle smaller than 60 degrees). Fig. 18a shows an example of the particle-identification data obtained from measurements in a single emulsion plate, and Fig. 18b, an expected refinement of it using all available emulsion layers. Particle identification for tracks with much smaller angles and higher momenta (up to 10 GeV/c) will be made in the special, thick emulsions which are forced for this purpose to have a large (400 microns) distortion, and the grain density can be easily counted. The lateral distance for these measurements extends as wide as 1 cm. The ultimate accuracy of momentum and grain density measurements should be about 1.5% and 3.5%, respectively (Fig. 18b). Because of such a superb accuracy, particle identification is possible, discriminating electrons, muons, pions, kaons, protons, hyperons and deuterons.

Fig. 18a. Single layer data.

Fig. 18b. Expected resolution with full emulsion measurements.

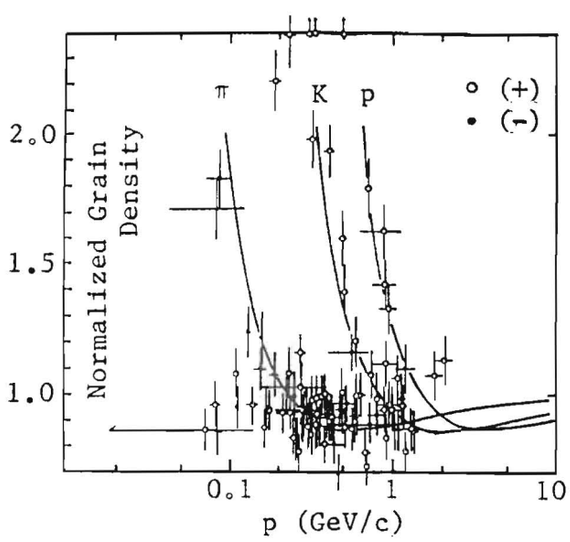

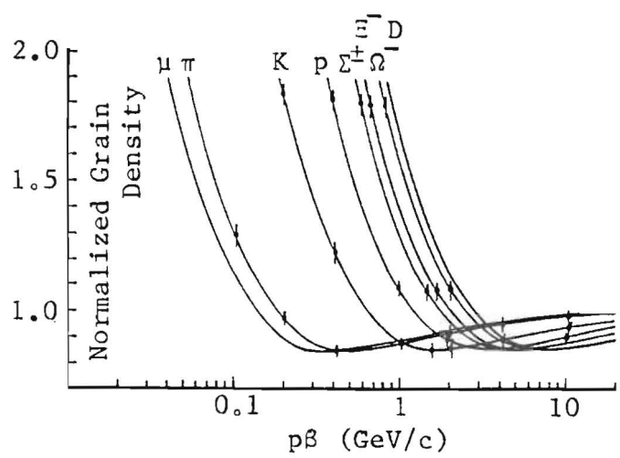

5-4. Use of MAGIC in Space - Super-JACEE type Experiments.

Use of these techniques in space will allow a study of very high density state of matter in heavy-ion collisions above several TeV/amu. A super-conducting magnet is necessary to allow a detailed track analysis in the MAGIC-type emulsion chambers. The planned construction at KEK of R & D magnet for Astromag (KEK report, Nishimura and Yamamoto et al., 1987) will meet requirements in accomodating MAGIC-type experiments. A Super-Conducting Japanese-American-Cooperative-Emulsion-Experiments (SUPER-JACEE), now under consideration, is one of such experiments. Fig. 19 illustrates a conceptual configuration of MAGIC in Astromag Prototype.

Fig. 19. A Conceptual Configuration of MAGIC in KEK's Prototype magnet considered for the Super-JACEE plan.

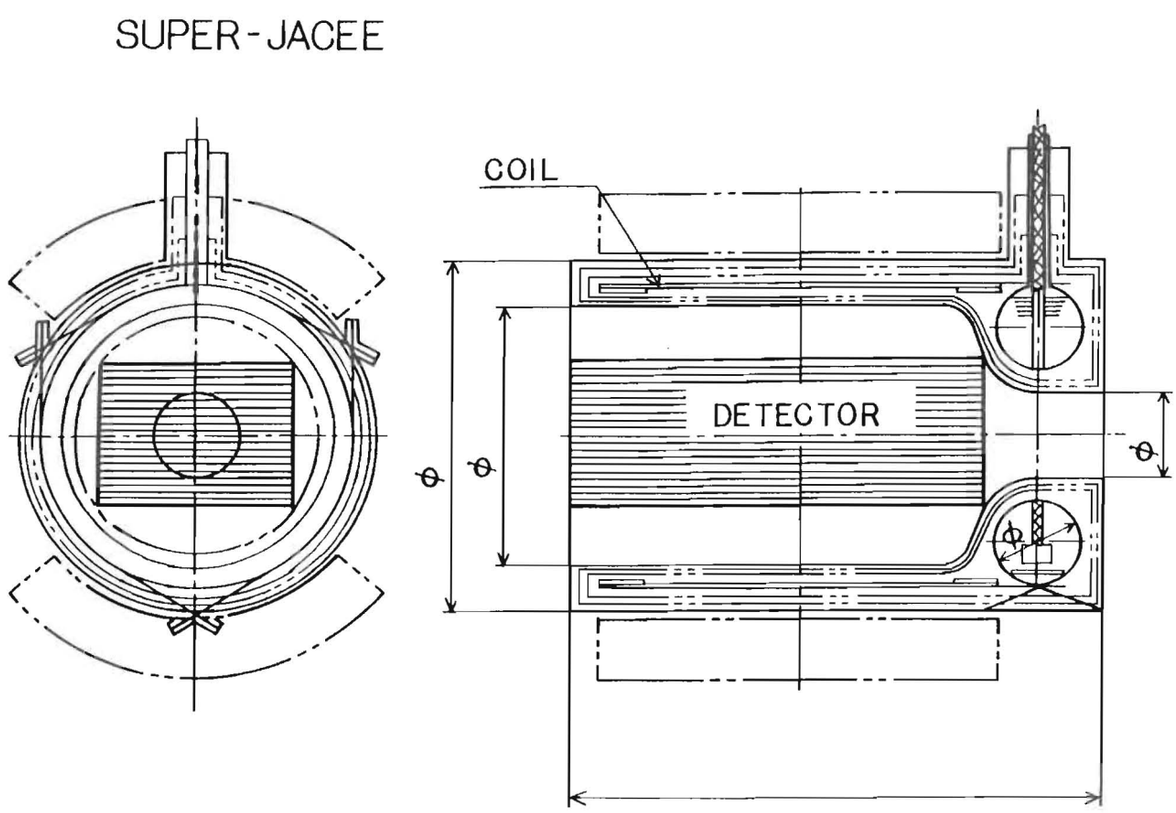

6. Experimental Plans

Here we summarize on-going and planned high energy experiments. Firstly, Long-Duration-Balloon-Facility (LDBF) of NASA in Australia has launched two emulsion chamber experiments in 1987 and 1988 for the JACEE emulsion chambers. Flight time of 150 hours and 120 hours were achieved in these Half-Around-the-World (HATW) flights. A full-scale, Around-the-World (ATW) flights for 200 - 400 hours will be restored in a few years, since several ballooning problems have been resolved gradually. In addition to these ATW from Australia, NASA plans HATW flights from Bermuda to California, and New Zealand to Argentine in a few years. Significant advancement in collecting high energy nuclei will be thus achievable in coming several years by using these balloon flights. A Super-JACEE type experiment is more safely conducted in the HATW from Bermuda because a chance to lose an expensive magnet in the ocean is negligible and a larger scientific payload (over 1.5 tons) could be accomodated in this campaign.

Several space-flights of emulsion chambers are authorized by NASA or under considerations. One of test Shuttle Flights will be conducted in the Get-Away-Special (GAS) on the Shuttle which is manifested for the State of Alabama experiments (Fig. 20a). Second next test flight with a full-size JACEE emulsion chamber is recently manifested in the Office of Space Application and Technology (OAST) of NASA for the University of Alabama JACEE team (Fig. 20b).

Fig. 20a. UAH's GAS Flight

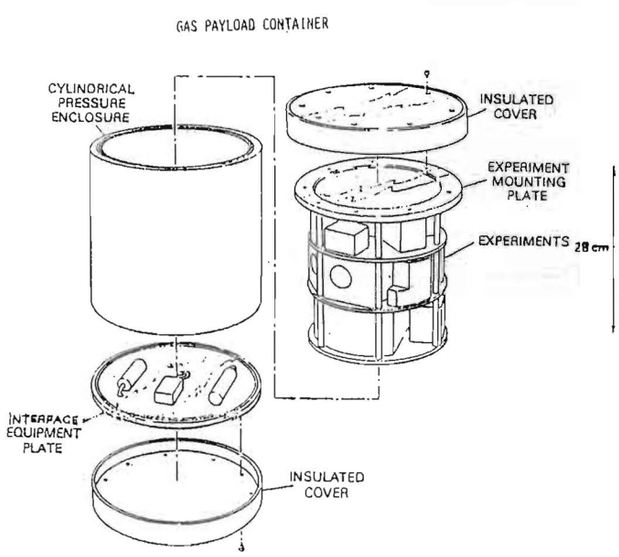

Fig. 20b. UAH's Shuttle Flight

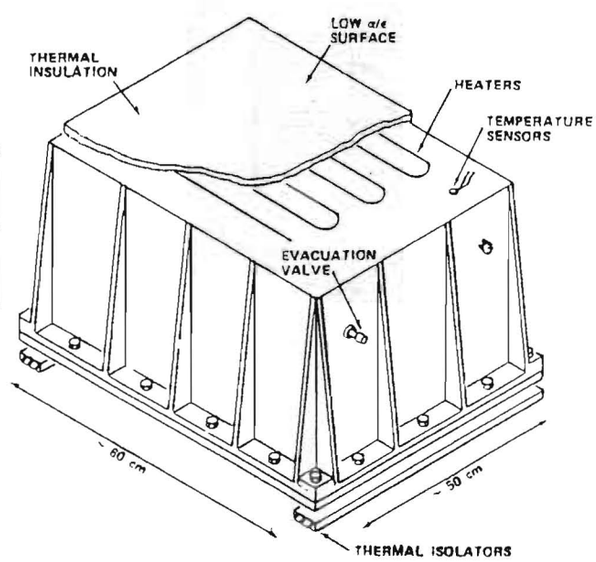

Full-size space experiments must necessarily await a plan in the Space Station. U. S. facility of A Small-Attached-Payload (ASAP) and Japan's JEM S-003 are those planned or discussed already (Fig. 21a and Fig. 21b, respectively). These will allow observations of cosmic particles and nuclei up to 10^{16} eV/nucleus by repeated several-months' exposures of a few m^2 detectors.

Other possible, known plans are Astromag (Fig. 24), Heavy-Nuclei-Collector (HNC) (Fig. 22), and Cosmic-Ray-Nuclei-Experiment (CRNE) (Fig. 23) facilities. These still remain as strawman and can accomodate exciting new ideas and instruments so that challenging studies are encouraged. A coupling of JACEE-type and MAGIC-type emulsion chambers with existing electronic counters and plastic detectors are also feasible in these future facilities.

Fig. 21a. ASAP Facility.

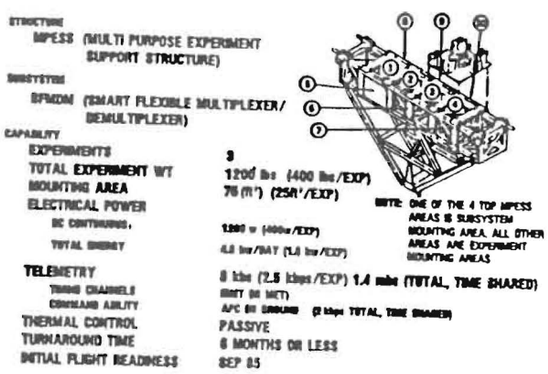

Fig. 21b. JEM S-003 Facility.

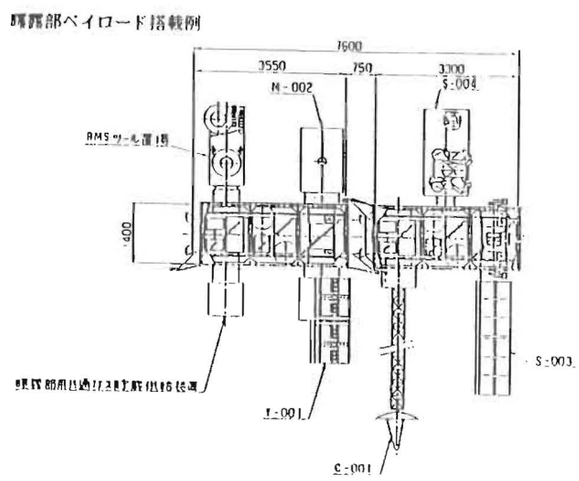

Fig. 22. HNC configuration.

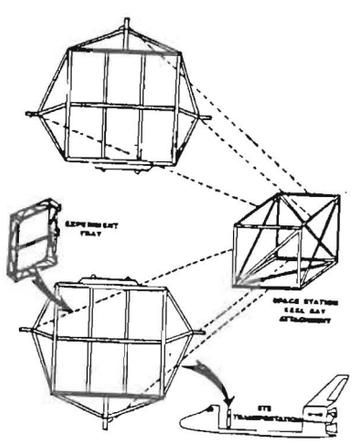

Fig. 23. CRNE configuration.

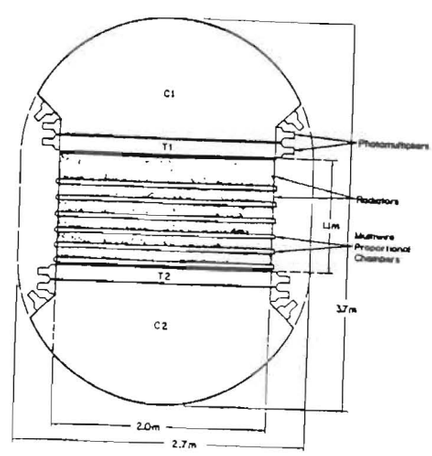

Fig. 24. Astromag configuration.

PARTICLE ASTROPHYSICS MAGNET SPECTROMETER (ASTROMAG)

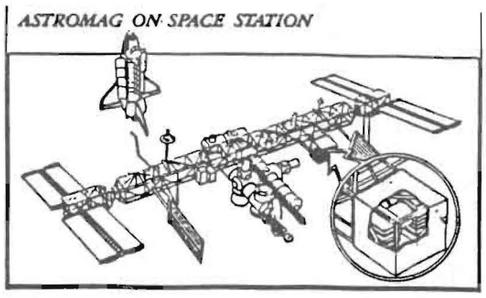

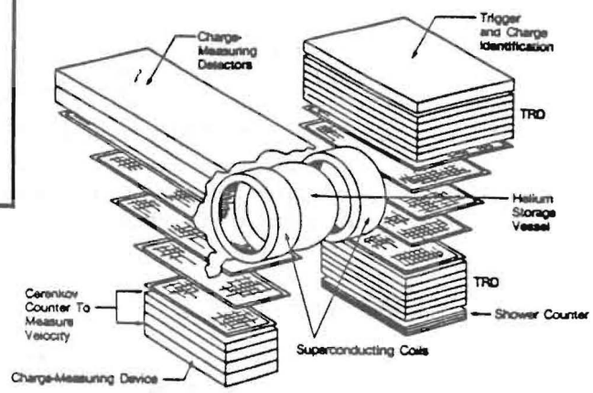

Headquarters Contact/Program Scientist
W. V. Jones, 202-453-1460

GSFC Contact/Project Scientist
J. F. Ormes, 301-286-5705

Requirements

Duty Cycle	100%
Payload Mass	5000 kg
Thermal/Active	-10 to +40 Deg. C
Pointing/Stability	None Required
Clearance	Anti-Earth (30 Deg); magnetic field below 3 gauss on Station
Location	Two-Bay Outrigger between Modules and Solar Panels
Power	28 VDC; 1 kW operation, 1.4 kW servicing (1day/yr)
Data Rates	1 kbps CMD, 100 kbps Science Data
Flight Duration	5-10 yr; experiment exchange each 1-2 years
Dimensions (m)	3.0 x 4.5 dia. (fits inside 5 cubic m bay)
Cryogen resupply	3.5 cubic meters/yr
Storage	10 cubic meters (Ancillary experiments; Cryogen/gas resupply)
Crew Utilization	1 day/year (Cryogen resupply)
Crew Console	"Button" as contingency for emergency Shutdown of Magnet

7. Summary

High energy particle and nuclear astrophysics is still at the early stage of evolution. Future balloon-flights and space-flight opportunities under discussions or preparations offer an opportunity to drastically advance knowledges of high energy particle composition and their origin. One of the most promising techniques for these experiments is an advanced emulsion chamber method. Its feasibility and usefulness described herein have been recognized for already some time, and its ground-based, further examinations, are recommended. The author is greatly indebted to the following people in summarizing status of the subject: The JACEE Collaboration, The CERN EMU04 and EMU05 Collaborations, Dr. J. Nishimura, and Dr. J. Ormes. Support and hospitality of workshop organizers and KEK Department of Physics are gratefully acknowledged.

8. References

1. W. R. Binns, et al., Ap. J. 324, 1106 (1988).

2. M. L. Bradt and B. Peters, Phys. Rev. 74, 1828 (1948).

3. S. Dake et al., Proc. 15th Int. Cosmic Ray Conf., Plovdiv, 7, 322 (1977).

4. J. D. Derrickson et al., EMU04 Collaboration: T. A. Parnell, J. D. Derrickson, P. B. Eby, W. F. Fountain, F. E. Roberts, J. W. Watts, J. C. Gregory, T. Hayashi, Y. Takahashi, S. Dake, M. Fuki, A. Iyono, T. Ogata, T. Tabuki, T. Tominaga, S. P. Ahlen, A. Marin, G. Tarle, J. A. Musser, Bull. Am. Phys. Soc. 33, 1068 (1988).

5. P. B. Eby, unpublished, 1988.

6. P. H. Fowler, C. J. Waddington, P. S. Freier, J. Naugle and E. P. Ney, Phil. Mag. 2, 157 (1957).

7. P. H. Fowler, R. A. Adams, V. A. Cowan, J. M. Kidd, Proc. Roy. Soc. A 301, 39 (1967).

8. P. H. Fowler et al., Proc. 19th ICCR, San Diego, 2, 119 (1985).

9. P. Freier, E. J. Lofgren, E. P. Ney and F. Oppenheimer, Phys. Rev. 74, 1818 (1948).

10. J. M. Grunfeld, et al., Ap. J. 327, L31 (1988).

11. D. Hartmann, S. E. Woosley and M. F. El Eid, Ap. J. 297, 837 (1985).

12. T. Hayashi et al., EMU05 Collaboration: Y. Takahashi, J. C. Gregory, T. Hayashi, J. H. Derrickson, P. B. Eby, W. F. Fountain, T. A. Parnell, F. E. Roberts, J. W. Watts, S. Nagamiya, S. Dake, M. Fuki, A. Iyono, T. Ogata, O. Miyamura, T. Tabuki and T. Tominaga, Bull. Ame. Phys. Soc. 33, 1068 (1988).

13. N. Hotta et al., Phys. Rev. D22, 1 (1980).

14. The JACEE Collaboration: T. H. Burnett, S. Dake, M. Fuki, J. C. Gregory, T. Hayashi, R. Holynski, J. Iwai, W. V. Jones, A. Jurak, J. J. Lord, O. Miyamura, H. Oda, T. Ogata, T. A. Parnell, T. Saito, T. Tabuki, Y. Takahashi, T. Tominaga, J. W. Watts, B. Wilczynska, R. J. Wilkes, W. Wolter, and B. Wosiek; Phys. Rev. Lett. 50, 2062 (1983)(a); Phys. Rev. Lett. 51, 1010 (1983)(b); Proc. Quark Matter 84 Conference, Helsinki, Lecture Notes in

Physics 221, 187 (1984)(a), Springer Verlag; Proc. Int. Symposium on Cosmic Rays and Particle Physics, University of Tokyo, Japan, eds. A. Ohsawa and T. Yuda, p. 740 (1984)(b); ibid., p. 468 (1984)(c); Nucl. Phys. A447, 189c (1985); Nuclear Instr. and Methods A251, 583 (1986)(a); Phys. Rev. Lett. 57, 3249 (1986)(b); Phys. Rev. D35, 824 (1987); Ap. J. (submitted) 1988.

15. W. V. Jones, presentation at Guntersville Workshop on A Small Attached Payload, NASA, February, 1988, and a private communication, 1988.

16. E. Juliusson et al., Proc. of 18th International Cosmic Ray Conference, Bangalore, 2, 21 (1983).

17. M. F. Kaplon, B. Peters, H. L. Reynolds and D. M. Ritson, Phys. Rev. 85, 2, 295 (1952).

18. C. O. Kim, University of Chicago preprint, 1965 (unpublished).

19. J. F. Ormes and R. E. Streitmatter, Proc. of the Workshop on Cosmic Ray and Gamma Ray Experiments for the Space Station Era, p. 340, Eds. W. V. Jones and J. P. Wefel, LSU, Baton Rouge (1985).

20. J.-P. Meyer, Proc. of 19th ICCR, San Diego, 9, 141 (1985).

21. P. Meyer, R. Ramaty and W. R. Webber, Physics Today, October, 1974, p. 23.

22. J. Nishimura et al., Ap. J. 238, 394 (1980).

23. J. Nishimura, Prog. Theor. Phys. Supple. 32, 72 (1964).

24. T. Tabuki et al., EMU05 Collaboration, Bull. Ame. Phys. Soc. 33, 1068 (1988).

25. Y. Takahashi et al., EMU05 Collaboration, Proc. of Intern. Conf. on Phys. & Astrophys. of Quark-Gluon Plasma, Tata Institute, Bombay, Feb. 8 - 12, 1988, ed. B. Sinha, World Scientific Pub., Singapore 1988(a), in press; Y. Takahashi et al., EMU04 Collaboration, Bull. Ame. Phys. Soc. 33, 1069 (1988)(b).

26. Y. Takahashi and J. C. Gregory, Proc. of the Workshop on Scientific Uses of the Space Station in Cosmic Ray and Gamma Ray Physics, UCSD, San Diego, ed. J. Klarman, p. 144, Washington University 1985.

27. Y. Takahashi, S. Miyaji, T. A. Parnell, M. C. Weisskopf, T. Hayashi and K. Nomoto, Nature 321, 839 (1986).

27. Y. Takahashi, Proc. Workshop on Cosmic Ray and High Energy Gamma Ray Experiments for the Space Station Era, ed. W. V. Jones and J. P. Wefel, p. 203, LSU Press 1985(a); Physics in Collision 5, Edition Frontieres, eds. B. Aubert and L. Montanet, p. 443 (1985)(b); Lecture Notes in Physics, Proc. of IAU Colloquium No. 107, September, 1987, University of Tokyo, ed. K. Nomoto, Springer Verlag (1988)(a); Nucl. Phys. A478, 675C (1988)(b); Bull. Ame. Phys. Soc. 33, 1069 (1988)(c).

28. Y. Takahashi, P. B. Eby, T. A. Parnell, J. C. Gregory and T. Hayashi, Proc. of Cosmic Ray and High Energy Gamma-Ray Experiments for the Space Station Era, ed. W. W. Jones and J. P. Wefel, p. 390 (1985), LSU Press.

29. C. J. Waddington et al., Proc. of 19th ICCR, San Diego, 9, 527 (1985).

30. W. R. Webber et al., Proc. of 19th ICCR, San Diego, 2, 88 (1985).

31. A. Yamamoto, Proceeding of Astromag Workshop, July 9 - 10, 1987, KEK REPORT 87-9, H, eds. J. Nishimura, K. Nakamura and A. Yamamoto, p. 13, (1987); also, S. Orito, op.cit., p. 111.

Searching for the Quark-Gluon Plasma

David S. Koltick
Purdue University
West Lafayette, Indiana
United States 47907

ABSTRACT

The search for the Quark-Gluon Plasma is discussed in
Proton-Antiproton collisions

Hadronic matter at extremely high density is a large unexplored region of physics which experiments are just now starting to investigate[1]. Matter at high density exists naturally in various forms and illustrates well the physical richness of such systems.

Nuclear Matter	$\cong$ 0.16 GeV/fm^3	
Proton	$\cong$ 0.5 GeV/fm^3	(1)
Neutron Star	$\cong$ 2 - 3 GeV/fm^3	

QCD should predict the behavior of hadronic matter at these densities, just as QED should be capable of explaining electrically charged matter which interacts in bulk. As a check of the correctness of this assumption we can turn to experiments done at the highest energy e^+e^- colliders. Here parts of 1st, 2nd and 3rd order in the theory can be checked down to distance scales of 10^{-18} cm. The check can be done by simply looking at the R-ratio, that is the ratio of hadronic production to muon pair production, as well as other effects in the production of hadrons. If QCD should start to fail, for example if new color fields should appear or the fundamental particles (quarks) should develop a size, such effects would alter the R-ratio. More subtle effects such as changes in the strength of the interaction will show up in the multiplicity distribution of produced hadrons and in other ways. Using the data from TRISTAN[2]:

Group	R-value	
TOPAZ	4.40 ± 0.34	
AMY	4.23 ± 0.29	(2)
VENUS	4.70 ± 0.58	
Wt. Sum	4.35 ± 0.24	
Theory	4.43	

a limit can be set on the minimum hadronic density at which QCD could fail. If we take the error in the weighted sum of the measurements as an indication of the size of a possible violation distance then,

$$QCD_{violation} = [\ \Delta R\ *\ \sigma_{\mu\mu}\ ]\ . \qquad (3)$$

This leads to a violation distance on the order of 10^{-18} cm or densities of the order $\rho = 10^{13}$ GeV/fm^3. So QCD should be good to unimaginably high densities. Comparing this number to the explored range of hadronic density above means there is a vast new region to be explored.

Exploring the region of a few GeV/fm^3 theoretically leads to the prediction of a phase transistion[3]. Of course there is ambiguity in the translation of these theoretical results into experimental predictions but estimates for the transition seem to be on the order of 10 times nuclear matter.

As is shown in Figure 1, the theoretical results are in the ε/T, $\beta=6/g$ space, where ε is the energy density, T is the temperature and g is the coupling constant on the lattice. The transition from these variables to experimentally measurable ones is as follows; starting with the standard thermodynamic variables

$$U = TS - PV \tag{4}$$

and then dividing by TV we find:

$$\varepsilon/T = \sigma - P/T \tag{5}$$

where σ is the entropy density. From modeling it is found that the pressure term is small and can be dropped. This means that the energy density and entropy density are simply related. Using the hydrodynamic model of Landua[4] or more modern variants, the energy tensor of the hadronic fluid is,

$$T_{\mu\upsilon} = (\varepsilon + p)\, u_\mu u_\upsilon - g_{\mu\upsilon}\, p \tag{6}$$

where u_μ is the velocity field of the fluid. While Bjorken[5] has relaxed the assumption made by Landua that the fluid must be noncompressible, both find that the number of particles, n_c, produced per unit of rapidity, y, is proportional to the entropy density. This then gives the experimentalist two relativistic invariant variables with which to work:

$$\delta n_c / \delta y \;\; \alpha \;\; \varepsilon/T \cong \sigma \tag{7}$$

$$< P_\perp > \;\; \alpha \;\; T \tag{8}$$

where $P_\perp$ is the transverse momentum of the particle. As is shown in Figure 1 the experimental variable can now be related to the theoretical results.

In order to accomplish these measurements, an experiment[6] (E735) has been set up in the C0 interaction region of the Fermilab collider to search for the plasma in proton-antiproton collisions at $\sqrt{s}$ = 1.8 TeV. The detector is shown in Figure 2. In the first run of the experiment the detector consisted of a 240 element multiplicity hodoscope surrounding the interaction region; covering about 6.5 units of rapidity and a magnetic spectrometer at $\approx 90^0$ which samples the charged particle spectrum with a solid angle coverage of 0.4 sr. The hodoscope system is then used to measure the average number of charged particles over its full rapidity range and the magnetic spectrometer is used to measure the transverse momentum of the particles that enter it. Thus the spectrometer measures only about 1% of the particles in an event.

The key idea used in the design of this experiment and in the analysis of its results is that of the thermodynamic ensemble. Each event is considered to be only one element of the ensemble. The average transverse momentum is then found using all those events within a fixed range of entropy density. This then allows the experimenter to plot effectively the temperature versus the energy density. Structure in the distribution of transverse momentum versus multiplicity density, such as a rise with a plateau followed by a second rise, could be interpreted as one of the signatures of a phase transition.

There has been some criticism of searching for a plasma in proton-antiproton collisions on the grounds that the size of the excited region may not be large enough nor persist long enough for the system to come to thermodynamic equilibrium. But the very fact that each of the data points consist of an average of thousands of events, (even though any given event by itself may be considered to be extreme) means that the abstracted state which is the ensemble average of all the particular states is in thermodynamic equilibrium. At this point in time the question that is being addressed by all experiments is whether or not a plasma state exists and not the finer details of its development. The goal is not to find a single quark-gluon plasma event.

Shown in Figure 3 are the data for events in which there are two or more tracks in the spectrometer arm. These events were used because a clear vertex can be formed using the multiple tracks, which can then be matched to the vertex formed using the timing information in the trigger hodoscope counters. These counter lie alone the beam line and cover the pseudorapidity intervals $3 \leq |\eta| \leq 4.5$. These events are found to be nearly background free, containing background at the level of a few percent. The average transverse momentum was found over the range 0.15 GeV/c $\leq P_\perp \leq$ 3.0 GeV/c. As is shown in the Figure, $\langle P_\perp \rangle$ rises steeply, followed by a plateau-like region. Then there seems to be a break at $\langle \delta n_c / \delta y \rangle = 15$, followed by a gradual rise. If four points on both sides of the step are fit with a simple level function $\langle P_\perp \rangle = b \langle \delta n_c / \delta y \rangle$, where b is a constant, the step is 36 ± 4.5 MeV/c. A straight line fit through the 8 points yields a χ^2/ D.O.F. =2.2.

The largest observed value $\langle \delta n_c / \delta y \rangle = 32$, using Bjorken's formula, represents an energy density of $\varepsilon \approx 4$ GeV/fm^3:

$$\varepsilon = \frac{1}{2\pi\tau_0} \left[\langle P_\perp \rangle^2 + M_\pi^2 \right]^{1/2} \frac{3}{2} \frac{\delta n_c}{\delta y} \qquad (9)$$

when τ_0 is set to 1 fm . This should be compared to energy densities obtained in heavy ion collisions which are about 3 GeV/fm^3. In Figure 4 is shown the expected probability to observe a given number of charged particles in the final state. In this experiment, events with over 200 particles have been observed. While the probability to observe such high densities is small the fall off as a function of increasing particle density is slow in comparison to that observed in heavy ion collisions. In heavy ion collisions the probability to observe a given energy density is at first very flat followed by a precipitous fall off at high density[7]. This may occur because while a single nucleon-nucleon collision may produce locally a very hot spot within the nucleus-nucleus collision, the probability that the entire nucleus obtains such a high density must ultimately be proportional to the same probability observed in nucleon-nucleon collisions raised to a large power n. Hence necleon-necleon collisions are undoubtedly the best place to obtain the very highest energy densities.

REFERENCES

1. L. McLerran, Rev. Mod. Physics, Vol. 58, #4, p.1021 Oct 1986.
2. T. Kondo and K.Takahashi, Ed., Physics in Collision 7, World Scientific, Teaneck N.J., 07666 U.S.A.
3. J. Polonyi et. al., Phy. Rev. Let. 53,644., L. Van Hove, Phys. Lett. 118b, 138 (1982).
4. L.D. Laudau, Izo. Akad. Nauk. SSSR, Ser. Fiz. 17 (1953) 51.
5. J.D. Bjorken, Phys. Rev. D27, (1983) 140.
6. T. Alexopoulos et. al., Phy. Rev. Let. V60,#16,p.1622 18 Apr. 88.
7. H. En'yo, in Proceeding of the Workshop on Physics of The Quark-Gluon Plasma, Ed., Y. Miyamura, J. Chiba, K.E.K. Japan,1988.

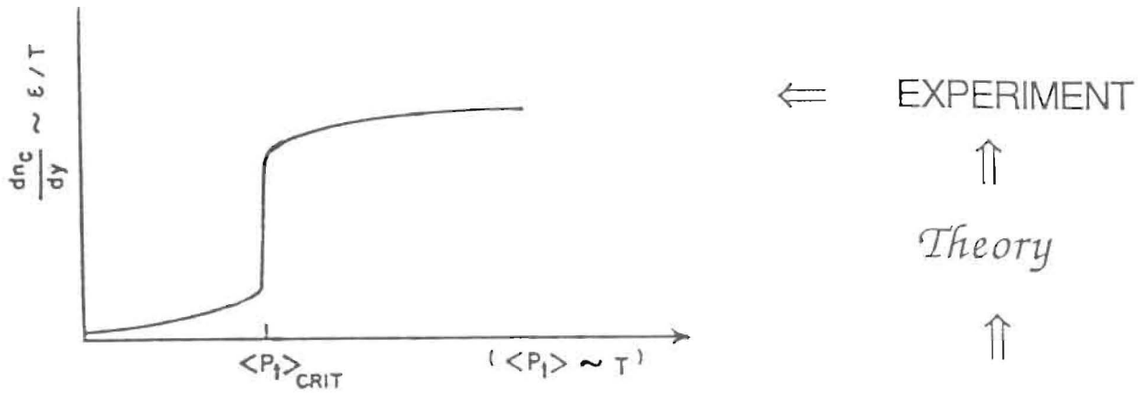

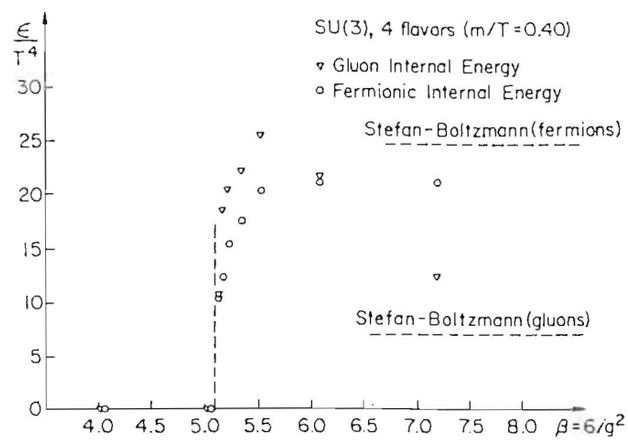

Figure 1. The conversion of theoretical predictions of QCD on a lattice to experimentally observable variables in terms of produced hadrons and their transverse momentum.

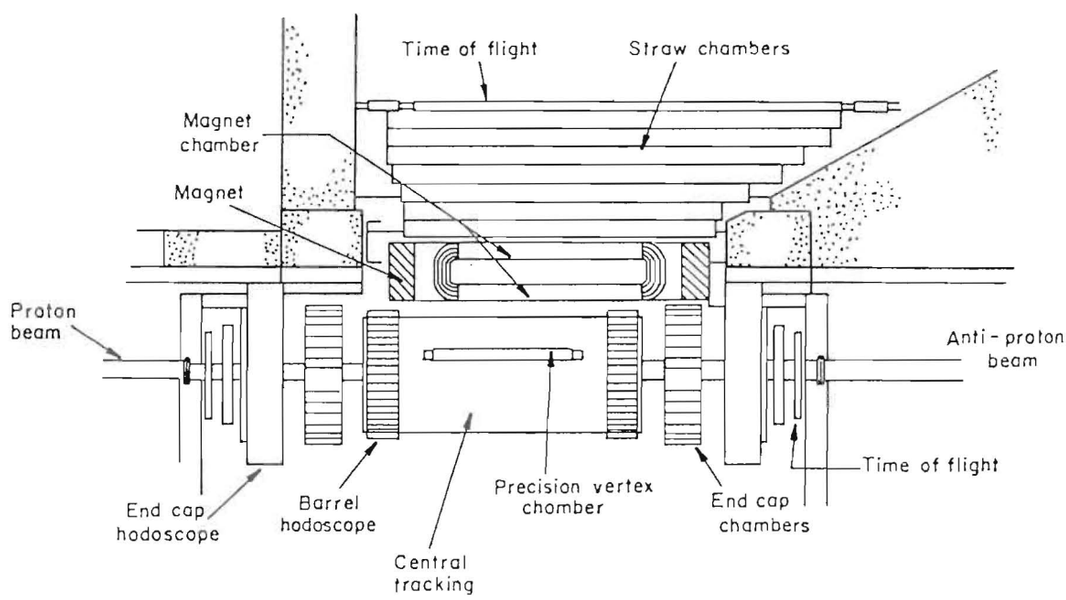

Figure 2. The C-0 detector. In the first run the central tracker was not installed.

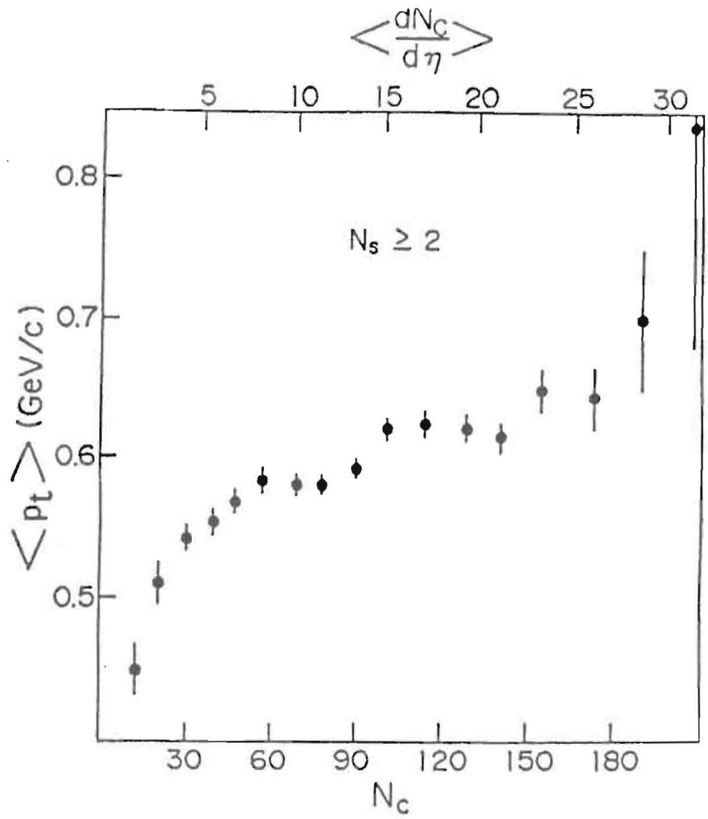

Figure 3. The data taken at $\sqrt{s}$ = 1.8 TeV in proton-antiproton collisions. The data points in the region $< \delta n_c/\delta\eta > \approx 15$ contain thousands of events each.

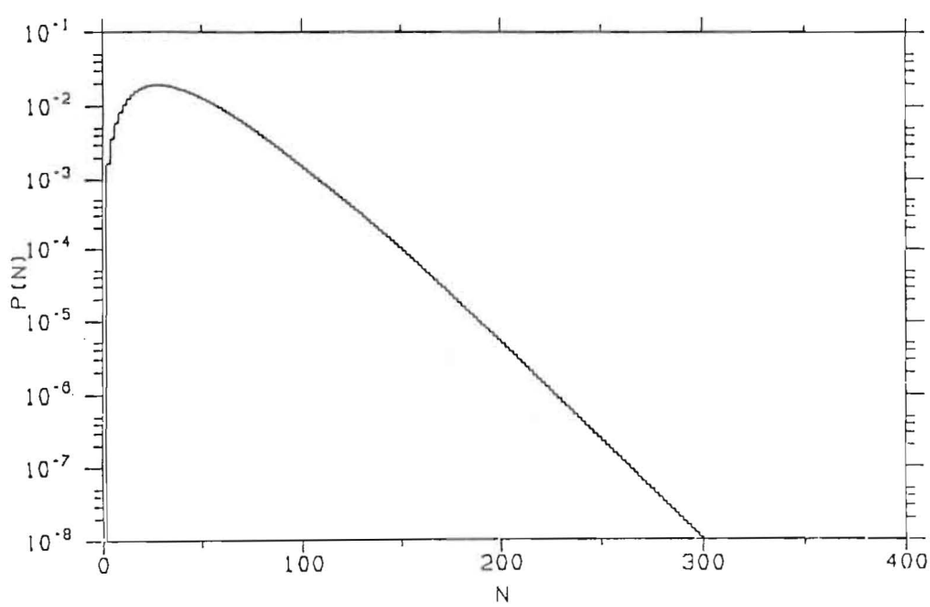

Figure 4. The probability to observed a given number of charged tracks N. A negative binomial was used to generate the plot. The probability to observe a given energy density has a very similar shape.